UNIVERSITAT POLITÈCNICA DE CATALUNYA BARCELONATECH

Possibilities and limitations of active battery management systems for lithium-ion batteries

Andreas Ziegler

ADVERTIMENT La consulta d'aquesta tesi queda condicionada a l'acceptació de les següents condicions d'ús: La difusió d'aquesta tesi per mitjà del repositori institucional UPCommons (http://upcommons.upc.edu/tesis) i el repositori cooperatiu TDX (http://www.tdx.cat/) ha estat autoritzada pels titulars dels drets de propietat intel·lectual **únicament per a usos privats** emmarcats en activitats d'investigació i docència. No s'autoritza la seva reproducció amb finalitats de lucre ni la seva difusió i posada a disposició des d'un lloc aliè al servei UPCommons o TDX. No s'autoritza la presentació del seu contingut en una finestra o marc aliè a UPCommons (*framing*). Aquesta reserva de drets afecta tant al resum de presentació de la tesi com als seus continguts. En la utilització o cita de parts de la tesi és obligat indicar el nom de la persona autora.

ADVERTENCIA La consulta de esta tesis queda condicionada a la aceptación de las siguientes condiciones de uso: La difusión de esta tesis por medio del repositorio institucional UPCommons (http://upcommons.upc.edu/tesis) y el repositorio cooperativo TDR (http://www.tdx.cat/?locale-attribute=es) ha sido autorizada por los titulares de los derechos de propiedad intelectual **únicamente para usos privados enmarcados** en actividades de investigación y docencia. No se autoriza su reproducción con finalidades de lucro ni su difusión y puesta a disposición desde un sitio ajeno al servicio UPCommons No se autoriza la presentación de su contenido en una ventana o marco ajeno a UPCommons (*framing)*. Esta reserva de derechos afecta tanto al resumen de presentación de la tesis como a sus contenidos. En la utilización o cita de partes de la tesis es obligado indicar el nombre de la persona autora.

WARNING On having consulted this thesis you're accepting the following use conditions: Spreading this thesis by the institutional repository UPCommons (http://upcommons.upc.edu/tesis) and the cooperative repository TDX (http://www.tdx.cat/?locale- attribute=en) has been authorized by the titular of the intellectual property rights **only for private uses** placed in investigation and teaching activities. Reproduction with lucrative aims is not authorized neither its spreading nor availability from a site foreign to the UPCommons service. Introducing its content in a window or frame foreign to the UPCommons service is not authorized (framing). These rights affect to the presentation summary of the thesis as well as to its contents. In the using or citation of parts of the thesis it's obliged to indicate the name of the author.

Universitat Politècnica de Catalunya

Departament d'Enginyeria Elèctrica

PhD thesis

Possibilities and Limitations of Active Battery Management Systems for Lithium-Ion Batteries

Author: **Andreas Ziegler**

Directors: **Daniel Montesinos i Miracle**
Ansgar Ackva

Barcelona, September 2022

Universitat Politècnica de Catalunya
Departament d'Enginyeria Elèctrica
Centre d'Innovació Tecnològica en Convertidors Estàtics i Accionament
Av. Diagonal, 647. Pl. 2
08028 Barcelona

Copyright © Andreas Ziegler, 2022

I would like to dedicate this thesis to my family, especially to my grandfather who passed away during the writing of this thesis in the corona pandemic.

Acknowledgements

I would first of all like to express my great gratitude to my supervisors Daniel Montesinos-Miracle and Ansgar Ackva. Throughout the last few years, I have been able to rely on their continuous professional support and encouragement during the process of writing this thesis. Especially during the corona pandemic, when many questions and problems arose regarding the continuation of the PhD project and the necessary long-term measurements, I could always rely on the advice of my supervisors. I would like to mention in particular their constant availability for online meetings and their help with even small, unexpected problems. Through their critical questions, scientific comments and further advices, they have made a decisive contribution to this work.

I would like to thank the reviewers Prof. Bernhard Arndt and Prof. Gunther Bohn who read and approved this thesis. Their comments and remarks have enabled me to further improve my work. I would also like to thank the members of the examination committee Prof. Francisco Díaz González, Prof. Andreas Sumper and Prof. Johannes Teigelkoetter for their support and willingness to be part of the panel.

I would like to thank my direct colleagues David Oeser, Thiemo Hein and Pavlo Ponomarov. In the last few years, it was especially their support in everyday questions and their willingness to participate in ongoing discussions that motivated me and made it possible to write this thesis. In this context, I would especially like to thank David Oeser, who has accompanied and supported me on my entire academic education since the beginning of my studies in electrical engineering. Furthermore, I would like to thank all my other colleagues and students at TTZ-EMO who accompanied me during this thesis.

Finally, I would like to thank my girlfriend Annika, for her constant support, encouragement and great understanding during the last few years. I would also like to thank my family. My parents Elisabeth and Manfred have supported me unconditionally for many years during my entire undergraduate education. They created the basis for my successful education, only because of them this was possible.

Abstract

Lithium-Ion Batteries (LIBs) are being used in more and more areas of application. At the same time, their chemical composition and their designs are constantly evolving. Major developments are also taking place in the field of Battery Management Systems (BMSs), which are essential for the safe operation of LIBs. The focus is on intelligent charge redistribution between individual cells as the main feature of active battery management, called Active Balancing (AB). This thesis deals with the possibilities and limitations of AB. An empirical long-term experiment provides new insights into the ageing behaviour of batteries that are actively balanced during their entire service life.

The main objective of this work is to to demonstrate influences on the ageing behaviour of batteries that are still unknown at present. A literature study shows that previous work in this area is often based on theoretical approaches and rarely has a functional proof through measurement results. Most significant statements from literature are examined. These include the increase in discharge capacity, energy efficiency and service life associated with active balancing, as well as lower parameter variation of the individual cells installed in the battery.

Before starting the empirical experiment, the current state of the art is captured and a universal AB topology is selected from a large number of known systems. The operating behaviour as well as the balancing algorithms are explained in detail in order to be able to understand the influences occurring during the ageing of the batteries. The ageing experiment itself is a comparison test between commercial Passive Balancing (PB) and the novel AB. Two identical battery packs are aged under uniform conditions, but with the two different BMSs mentioned above. At the end of the ageing process, the battery packs are disassembled and the parameters of all individual cells are determined for further investigation.

The main contribution of this work is the proof of effects through AB, especially with large battery loads. Both the increase in discharge capacity and the service life are demonstrated. The work shows how parameter variation of individual cells can be made visible during operation. It also presents diagnosis and calculation methods. The energetic efficiency of the batteries cannot be increased, since the self-consumption of the power electronics of

the AB system is always higher than with PB. However, the overall efficiency of the battery increases due to an increase in capacity and an extension of the service life. The thesis also shows that with lower battery loads, the use of AB is not beneficial any more or may lead to negative effects. In such applications conventional PB is sufficient. The results obtained during pack ageing are additionally substantiated and extended by the measurement results of the individual cells.

At the end of the thesis, all results and contributions are summarised. Suggestions for optimisation as well as further research ideas are presented as a possible starting point for further scientific studies.

Resum

Les bateries d'ions de liti (Lithium Ion Batteries, en anglès) s'usen en més aplicacions. Al mateix temps, la seva composició química i dissenys estan en evolució constant. Els sistemes de gestió del bateries (Battery Management Systems, en anglès), que són essencials per l'operació de les LIB, també estan en constant evolució. El focus principal està en la distribució intel·ligent de càrrega elèctrica entre cel·les individuals, l'anomenat balanceig actiu (Active Balancing, en anglès). Un assaig empíric, de llarga durada, com el dut a terme en aquest treball, dona molt informació en el procés d'envelliment de les cel·les durant tota la seva vida.

El principal objectiu d'aquest treball és demostrar les influències encara desconegudes en el procés d'envelliment de les cel·les. L'estudi de la literatura mostra que el treball previ en aquesta àrea està sovint basat en aproximacions teòriques i estranyament ensenya resultats empírics que ho corroborin. En aquest treball s'examinen la majoria de presumpcions que es poden trobar a la literatura. Aquestes inclouen l'increment en la capacitat, l'eficiència energètica i la vida útil associada a un balanceig actiu de les cel·les, així com la reducció de la variació dels paràmetres de cada cel·la en una bateria.

Abans de procedir amb l'experiment empíric, es revisa l'estat de l'art en els aspectes fonamentals per aquest estudi. També se selecciona una tipologia de sistema de balanceig actiu per tal de realitzar l'experiment. El treball detalla el procediment d'operació així com l'algoritme de balanceig actiu implementat per tal d'entendre els fenòmens que influencien la degradació de les cel·les durant la seva vida. L'experiment d'envelliment és una comparació entre un sistema de balanceig passiu (Passive Balancing, en anglès) i un de balanceig actiu. Per això s'escullen dues bateries idèntiques, però gestionades diferentment per dos sistemes de gestió diferents. Al final de l'assaig, les bateries es desmunten i s'analitza cada cel·la de forma individual per tal de determinar-ne els seus paràmetres i el seu envelliment.

La principal contribució d'aquest treball es el demostrar els efectes del balanceig actiu, sobretot en bateries amb una càrrega elevada. El treball demostra que el balanceig actiu millor gla capacitat de la bateria i la vida útil. El treball també mostra com la variació dels paràmetres de les cel·les es pot fer visible durant la seva operació. També presenta nous mètodes de diagnosi i càlcul d'aquests paràmetres. L'eficiència energètica de les bateries no es

pot augmentar degut al consum propi i les pèrdues del sistema de balanceig actiu basat en electrònica de potencia. Si que augmenta l'eficiència global de la bateria, ja que augmenta la seva capacitat i la vida útil. El treball també mostra que en bateries sotmeses a baixa càrrega, el balanceig actiu no aporta cap avantatge respecte el balanceig passiu. Fins i tot en algunes situacions, els efectes del balanceig actiu són negatius. En aquestes aplicacions, es recomana l'ús d'un sistema de balanceig passiu. Els resultats obtinguts durant l'assaig de la bateria queden reforçats quan es fa l'anàlisi de cada cel·la de forma individual.

Al final del treball, es resumeixen tots els resultats a més de proporcionar suggerències per la optimització així com possibles línies de futures investigacions.

Contents

List of Figures

List of Tables

Acronyms

AB	Active Balancing.
AC	Alternating Current.
BAT	Battery.
BMS	Battery Management System.
BOL	Begin Of Life.
CC	Constant Current.
CV	Constant Voltage.
DC	Direct Current.
DOD	Depth Of Discharge.
EFC	Equivalent Full Cycle.
EIS	Electrochemical Impedance Spectroscopy.
EMI	Electromagnetic Interference.
EOC	End Of Charge.
EOD	End Of Discharge.
EOL	End Of Life.
EV	Electric Vehicle.
HV	High-Voltage.
IEEE	Institute of Electrical and Electronics Engineers.
LCO	Lithium-cobalt-oxide.
LFMP	Lithium-iron-manganese-phosphate.
LFP	Lithium-iron-phosphate.
LIB	Lithium-Ion Battery.
LIC	Lithium-Ion Cell.

MOSFET	Metal Oxide Semiconductor Field Effect Transistor.
MUX	Multiplexer.
NCA	Lithium-nickel-cobalt-aluminium-oxide.
NMC	Lithium-nickel-manganese-cobalt-oxide.
OCV	Open Circuit Voltage.
PB	Passive Balancing.
PHEV	Plug-In Hybrid Electric Vehicle.
PWM	Pulse-Width Modulation.
RC	RC element.
RPT	Reference-Parameter-Test.
SEI	Solid-Electrolyte Interphase.
SOC	State Of Charge.
SOH	State Of Health.

List of Symbols

C	Capacitance.
Δ	Difference.
D	Diode.
E^0	Normal Potential.
η	Energy Efficiency.
f	Frequency.
I, i	Current.
$\hat{I}$	Current Amplitude.
Im()	Imaginary Part.
L	Inductance.
n	Number/Amount.
P, p	Active Power.
φ	Phase Difference Angle.
Q	Amount of Charge.
Re()	Real Part.
R	Resistance.
S	Switch.
t	Time.
T	Temperature.
τ	Time constant.
Tr	Transformer.

U, u	Voltage.
$\hat{U}$	Voltage Amplitude.
Z	Impedance.
$\underline{Z}$	Complex Impedance.

List of Subscripts

avg	Average.
b	Balancing value.
bat	Battery value.
c	Cell value.
cap	Battery capacity.
cb	Related to capacity based balancing.
ch	Related to charging process.
D	Related to double layer effects.
DC	Direct current.
diff	Difference.
disch	Related to discharging process.
EOC	End of charge.
EOD	End of discharge.
i	Individual value.
K	Related to diffusion process.
lim	Limit.
max	Maximum value.
meas	Related to measurement.
min	Minimum value.
N	Nominal value.
oc	Open circuit.

prev	Previous.
p	Pulse.
R	Related to resistance.
sd	Related to self discharge.
step	Balancing step.
sum	Sum.
tb	Related to voltage based balancing.

Chapter 1

Introduction

1.1 Background

Due to an increasing demand in the mobility sector and in the area of stationary storage systems LIBs are becoming more and more important [1]. They are used in many areas of application with a multitude of possible designs and shapes [2]. For example, the type and number of cells installed as well as their internal interconnection as series and parallel circuits vary. While a large number of cells must be connected in series in cars and trucks in order to achieve the necessary operating voltage of e.g. 400 V, only a few cells are required for e-bikes, e-scooters or other vehicles in the so-called last-mile segment in order to provide the necessary operating voltage of 36 V - 48 V. Based on the required battery capacity, additional cells are connected in parallel depending on the application.

Independent from the application, design and size of a LIB it must be equipped with a BMS [3]. Beside a large number of tasks this BMS is responsible of keeping the individual cells installed in the battery within their operating parameters and thus protecting them against deep discharge, overcharging or an excessively high or low operating temperature [4]. In order to fulfil this task, the BMS is connected to each individual battery cell in the series connection as well as to temperature sensors installed between the cells. A BMS is also capable of measuring the load current of a battery and, if necessary, interrupting it by a suitable hardware switch. The components mentioned can be seen in the schematic illustration of Figure 1.1. The figure shows four cells connected in series where each stands for n parallel cells.

Similar to the variety and individuality of LIBs, a variety of different BMSs in general, and in particular a variety of cell balancing topologies, have been established [5]. Cell balancing generally refers to the change in the State Of Charge (SOC) of individual cells by an electronic system integrated

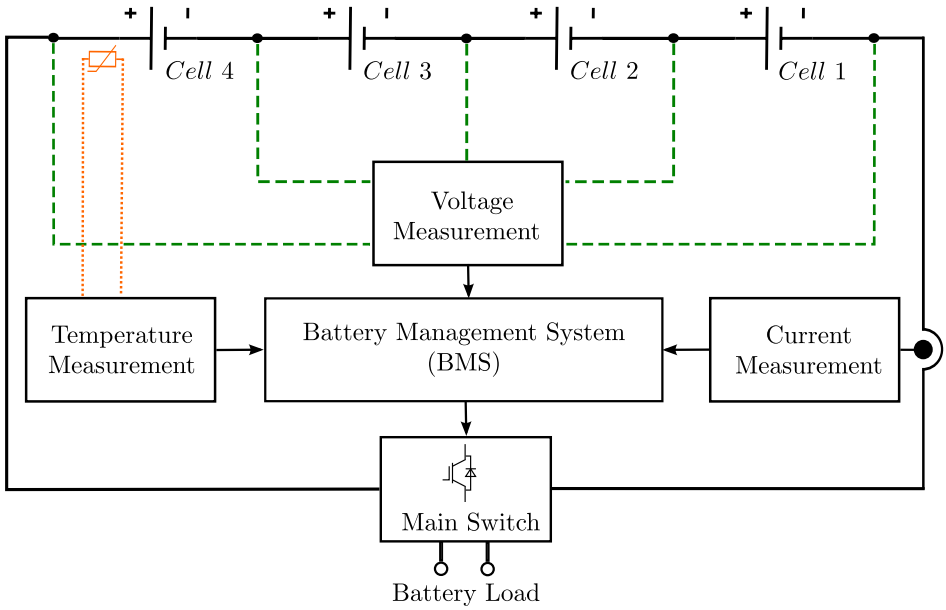

Figure 1.1: Basic components of a battery management system.

in the BMS. This is necessary because the SOC of the cells can change independently of each other due to a number of individual ageing effects, thus limiting the usability of the battery capacity [3]. Different balancing topologies can be separated in two categories. With so called PB, excess energy in weak cells is converted into heat by resistors in order to be able to fully charge stronger cells. With AB energy is distributed between the cells. Although AB seems to have some advantages over PB because of this fact, it has not established on the market.

This thesis deals with the balancing topologies of BMSs, their differences and the resulting advantages and disadvantages. Literature reveals a gap in the field of system validation with measurements and corresponding remaining research questions to be answered during the progress of this thesis. Assumptions including facts that AB, as opposed to PB, can increase the usable battery capacity, increase the energy efficiency, reduce the parameter variation between individual cells and finally extend the lifetime of the entire battery have to be proven or disproved.

1.2 Motivation of Research

In the last three decades the further development of LIBs and the associated BMSs have been advanced constantly. While LIBs are used in ever more differentiated areas of application with widely varying designs, the BMSs are often constructed to operate according to the same functional principle of passive balancing. Although a wide variety of active BMSs are known from literature and constantly further developed, they are rarely used in practice.

Research activities in the field of active balancing are manifold and usually divided into two areas, hardware topologies and balancing algorithms. Both fields have strongly been developed, especially since the 2000s. Today, there is a multitude of different topologies with different transmission techniques for energy exchange between the battery cells. They need a higher-level intelligence to decide which battery cells should be balanced. For this purpose, calculation methods and algorithms from literature propose how to control and monitor the energy transfer.

Many advantages of the active BMSs thus seem logical since energy exchange between the cells means that energy no longer has to be wasted due to passive balancing resistances and the battery can be used more efficiently. An increase in efficiency and service life are the direct consequences. The literature also identifies these advantages and proves them by means of comparative studies, most of which are based on simulation. A good example is the extensive work of Daowd et. al. [6] which compares different passive and active topologies and confirms decisive advantages for active topologies.

A validation of the findings presented in existing studies through simulation can hardly be found in the current literature. Important and consistent reasons explain this situation, including:

- Safety: Handling LIBs can be dangerous and requires a high level of test safety measures and fire protection.
- Time: A lot of time is required to age LIBs together with different BMSs. Battery ageing often lasts several months.
- Equipment: Appropriate battery test systems and temperature chambers for long-term tests are necessary, which often are not sufficiently available in laboratories.

In this work, however, long-term measurements are run in the laboratory on a large scale. This is an opportunity and motivation to carry out the validation measurements that are missing in literature. The aim is to prove the possibilities and limitations of active balancing systems through measurement in order to justify either the current approach of relying on passive systems or to justify the benefits of using active balancing in practice.

1.3 Objectives of Research

The aim of this work is to verify the positive and negative characteristics of AB as a component of a BMS in comparison to conventional PB, here called possibilities and limitations. The design and set-up of the empirical experiment is complex, as both the basics of LIBs and the state of the art of AB circuits have to be fully covered first. The AB system used must be fully understood and be able to be operate reliably in a long-term experiment. It is important for this work that the comparative tests between active and passive balancing are designed in such a way that they provide sufficient and conclusive data sets for further evaluation. From this aim a number of objectives are generated, which are summarised as follows:

- Obtain a basic understanding of lithium-ion batteries and their ageing behaviour based on recent literature.
- Acquire a complete technical understanding of balancing systems from literature, including a functional description of relevant topologies and algorithms of passive and active balancing.
- Define a suitable balancing architecture for the specific context of this thesis, including a complete description of the related hardware and balancing algorithms.
- Design the empirical comparative experiment suitable for data collection.
- Monitor and evaluate the differences between AB and PB over the entire battery life. Study the effects on the individual cells inside the battery.
- Collect, process and analyse the data obtained. Identify dependencies, advantages and disadvantages of active balancing systems.

1.4 Contributions of Research

The scientific contributions of this work can briefly be summarised as follows, based on the objectives mentioned above:

- This thesis presents a universal active balancing system in terms of hardware and software and allows a complete system understanding. Based on the latest state of the art in both lithium-ion batteries and BMS, especially balancing topologies, the requirements for such a system are given in detail. Balancing algorithms are presented transparently and their calculation principles are described in detail.
- The approach of the empirical experiment for comparing active and passive balancing through a number of long-term tests is presented in this thesis. A literature review has revealed a significant gap in this area, as, so far, mainly simulations have been chosen for comparative experiments. Through extensive data collection ageing effects related to the BMS are identified over the complete lifetime of the battery packs. In addition to an increase in capacity during operation, influences on energy efficiency, deviations of internal cell parameters and the service life of the battery packs are investigated and proven.
- Another important contribution of this work results from the single cell measurements provided. By disassembling the tested batteries, a large amount of single-cell data is evaluated. These data support the previous results and also show further influences of active balancing in terms of parameter variation. AB is able to homogenise the ageing process of the individual cells and thus increase battery utilisation.
- In conclusion, this work provides a novel overview of the possibilities and limitations of an active balancing system that exceeds the latest state-of-the-art in literature. AB has the potential for a higher battery usability. However, battery load, battery design and the balancer itself have major impacts on the result.

1.5 Thesis Outline

Chapter 1 contains a short introduction to the subject and its background. Furthermore, the motivation, the objectives of the work and its contributions to science are explained.

Chapter 2 presents an overview of the state of the art of lithium-ion batteries. Frequently used designs, chemical compositions, important terms and definitions from battery technology, information about common aging mechanisms and modelling possibilities are explained. Finally, the chapter contains information about the determination of important battery parameters by measurement and possible effects of parameter variation.

Chapter 3 summarizes the state of the art in battery management systems, with a focus on balancing topologies. A variety of cell balancing topologies are explained and evaluated. The different possibilities for energy transport within a battery pack are explained as well as the selection of deviating cells relevant for balancing.

Chapter 4 explains a self developed BMS hardware and its balancing algorithms. First, the flyback converter is described as the most important component for the energy transfer. The behaviour of the balancing currents during operation of the entire system is explained in detail. Second, calculation methods and algorithms necessary for balancing are described. Three different routines their interaction ar explained.

Chapter 5 gives an insight on relevant literature used to define the relevant literature gap and the objectives of the empirical test approach with several battery packs. A full description of the experimental study design, the test conditions, the test procedure as well as a description of all relevant measurement parameters and further evaluation methods are provided. Finally, pack test results are explained and discussed.

Chapter 6 continues the empirical test approach from Chapter 5 with single cell measurements. In analogy to the pack tests, a full description of the experimental study design, the test conditions, the test procedure as well as a description of all relevant measurement parameters and further evaluation methods are provided. To conclude the chapter, cell test results are explained, discussed and compared to battery pack tests.

Chapter 7 concludes the work and summarises the thesis. Furthermore, the contributions of this thesis are listed and possibilities and suggestions for further research are provided. A list of all publications and patent applications of the author is shown at the end of the chapter.

Chapter 2

Lithium-Ion Batteries

According to [7], rechargeable batteries are the most widely used electrical energy storage devices today. They store electrical energy in the form of chemical energy. The technology of the LIB is promising. Compared to other battery types, the advantages of LIBs are their high efficiency, high energy density and long service life. The amount of installed LIBs is expected to continue to grow rapidly. It is expected to be the predominant battery storage technology in the future. It is therefore essential to be able to understand the basic features of this technology.

2.1 Functionality, Chemistry and Construction

Although the lead-acid battery was predominant for decades the Lithium-Ion Cell (LIC) is considered the best researched technology of all chemical energy storage devices nowadays [1]. With a density of 0.534 g/cm^3 at 20 °C, lithium is the lightest of all metals and with its normal potential of $E^0 = -3.045$ V it enables building batteries with high energy and performance [8]. In ionised form, lithium enables a high cell voltage and thus a high energy density of the battery. The reason for this is not only the electrochemical potential difference to graphite, for example, but also the significantly faster kinetics of the lithium ions in the various oxide cathode materials. In addition, unlike the other alkali metals, lithium ions can be reversibly intercalated into graphite or silicon. [9]

Figure 2.1 schematically shows the structure of a LIC. In this example image the LIC consists a metal-oxide cathode. Between the two electrodes is the ion-conductive electrolyte (which contains lithium conducting salt) and a separator. The separator is a porous membrane that electrically isolates the two electrodes from each other. During discharging and charging of the cell, lithium ions migrate back and forth between the electrodes and are stored

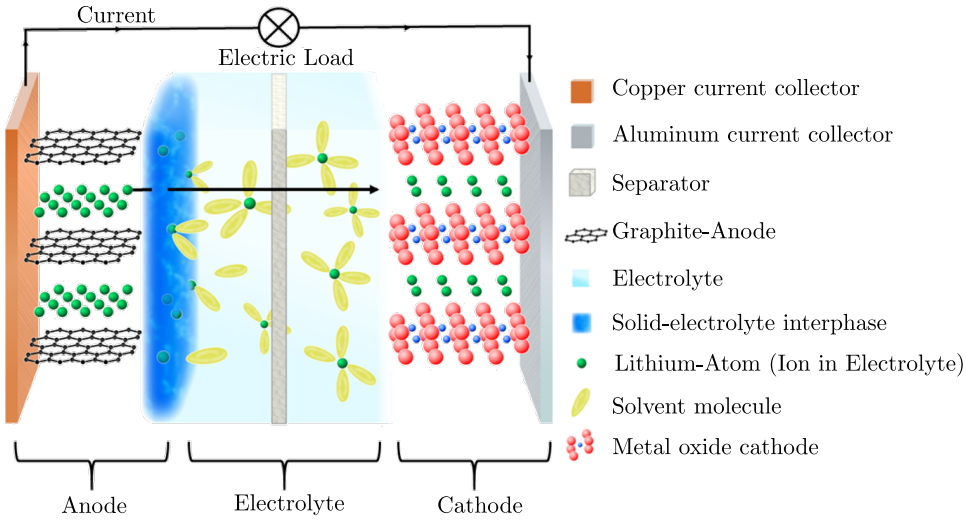

Figure 2.1: Functionality of a LIB, based on [1].

in the active materials of the electrodes. As active materials the positive electrode consists of mixed oxides (e.g. Lithium-nickel-manganese-cobalt-oxide (NMC) or Lithium-nickel-cobalt-aluminium-oxide (NCA)), whereas graphite is usually used for the negative electrode. During the process of de-intercalation of lithium from the negative electrode (copper as a current collector), electrons are released. This is therefore an electrical discharge process. When discharging, lithium ions migrate from the anode through an electrolyte and a separator to the cathode. At the same time, the electrons flow from the anode via an external electrical connection (cable connection, circuit board) to the cathode (aluminium as current collector). Any electrical consumer can be supplied with energy via the external electrical connection by the resulting current flow. When charging, this process is reversed, so that in this case lithium ions migrate from the cathode through the electrolyte and the separator to the anode. [9]
In principle, the more positive lithium ions can be intercalated in the cathode, the more free electrons are available for energy storage. The chemical composition of the cathode and its size therefore determines its capacity and is therefore also decisive for the capacity of the battery cell itself. [1]

The development and use of suitable cathode materials is essential for improving the performance of LIBs to meet the increasingly demanding requirements for energy storage. The cathode materials, as active materials,

must be capable of repeatedly (for recharging) and rapidly (at high current) absorbing and releasing lithium-ions [10].
LIBs are named after their active materials, with the designations written either in full text or abbreviated by their chemical symbols. For example, lithium cobalt oxide, one of the most common LIBs, has the chemical description $LiCoO_2$ and the abbreviation LCO [10]. For the sake of simplicity, the abbreviation Li-cobalt can also be used for this battery. Cobalt is the most important active material that gives this battery its properties. Other Li-ion chemicals are given similar abbreviations [11].
A hexagonal field to represent battery properties, as shown in Figure 2.2, is commonly used in the literature (see [9, 11]) to summarize the properties of different battery chemistry. Properties such as manufacturing costs, specific energy and capacity density, performance and expected life time at identical battery usage are shown. The safety aspect refers to stability at hot and cold temperatures, the release of gases and the associated flammability. In order to explain the influence of the cathode materials on the properties of the battery in more detail, the compositions that appear in the figure are briefly presented below from a users perspective:

- LCO: Lithium-cobalt-oxide ($LiCoO_2$)
  This chemistry has a relatively high theoretical specific capacity, low self-discharge, high discharge voltage, associated power and good cycle performance (lifetime). The main limitations are high cost, low thermal stability and fast capacity decrease at high currents or during cycles with a high Depth Of Discharge (DOD). Lithium-cobalt-oxide (LCO) batteries are relatively expensive due to the high cost of cobalt [12]. Due to its high specific energy density, LCO is often used in mobile phones, laptops and digital cameras [11].
- NMC: Lithium-nickel-manganese-cobalt-oxide ($LiNiMnCoO_2$)
  One of the most common Li-ion systems is a cathode combination of nickel-manganese-cobalt [11]. In the development of LIBs, it has replaced the chemistry LCO due to its better stability during cycles even at elevated temperatures, higher capacity and better thermal stability in the charged state [13]. NMC has a similar or higher achievable specific capacity density as LCO and a similar operating voltage at slightly lower cost due to reduced cobalt content [12].
- NCA: Lithium-nickel-cobalt-aluminum-oxide ($LiNiCoAlO_2$)
  Lithium-nickel-cobalt-aluminum batteries or NCA has great similarities with NMC chemistry. They offer high specific energy, good specific

performance and long life. Less advantageous are safety and also high costs. NCA is a further development of lithium-nickel-oxide, the addition of aluminium gives the chemistry a better stability [11]. The NCA cathode has found a relatively widespread commercial use, for example in Panasonic batteries for Tesla Electric Vehicles (EVs). NCA has a high usable discharge capacity compared to a conventional cobalt-based oxide cathode. [12]

- LFP: Lithium-iron-phosphate ($LiFePO_4$)
  $LiFePO_4$ is chemically and thermally resistant, has a high cycle stability, is inexpensive, resists high temperatures without decomposition (up to 300 °C), is quite stable against overcharging and short circuits, does not release oxygen compared to other battery materials and therefore does not tend to burn [8]. Compared to NMC and NCA it offers the advantage of safety combined with a lower energy density. LFP is often used as a replacement for the lead-acid starter battery in motor vehicles. Four cells in series produce 12.80 V, a similar voltage to six 2 V lead-acid cells in series. [11]

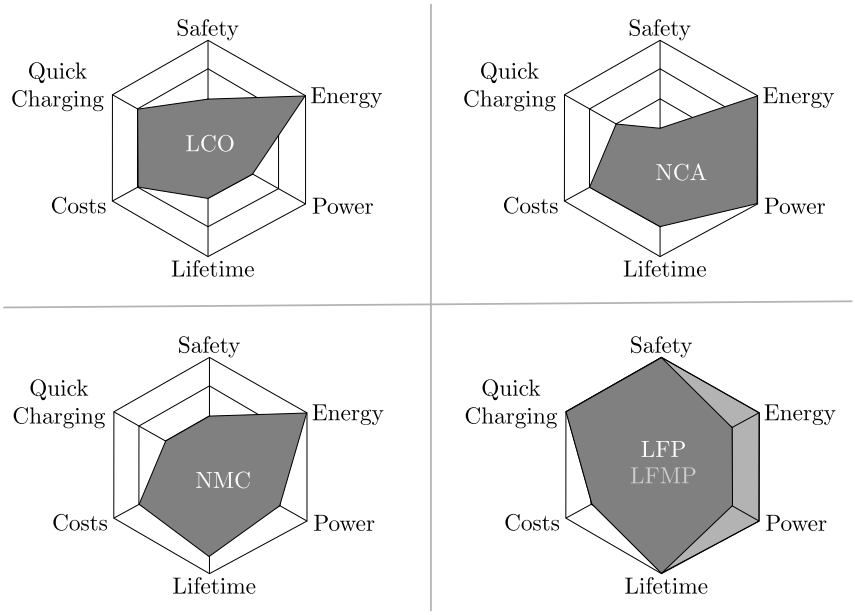

Figure 2.2: Battery properties depending on chemistry, based on [9].

- LFMP: Lithium-iron-manganese-phosphate ($LiFeMnPO_4$)
  Besides LFP, LFMP is the only cathode material that is both fast dischargeable and fast chargeable. LFP has not yet reached the high energy (Wh/kg) and power (W/kg) densities of the oxide cathode materials. By using manganese in LFMP, the LFP values can be increased by 20%. [9]

The electrical properties of the materials are summarized in Table 2.1. The final discharge voltage U_{EOD}, the nominal voltage U_{N}, the final charge voltage U_{EOC}, the capacity density in Ah/kg and the energy density in Wh/kg depend on the battery chemistry used.

Chemistry	$U_{\mathrm{EOD}} - U_{\mathrm{EOC}}$	U_{N}	Ah/kg	Wh/kg
LCO	2.5 – 4.2 V	3.6 V	160	624
NMC	2.5 – 4.2 V	3.7 V	160	592
NCA	2.5 – 4.2 V	3.7 V	200	740
LFP	2.0 – 3.7 V	3.3 V	160	544
LFMP	2.0 – 3.7 V	3.3 V	150	590

Table 2.1: Electrical properties depending on battery chemistry [9, 11].

Besides a variety of different chemical compositions, LIBs are also available in different forms. Based on Kurzweil et al. there are cylindrical, prismatic and flat cells (pouch cell, coffee-bag, softpack). The round cell of type 18650 for example has a diameter of 18 mm and a length of 65 mm. It contains a cylindrical winding of anode, separator, cathode, separator, as shown in Figure 2.3. Prismatic cells contain a flat coil or stacked units in a rectangular housing (hard case) or foil (soft pack). Thin, flexible electrodes are always used except in coin cells. Flat cells are more complex to manufacture, but offer price advantages in materials compared to cylindrical cells. All commercial batteries are hermetically sealed. [8]
According to Korthauer (2013), the 18650 round cell is a standard type and the most common cell on the market. It is produced at lower cost than other cell types and is used especially for laptops and power tools in the consumer sector. In the automotive sector, round cells are also used alongside prismatic cells and pouch cells. Pouch cells are frequently used in the consumer sector in smart-phones and can also be found in new types of ultra-thin laptops. A further product, however, are lithium-ion coin cells. These are used for example for Blue-tooth applications and other miniature devices.

All LICs on the market today have metallic housings or packaging material. This prevents humidity from entering the cell and also prevents solvents from escaping the cell by diffusion. A plastic housing cannot be used, since all plastics are permeable to humidity and are not diffusion-resistant to some organic solvents. [9]

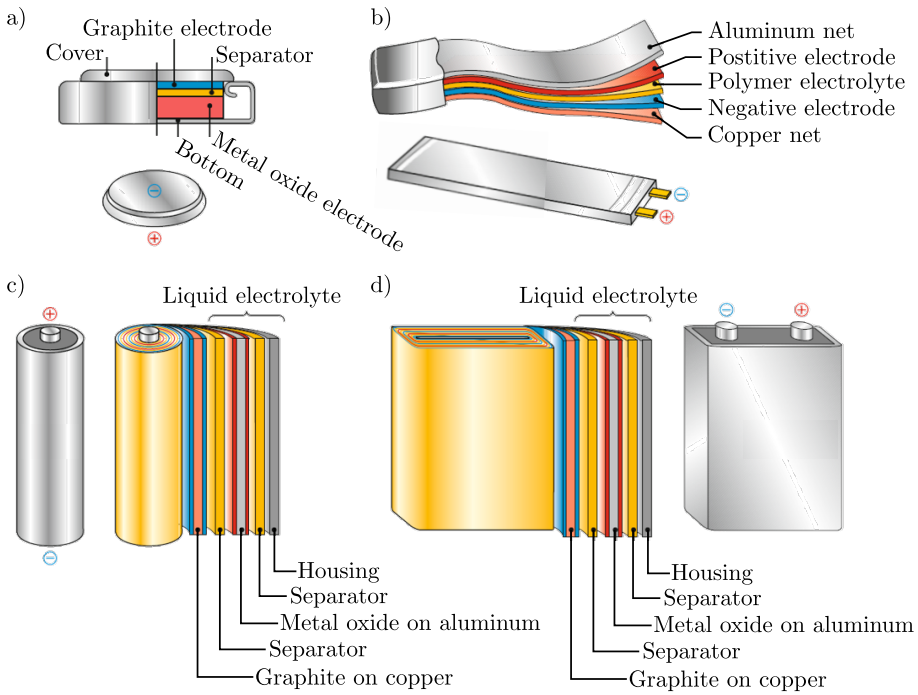

Figure 2.3: Mechanical construction of LIBs, based on [8]. Cell types shown: a) coin cell, b) pouch cell (coffee-bag, softpack), c) cylindrical (round) cell, d) prismatic cell. Cells b), c) and d) are provided with exemplary battery parameters.

2.2 Terms and Definitions

Important terms and definitions for LIBs based on [14]:

- Nominal Voltage
  The nominal voltage is the average value from the linear range of the cell voltage characteristic curve. The regions of the characteristic curve with large voltage changes at the beginning and end are neglected.
- Capacity (general)
  The term capacity refers to the maximum amount of charge Q that can be released by a pre-charged battery. The SI unit for measuring the amount of charge is coulomb (C). The product of current and time can also be used (Ah or mAh) as battery capacity C_{cap}. More precisely, this quantity of charge is the integral of the discharge current i (whether constant or variable) over the duration of the discharge t_{disch}. The amount of charge removed from the battery is also referred to as Q_{disch}.
  $$C_{\text{cap}} = \int_0^{t_{\text{disch}}} i(t)dt = Q_{\text{disch}} \tag{2.1}$$
- Nominal Capacity
  The nominal capacity (or rated capacity), noted as C_{N}, appears in the manufacturers' manuals and on the battery's nameplate. It is given for a discharge duration defined by international standards, depending on the application.
- Depth Of Discharge (DOD)
  The DOD is an indication of the amount of charge already removed from a battery in relation to C_{cap}. A DOD of 90%, for example, corresponds to a deep discharge, since the theoretical maximum is 100%.
  $$\text{DOD} = \frac{\int_0^{t_{\text{disch}}} i(t)dt}{C_{\text{cap}}} \tag{2.2}$$
- State Of Charge (SOC)
  The SOC is an indicator of the amount of charge remaining in the battery in relation to C_{cap}. It is a unitless value, usually expressed as a percentage.
  $$\text{SOC} = \frac{C_{\text{cap}} - \int_0^{t_{\text{disch}}} i(t)dt}{C_{\text{cap}}} \tag{2.3}$$
  $$\text{SOC} = 1 - \text{DOD}\ , \quad \text{DOD} = 1 - \text{SOC} \tag{2.4}$$

- State Of Health (SOH)
  The SOH is an indicator of the ageing condition of a battery. It can be evaluated as the amount of charge measured during a complete discharge in relation to the nominal capacity.

$$\mathrm{SOH} = \frac{Q_{\mathrm{disch}}}{C_{\mathrm{cap,N}}} \tag{2.5}$$

  This parameter thus characterizes the degradation of a battery during use and provides information about the End Of Life (EOL). The SOH is usually expressed as a percentage.

- Begin Of Life (BOL) and End Of Life (EOL)
  The condition of the battery immediately after production is called BOL. During use, the ageing of a battery leads to a reduction in its capacity and an increase in its internal resistance. If these parameters reach a certain level of deterioration, the battery can no longer perform its intended function. It is called the EOL even if it is still functional.

Further definitions with significance based on [15]:

- End Of Charge (EOC) and End Of Discharge (EOD) Voltage
  The charge and discharge cut-off voltages U_{EOC} and U_{EOD} describe the upper and lower cell voltage limit, which is specified by the manufacturer depending on the cell chemistry for safety reasons.

- Open Circuit Voltage (OCV)
  The OCV, is the voltage that is set at the terminals of the cell in an unloaded state when all equalization processes and secondary reactions in the cell have been completed. However, this state can only be reached approximately, since self-discharge in particular is present continuously as a side reaction.

- Current Rate
  The current rate or C-rate indicates the charge or discharge current in relation to the nominal capacity. For example, under nominal conditions, the discharge of a previously fully charged cell takes half an hour at a current rate of 2C.

- Current Direction
  The current direction is chosen in a way that a positive charging and negative discharging current results. This has the advantage that the cell voltage response follows the change in charge current with the same sign.

- Partial Cycle, Full Cycle
  A full cycle, starting from a fully charged state, corresponds to a full discharge and subsequent charge of the cell within the maximum voltage limits specified by the manufacturer. A partial cycle therefore corresponds to a charge/discharge cycle where the maximum voltage limits are not reached. For a partial cycle, the DOD is less than 100%.
- Equivalent Full Cycle (EFC)
  An equivalent full cycle corresponds to the total charge turnover in the cell in relation to the charge turnover of a full cycle with nominal capacity. In ageing tests, the number of cycles completed from the cell is sometimes expressed in equivalent full cycles.

2.3 Ageing Mechanisms

A detailed analysis of the ageing mechanisms of individual battery components is going beyond the context of this thesis. However, the most important aspects with influence on battery life should be considered.
The ageing of cells is divided into two major areas. These include ageing by cycle ageing (battery usage) and calendar ageing (battery storage) [16]. Since ageing is associated with electrochemical reactions in the cell, the temperature dependence can be estimated using Arrhenius' law [17].

2.3.1 Cycle Ageing

During cycle ageing, two main ageing effects can be observed in the cell: the loss of active material and the loss of cyclizable lithium. This loss is e.g. due to mechanical stress caused by changes in the volume of the active material during charging and discharging through the intercalation of lithium ions. Parts of the active material may crack or break off. [17, 18, 19]
The most common and fundamental source of capacity loss in LIBs is the loss of cyclizable lithium to cover layers like the Solid-Electrolyte Interphase (SEI) film that forms on the surface of the negative graphite electrode during recharging. Initially, SEI formation protects the electrolyte from decomposition, but over time it leads to a gradual decrease in capacity as the SEI layer becomes thicker. In general, SEI growth results from irreversible electrochemical decomposition of the electrolyte. The product of this decomposition forms a solid layer on the surface of the active material. The consequences are a decrease in capacity due to the irreversible reaction of lithium with the electrolyte, as well as an increase in internal resistance due to the increasing SEI layer thickness. [20]
An additional ageing process, the so-called lithium plating, takes place especially at high charge currents and simultaneously at low temperatures. The deposition of lithium (plating) occurs because the lithium ion concentration on the surface of the active material (anode side) increases due to the slowed diffusion process and the lithium ions are not stored fast enough. The lithium metal reacts strongly with the electrolyte, which in turn leads to passivation (and further SEI growth) and gas formation. Lithium metal tends to deposit at these sites during further cycles, which leads to the growth of dendrites (depends on cell current). In the worst case, the separator can be pierced by tall dendrites and an internal cell short circuit can occur. [21]

The decrease in capacity generally shows a linear dependency with an increasing number of cycles, but at certain residual SOH, depending on the chemistry and the actual ageing (e.g. about 80%), it turns non-linear at a turning point (see Figure 2.4). It is assumed that a thickening of the SEI film is the dominant ageing mechanism before the turning point. Subsequently, the deposition of lithium (plating) and thus the loss of cyclizable lithium is the main reason for the non-linear decrease in capacity until reaching EOL. [22]

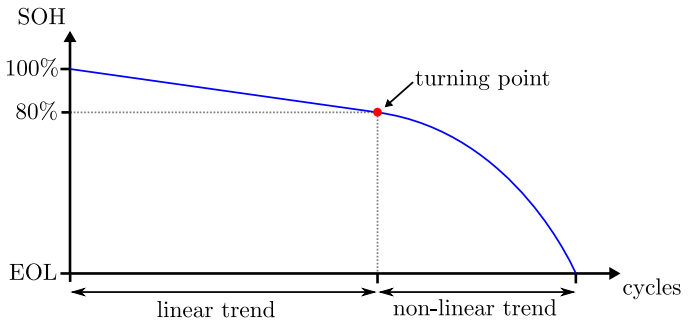

Figure 2.4: Battery capacity decrease depending on different ageing mechanisms.

2.3.2 Calendar Ageing and Self Discharge

Calendar ageing is one of the main disadvantages of LICs, as it does not depend on the use of the cells. Calendar ageing increases with temperature and SOC and is considered to be a limiting ageing mechanism with a concomitant loss of capacity and growth of internal resistance. [17]
According to [14], during a charging process, even if the battery is not subsequently discharged, the fully charged state is never completely reached. The batteries experience self-discharge phenomena in real life. These self-discharge phenomena are associated with redox reactions at each electrode, which are caused by the actually normal discharge reaction of the electrode itself. Since this is a chemical reaction, the higher the temperature, the greater the self-discharge - as well as the calendar ageing. In lithium batteries with a negative graphite electrode, self-discharge occurs more quickly at high SOC, since it is essentially due to reactions of the negative elec-

trode with the electrolyte. There is an oxidation/reduction of the lithium present, which reacts with the molecules of the solvent in the electrolyte (or the lithium salt) [23]. This process is comparable to the SEI layer formation and its growth with increasing battery age [20]. A part of the lithium is irretrievably lost, which leads to an irreversible decrease in the capacity of the battery cell.

A comparison between calendar and cycle ageing showed that cycle ageing of the battery leads to additional degradation in both capacity and resistance compared to storage [24]. Depending on the application area of the battery, cycle and calendar ageing exist in different dominance.

2.4 Battery Modelling and Model Parametrisation

The aim of the modelling is to achieve the best possible replica of the real battery cell, which reproduces all relevant effects with sufficient accuracy. The best possible reproduction of the battery cell is of great importance for the determination of their parameters in a BMS. The model approaches known in the literature can in principle be divided into three categories: [25, 26]

1. Multidimensional physical and chemical motivated models. (White-Box-Models)
   This type of model attempts to reproduce the structure of the individual materials inside the battery as accurately as possible to express the potential and diffusion gradients in different spatial directions by means of several coupled differential equations. This is often simulated with an FEM tool, although the spatial resolution can vary.
2. Electrical equivalent circuit diagrams. (Grey-Box-Models)
   Grey-Box-Models can be described as electrical equivalent circuit diagrams that were already used in technical applications before the use of LIBs. In this model category the electrical behaviour is simulated by simple components such as voltage sources, resistors, capacitances and inductors. The advantage of this modelling method is its high flexibility. This allows an easy adaptation of the model complexity to the requirements of the respective application.
3. Mathematical models. (Black-Box-Models)
   This includes all approaches based on mathematical models that are not oriented to the physical-chemical functional principles, but are merely mathematical approaches that suitably combine input and output variables of a battery according to empirical findings. The black box models include artificial neural networks and fuzzy logic or nonlinear autoregressive moving average models with exogenous inputs. Furthermore, these models are mainly used for diagnostic purposes and not for reproducing the current/voltage behaviour of a LIB.

In the field of electrical engineering, electrical equivalent circuit diagrams are preferred. In general, a voltage source which represents the OCV of the battery is combined with resistors, inductors and capacitors. The additional passive components approximate the dynamic battery behaviour. Figure 2.5 shows equivalent circuit diagrams of varying complexity:

a) The first equivalent circuit diagram consists of an ideal voltage source U_{oc} and a series connected resistor R_{DC}. U_{oc} represents the internal cell voltage and R_{DC} the internal resistance of the battery. If a load current is set at the terminals, voltage drops at the internal resistance. The step response of the system is rectangular and can hardly reproduce the dynamic battery behaviour.

b) The first equivalent circuit diagram is extended by an RC element (RC). The step response of the RC is exponential (PT1 element). Thus R_{DC} together with RC_1 better simulate the dynamic battery behaviour.

c) To further improve the dynamic behaviour, a further RC element is added. The battery model is now able to reproduce the voltage and current behaviour of a battery cell almost identically by overlaying R_{DC}, RC_1 and RC_2. This equivalent circuit diagram is the basis for battery modelling in various publications [27, 28, 29]. In [30] a third RC element was added to furhter improve accuracy.

d) A final increase in accuracy is achieved by using Warburg impedances. This form of battery modelling is difficult to compute. Basically, according to Keil et al., the two Warburg impedances simulate finite diffusion paths according to Fick's laws. They differ in the boundary condition at the end of the diffusion path. With an ideal reservoir (here Z_{W1}), the value at the end of the diffusion path always remains constant, with an impermeable wall (here Z_{W2}), all inflowing charges are stored within the diffusion path and released again when discharging. [26]

To verify the accuracy of the modelling, the step response of the systems can be evaluated. According to Waag et al., the immediate voltage drop after switching on the load is caused by the ohmic resistance of the cell and results from the conductivity of current collectors, active material, electrolyte, separator and the passivation layers, such as the SEI film or the corrosion layers on the current collectors. Especially the almost anhydrous electrolyte influences the ohmic voltage drop due to its low conductivity. At the same time, the electrolyte is highly temperature-dependent, with conductivity increasing with rising temperature. [31]
According to Jossen et al., the further time-dependent voltage drop is caused by the charge transfer, the effects of the double-layer capacitance and the diffusion process. The voltage drop during charge transfer causes the transition from ionic to electrical conduction and vice versa. Charge carriers are

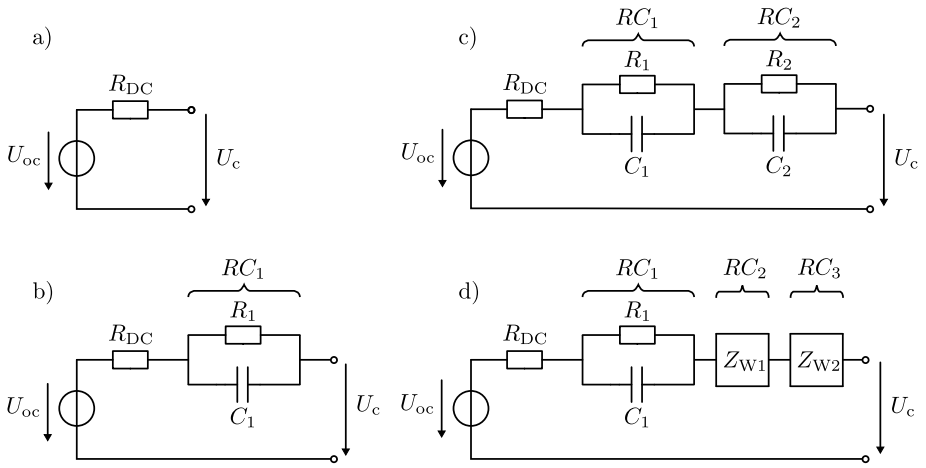

Figure 2.5: Electrical equivalent circuit diagrams for LIBs.

thus exchanged between electrode and electrolyte. Charge transfer is made up of a back and forth reaction, which are of equal magnitude in dynamic equilibrium. In dynamic equilibrium, the overlapping of both reactions to the outside means that no charge transfer and thus no change in voltage can be observed. If, for example, an imbalance between the forward and backward reaction occurs due to a load current, this leads to an effective charge transfer and thus to a change in voltage. However, a change in current does not immediately result in a voltage drop, but rather in an exponential change over time and follows the transient response of an RC element. This time-dependent behaviour also results from the buildup of a double layer capacitance in the electrode/electrolyte interface. The effect of the double-layer capacitance occurs when charge carriers of different polarization are close to each other in the electrode/electrolyte interface. From a physical point of view, a capacitor is formed. The diffusion voltage is caused by charge transport or ion transport within the electrolyte. With increasing temperature the diffusion is noticeably faster, thus the diffusion voltage is reduced significantly with increasing temperature. Besides the temperature, the geometry of the diffusion path also plays a important role. According to this, the ion transport is influenced by the porosity of the separator and active material as well as their thickness. [17]

2.4.1 Parametrisation with Step-Response

In Figure 2.6 the step response of a battery cell and the step responses of the presented equivalent circuit diagrams can be observed in a qualitative illustration. A fictitious load of 1C is applied at t_1, before that the battery is at rest. The step response is evaluated at t_2 and t_3, which are typically only a few seconds after t_1. The above presented charge transfer in connection with the effect of the double layer capacity can be simulated by an RC element, as in equivalent circuit diagram b). By adding a further RC element to the equivalent circuit diagram c), the effect of diffusion, and thus the entire step response, is reproduced. The RC elements use different time constants to reproduce the duration of the underlying chemical processes. [27]

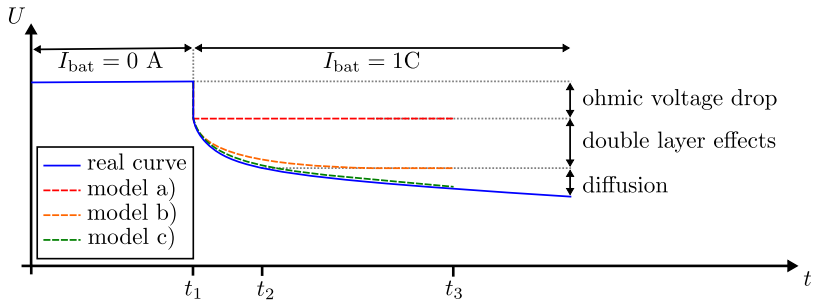

Figure 2.6: Step response of different electrical equivalent circuit diagrams.

Based on numerous experimental validations in the literature, the use of two RC time constants is the best compromise between accuracy and complexity [28]. In the following the equivalent circuit diagram c) is used for battery modelling.
In order to integrate further effects such as the SOC of the cell and ageing effects into the model, the ideal voltage source U_{oc} must be controlled. For this purpose, the equivalent circuit diagram c) is supplemented in Figure 2.7 according to Chen et al. by the control of the voltage source U_{oc} with further electrical components. Here, the voltage U_{oc} results from a parallel connection of the polarized battery capacity C_{cap}, the self-discharge resistor R_{sd} and the current source I_{bat}. Here C_{cap} must be selected in such a way that the voltage at the capacitor corresponds to the battery voltage depending on its SOC. For example, 0 V at 0% SOC and 1 V at 100% SOC can be assumed. [28]

Finally, the parametrisation of such an equivalent circuit diagram shall be

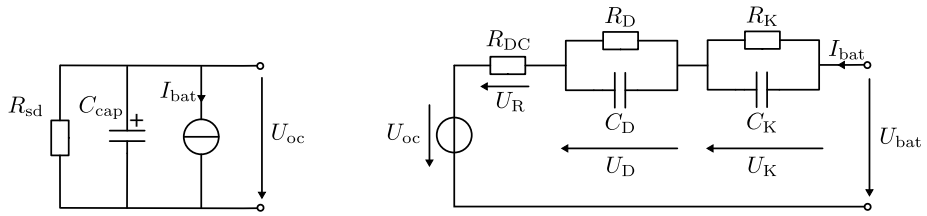

Figure 2.7: Full equivalent electronic circuit diagram of a LIC.

considered. While R_{sd} (see [32]) and C_{cap} (see Chapter 2.5.1) are determined by measurement, further parameters can be calculated from the step response of the battery cell according to [27] and [33]. In Figure 2.7 the elements are renamed accordingly. U_{bat} and I_{bat} are the terminal voltage and the current, U_{oc} is the OCV, R_{DC} is the constant part of the internal resistance (connectors, electrodes, electrolyte), R_D and C_D describe the effects on the surface of the electrodes (double layer capacitance), R_K and C_K describe the diffusion processes in the electrolyte. The electrical behaviour of the circuit can be described with the following equations:

$$U_{bat} = U_{oc} - I_{bat}(t) * R_{DC} - U_D(t) - U_K(t) \tag{2.6}$$

$U_D(t)$ and $U_K(t)$ correspond to the differential equations:

$$U_D(t) = I_{bat} * R_D - \frac{dU_D(t)}{dt} * C_D * R_D \tag{2.7}$$

$$U_K(t) = I_{bat} * R_K - \frac{dU_K(t)}{dt} * C_K * R_K \tag{2.8}$$

The internal resistance of the cell is calculated from the abrupt voltage change when the load is switched on, where $U_{bat}(t_1, I_{bat} = 0\ A)$ is the voltage right before and $U_{bat}(t_1,\ I_{bat} = 1C)$ is the voltage right after switching on the current:

$$R_{DC} = \frac{U_{bat}(t_1, I_{bat} = 0\ \text{A}) - U_{bat}(t_1,\ I_{bat} = 1\text{C})}{I_{bat}} \tag{2.9}$$

To determine the two RC elements, the voltage curve from Figure 2.6, between the points $t_1 - t_2$ (without initial voltage drop) and $t_2 - t_3$ is considered in two separate sections. According to [27, 33], to define the time range for

determining the first RC element ($R_\mathrm{D},\ C_\mathrm{D}$), the first tenth of the step response should be considered and for the second RC element ($R_\mathrm{K},\ C_\mathrm{K}$) the remaining duration of the pulse. The time constants τ_D and τ_K can be estimated in these two sections. The remaining parameters can then be calculated to finish the model parametrisation:

$$R_\mathrm{D} = \frac{U_\mathrm{D}(t_1,\ I_\mathrm{bat} = 1\mathrm{C})}{I_\mathrm{bat}(t_1)}\ ,\quad R_\mathrm{K} = \frac{U_\mathrm{K}(t_2,\ I_\mathrm{bat} = 1\mathrm{C})}{I_\mathrm{bat}(t_2)} \tag{2.10}$$

$$C_\mathrm{D} = \frac{\tau_\mathrm{D}}{R_\mathrm{D}}\ ,\quad C_\mathrm{K} = \frac{\tau_\mathrm{K}}{R_\mathrm{K}} \tag{2.11}$$

2.4.2 Parametrisation with Impedance Spectroscopy

Impedance spectroscopy is another possibility for parametrising an equivalent circuit diagram. With impedance spectroscopy, the Alternating Current (AC) resistance is determined as a function of frequency. If this is used to characterize LIBs, it is called EIS. It depicts the complex internal resistance of the cell and thus also describes the internal electrochemical processes [17]. For this purpose, in the EIS, a current signal (galvanostatic) or a voltage

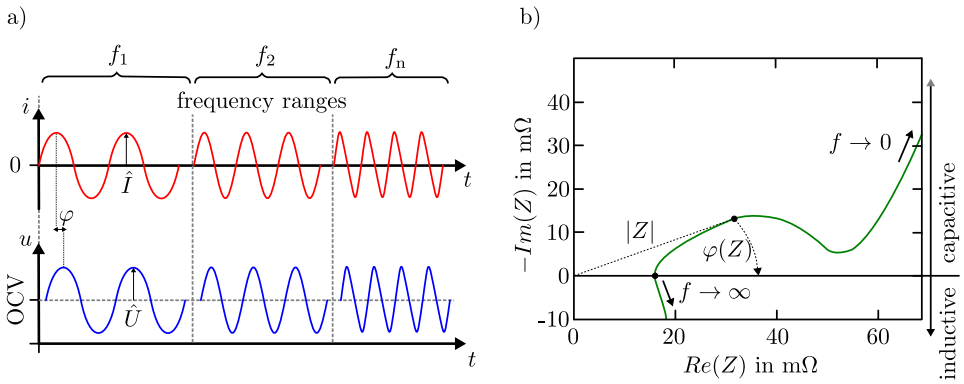

Figure 2.8: a) Voltage and current signal during Electrochemical Impedance Spectroscopy (EIS) measurement with frequency f
b) Nyquist plot of a impedance spectrum of a HP-LFP1 cell at 90% SOC and $T = 15°\mathrm{C}$, based on [25, 34].

signal (potentiostatic) is applied and voltage/current response is measured, the impedance can be determined by evaluating the amplitude and phase offset [35]. In order to obtain an impedance spectrum over the entire relevant frequency range, the excitation is carried out at different frequencies to be defined (see Figure 2.8).

With regard to investigations on LIBs, the galvanostatic measuring method is to be used, since the SOC of the cell is not changed during the measurement [36]. For evaluation, the impedance curve is plotted in a Nyquist plot, whereby the negative imaginary part of the resistance is plotted over the real part. The impedance curve of LICs shows a characteristic behaviour [35].

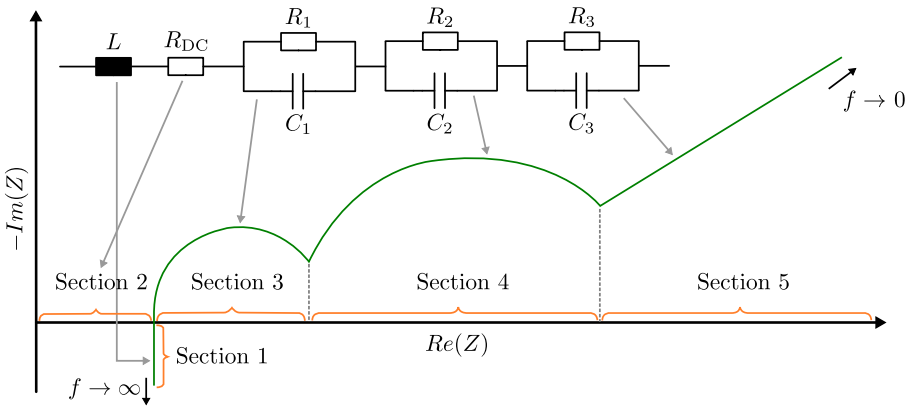

Figure 2.9: Ideal impedance spectrum of a LIC with equivalent circuit diagram, based on [35, 37].

The sectors shown in Figure 2.9 can be described as follows: [35]

- Section 1: At high frequencies metallic elements in the cells and connecting wires show inductive behaviour in the spectrum caused by their inductive reactances.
- Section 2: Sum of the ohmic resistances of current collectors, active material, electrolyte and separator at the intersection with the real axis.
- Section 3: First semi-circle associated typically with the SEI, which is formed during cycle ageing on the surface of the anode.
- Section 4: The double layer capacity and charge transfer resistance at the electrodes represent the second semi-circle.

- Section 5: At low frequencies, diffusion processes occur in the active material of the electrodes.

To quantify the processes measured by EIS and to determine resistances and time constants, the impedance can be described with an equivalent circuit diagram model [34]. Figure 2.10 shows the impedances of different elements of the equivalent circuit diagrams:

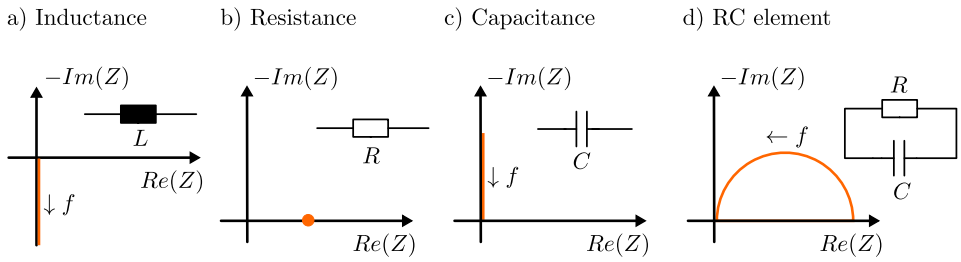

Figure 2.10: Impedance curves of various standard elements for building battery models.

The total impedance of the electrical equivalent circuit diagram Figure 2.9 can be mathematically described as follows:

$$\underline{Z} = j\omega L + R_{\mathrm{DC}} + \frac{1}{1/R_1 + j\omega C_1} + \frac{1}{1/R_2 + j\omega C_2} + \frac{1}{1/R_3 + j\omega C_3} \tag{2.12}$$

At high frequencies, the impedance behaviour is simulated by an ideal inductance L and resistance R_{DC}. R_{DC} corresponds to the internal resistance of the cell. The first semicircle, which describes the behaviour at the SEI layer, is reproduced by the first RC element (R_1; C_1). The second RC element (R_2; C_2) characterizes the behaviour at the double layer capacitance of the electrode/electrolyte interface, which is represented in the Nyquist diagram by the second semicircle. The third RC element (R_3; C_3) describes the diffusion processes of lithium ions within the cell, which are in the range of low frequencies. [37]
The parameters of the model can be determined by numerical optimization methods. The *Gamry Instruments* measuring device used at the FHWS offers its own software for this purpose, the *Gamry Echem Analyst* with integrated model editor. This allows to create own electrical equivalent circuit diagrams and to calculate their parameters similar to [37].

The presented types of modelling with subsequent parametrisation can electrically replicate various battery chemistry with varying degrees of accuracy. The determination of the voltage U_{oc} and the ageing factors necessary for the modelling is also possible by means of a previously measured OCV curve and further measurement results in battery operation [38]. The determination of the OCV curve is explained in the next chapter. Hybrid models are also used in the literature as a combination of different modelling variants for the dynamic control of U_{oc} [39]. In [40] different modelling approaches are explained in a comprehensive review.

2.5 Determination of Battery Parameters

The measurement methods for determining battery parameters are diverse. In this section the parameter determinations that are important for this work will be explained. Not all battery parameters can be measured directly, the SOH and SOC of a battery are usually estimated.

2.5.1 Measurement of Capacity and Internal Resistance.

According to the literature, the capacity of LIBs is generally determined by discharge at a Constant Current (CC) after a complete charge consisting CC and Constant Voltage (CV) phase. The current intensity during discharge, the cut-off (EOD) voltage and the charging procedure by the cell manufacturer are given in the data sheet [25]. The actual capacity determination is done by integrating the discharge current, the so-called *Coulomb Counting* via Equation 2.1. The smaller the current, the more precise the capacity determination. A higher current intensity causes higher losses and thus an earlier termination of the discharge, because the EOD voltage is reached earlier. Thus a resistance increase can be mistakenly interpreted as a loss of capacity [34]. An example of a capacity measurement can be seen in Figure 2.11.

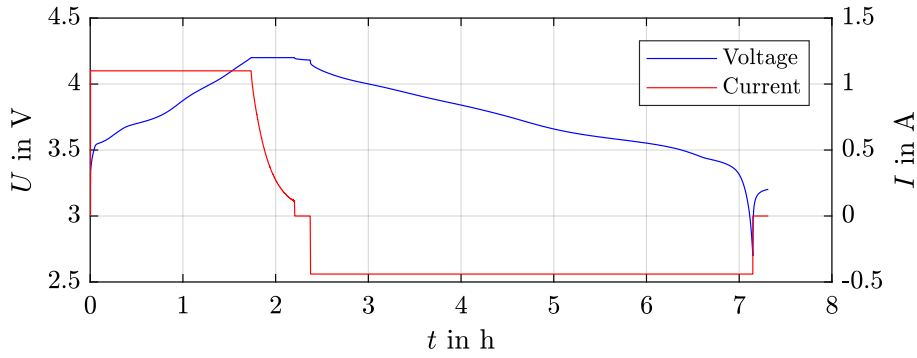

Figure 2.11: Capacity measurement with the example of a Samsung ICR18650-26F cell at $T = 25°C$ and a current of $I_{bat} = 0.2C$.

The internal resistance R_{DC} of a battery cell can be determined using a current pulse method, which is used for example in ISO standard 12405 [41] and in [42]. By this kind of measurement the measured value is also called pulse resistance. The calculation is based on the voltage difference due to

the current pulse, the value of the current pulse and a defined period of time from the moment of switching on to the moment of measurement. The formula for calculating the R_{DC} using Figure 2.12 is:

$$R_{\mathrm{DC}}(\Delta t) = \frac{U_0 - U_{10}}{I_{\mathrm{bat}}} \tag{2.13}$$

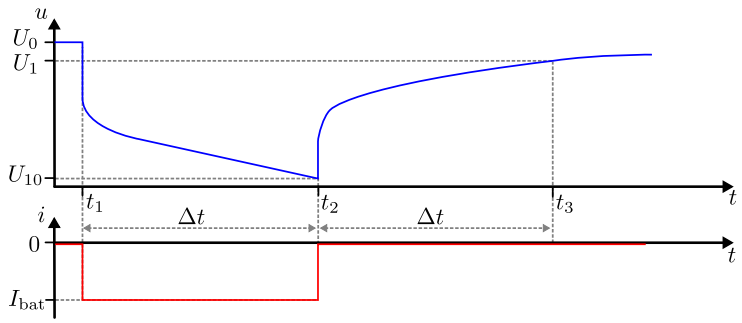

Figure 2.12: R_{DC} measurement with current pulse method.

According to Gantenbein (2019), the SOC of the cell changes during a pulse in the measurement, depending on the current intensity and the pulse duration. Since the OCV also changes as a result, the difference in cell voltages at the end and beginning of a pulse does not only include the losses or the internal cell resistance. If the pulses are sufficiently short or the currents are low and depending on the SOC under consideration, their change can be neglected. If the change is too large, the problem can be counteracted by calculating the internal resistance from the relaxation phase, during which no change in the SOC occurs and the cell is in a stationary state. [34]

The R_{DC} is then calculated in the same way as equation 2.13 with:

$$R_{\mathrm{DC}}(\Delta t) = \frac{U_1 - U_{10}}{I_{\mathrm{bat}}} \tag{2.14}$$

2.5.2 Estimation of SOC and SOH

For estimating the SOC and SOH, there are a variety of known methods in the literature, but not all of them are applicable to LIBs. A selection of the applicable methods can be summarized as follows: [43, 44]

Technique	**Field of Application**	**Advantages**	**Disadvantages**
Discharge test	Used for capacity determination at BOL.	Easy and accurate, independent of SOH	Offline, time intensive, modifies the battery state, waste of energy
Ah-Counting (Coulomb-Counting)	most applications (consumer, EV)	Online, easy to implement, accurate if enough re-calibration points	Dependent on the initial SOC, not suitable in EVs with frequent charging/discharging profiles
Open Circuit Voltage (OCV) measurement	Suitable for all battery types	Online, cheap	Low dynamic, needs the battery to be in the resting mode for a long time
Impedance Spectroscopy	Suitable for all battery types	Gives information about SOH and internal conditions.	Temperature sensitive, cost intensive
Kalman filter	Suitable for all battery types	Online, Dynamic	Large computing capacity, needs suitable battery model, problem of determining initial parameters

Table 2.2: SOC and SOH estimation methods.

In this thesis the methods of Coulomb-Counting and SOC determination using the OCV curve are selected as suitable methods. According to [43] Coulomb-Counting is the most frequently used method and according to [45] OCV curves are often used for further analyses in battery systems, they prove to be a good indicator for the SOC of LIBs according to [46]. Furthermore, both methods can be performed online during battery operation (cycle operation with resting times) and are therefore well suited for later use in a BMS. In addition, both methods can be used in combination because the OCV-SOC technique is able to correct errors in dynamic processes such as Coulomb-Counting [46].
Discharge test and Coulomb-Counting determine the SOC using the known Equations 2.1 and 2.3. For a SOC determination based on the OCV curve, the curve must first be measured. Besides a variety of possibilities in [47], the literature offers two main methods:

- Relaxation measurements (Coulometric titration) [26, 25, 48]
  In stationary measurement, the fully charged battery is discharged step by step and after each partial discharge the voltage is waited to relax. The voltage obtained in this way is the OCV for the set SOC. The OCV characteristic curve for the discharge $OCV^{-}(SOC)$ is obtained for several interpolation points. This process can also be reversed: if the battery is subsequently recharged in partial charges, the OCV characteristic $OCV^{+}(SOC)$ is recorded for the charging process. The two open-circuit characteristics do not necessarily lie on top of each other, which is called hysteresis. By extrapolating the measured rest points with an exponential function, the OCV in the steady state can be estimated. The test duration can be shortened accordingly by reducing the number of interpolation points and waiting pauses. Good results can be obtained from pause times of about 1 hour. Only in the range of low SOC (<10%) it takes a long time until a state of equilibrium is reached. The duration of the pulses depends on the amount of charge within the battery cell and must be calculated in advance. For example, one pulse can correspond to a discharge of 1% SOC. An example measurement is performed in Figure 2.13.

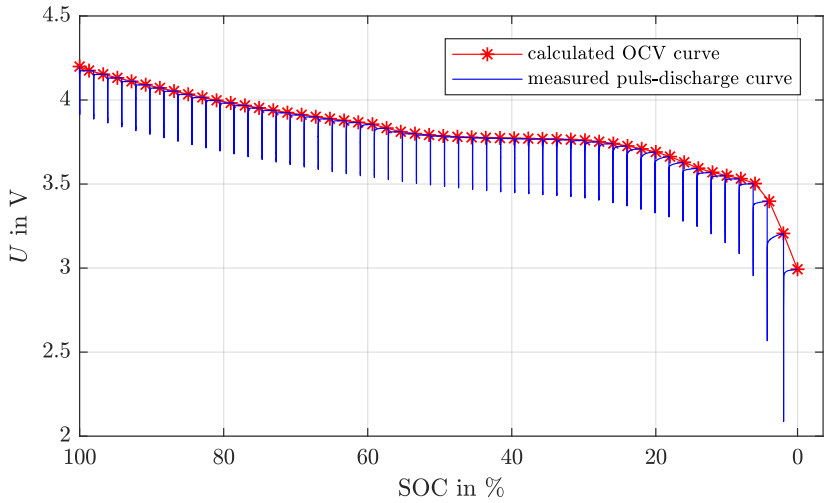

Figure 2.13: Example measurement of a $OCV^{-}(SOC)$ curve with coulometric titration. Cell-type: ICR18650-26F, pulse current: $I_{bat} = 1C$, pulse duration: 36s (2% SOC), $T = 25°C$.

- CC measurement (Chronopotentiometry) [26, 25, 49, 50]
  In CC measurement, the cell is charged or discharged with a low, constant current. Once the EOD voltage has been reached, the direction of the current can be reversed and a cyclical process is obtained. By integrating the current, the cell voltage can be plotted either over the charge removed, or normalized over the SOC. In contrast to the relaxation measurement, the terminal voltage differs from the OCV due to polarization effects and influences from the internal resistance. If the current is chosen sufficiently small, these influences can be neglected. In the literature C rates between C/10 and C/40 are recommended for chronopoteniometry. This is because at higher currents the internal resistance has a significant influence on the voltage characteristic curve. At lower currents, this influence decreases at the expense of time. Chemical reactions that occur when lithium ions are deposited (plating) on the electrodes and lead to distortions of the voltage characteristic curve, do no longer take place. An example measurement is performed in Figure 2.14.

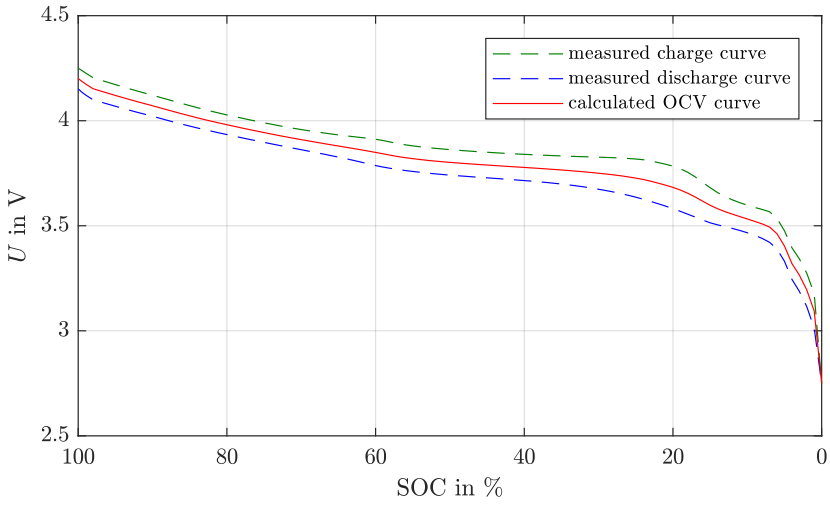

Figure 2.14: Example measurement of a OCV(SOC) curve with chronopotentiometry. Cell-type: ICR18650-26F, current: $I_{bat} = 0.1\text{C}$, $T = 25°\text{C}$

The SOH can be determined by impedance spectroscopy as shown in Table 2.2. It is also possible to estimate it from the internal resistance of the battery [51], to analyse it from the voltage curves during operation [52], or to determine it from a Kalman application together with the SOC [53]. In this PhD thesis the SOH calculation with Equation 2.5 in the context of a complete discharge is used. Based on [54], the determination of the SOH by Coulomb-Counting is a well used technique, similar to the SOC determination. Due to intelligent algorithms, as performed in [55], this determination type is used in many applications.

2.6 Parameter Variation and its Consequences

According to Lelie et al., the SOC of several individual cells in a serial connection can have different values at a certain point in time for various reasons. Figure 2.15 shows the possible causes that can lead to inhomogeneities between the individual cells in a battery pack. The reasons for the inhomogeneities are on the one hand production-related differences and on the other hand different operating and environmental conditions, e.g. temperature. These causes can lead to different initial conditions, different ageing and therefore different self-discharge rates, which then result in different SOC, capacity and resistance values. [56]

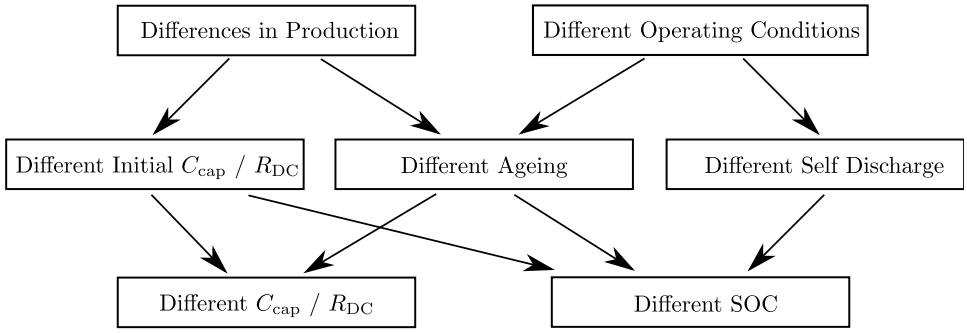

Figure 2.15: Possible causes of inhomogeneities in battery packs, based on [56].

Within a battery pack, an unbalanced ageing behaviour between serial or parallel connected cells is often observed [57]. Different thermal influences cannot always be observed as the cause, or more severely aged cells cannot always be assigned to the local thermal hotspots of a battery, so a random and unavoidable type of parameter variation within battery packs can be assumed [58]. Furthermore it is shown in [59] that the variance in the self-discharge rate already mentioned above is one of the main issues of parameter variation.
Based on Baumhoefer et al., even in mass production lines for LIBs there are deviations in material properties and process parameters that lead to different behaviour of the individual cells. From the base materials (such as the particle size distribution of the active materials) to process parameters during production (such as the layer thicknesses or drying times) to the forming process and storage times, everything contributes to variations

in the properties of the cells. Modern process control and quality assurance techniques can help to reduce the uncertainties, but due to the complex dependencies some uncertainties will remain. Figure 2.16 shows results from an ageing test of 48 identical cells from a common mass production line. During cyclic ageing the capacity decrease was investigated. The results show how large the differences in ageing identical cells can be. [42]

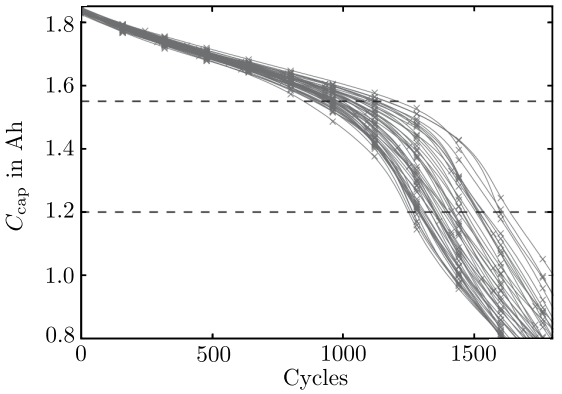

Figure 2.16: Results from an cyclic ageing test of 48 identical cells from a common mass production line, based on [42]. Cell-type: Sanyo/Panasonic UR18650E, Test-cycle: partial cycles between 20% and 80% SOC, $T = 25°C$

Without a BMS, several problems threaten to occur according to Andrea (2010). Basically all cells in a battery should have the same voltage within a series connection. However, if the parameters of the cells deviate from each other, imbalances are possible. The larger the number of cells connected in series, the greater the probability of unequal voltages, regardless of the battery chemistry. Basic scenarios are shown in Figure 2.17 using the example of 4 cells connected in series. [3]
Illustration a) shows a four-cell LIB that is charged up to 16.8 V. When the cells are balanced and perfectly charged, the total voltage is evenly distributed to 4.2 V per cell. In practice, Illustration b), the cells will be unbalanced and one cell will be fully charged first, and in the worst case even overcharged. In this example, the second cell will be overcharged to 6.3 V, while the others will be around 3.5 V. Despite the fact that the total voltage is fully charged at 16.8 V, three of the cells in this battery are not fully charged, and one of the cells is in danger of being irreversibly damaged.

It is therefore essential that a BMS monitors such a battery, primarily to prevent a cell from overcharging.
In illustration c) the same battery is discharged to 12.0 V. When the cells are perfectly balanced, the total voltage is evenly distributed to 3.0 V per cell, which is set as EOD voltage in this example. In practice, Figure d), the cells will be asymmetrical, and one of them will first be fully discharged and in the worst case subjected to a deep discharge. If their voltage drops below a certain level, depending on the chemistry, irreversible damage can occur. In this example, one cell is discharged to 1.5 V, while the others have about 3.5 V. Despite the fact that the total voltage is 12 V, three of the cells in this battery are not fully discharged and one of its cells is under a certain risk to be damaged. Therefore, it is important that a BMS monitors such a battery to prevent a cell from being deeply discharged and damaged.

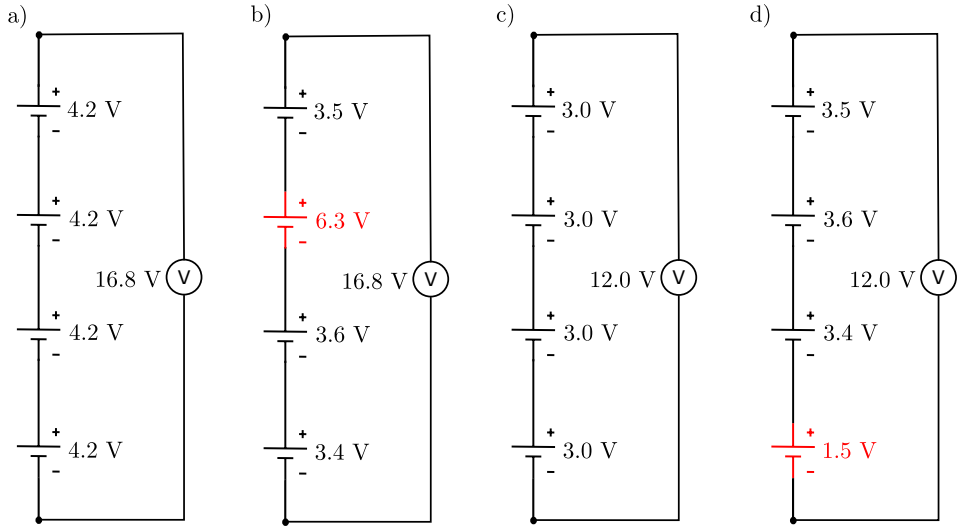

Figure 2.17: Voltage distributions in series connected cells at EOC and EOD, based on [3].
a) Equally distributed voltages at EOC.
b) Unequally distributed voltages at EOC.
c) Equally distributed voltages at EOD.
d) Unequally distributed voltages at EOD.

Furthermore, [3] shows that there are different scenarios to be considered in relation to the SOC of the cells, which allow conclusions about the consequences of the parameter variation. First of all, it is decisive how large the deviation of the self-discharge rate between the cells is. This determines

how far apart the cells are over time. Figure 2.18 shows the effects of the self-discharge rate on the SOC of the cells. In reality, all batteries behave as shown in illustration d). The cells are not ideally balanced and also have different self-discharge rates. As a result, the battery becomes more and more out of balance with increasing time. Once the battery is balanced, it behaves as shown in figure c), and loses its balanced state over time due to the different self-discharge rates.

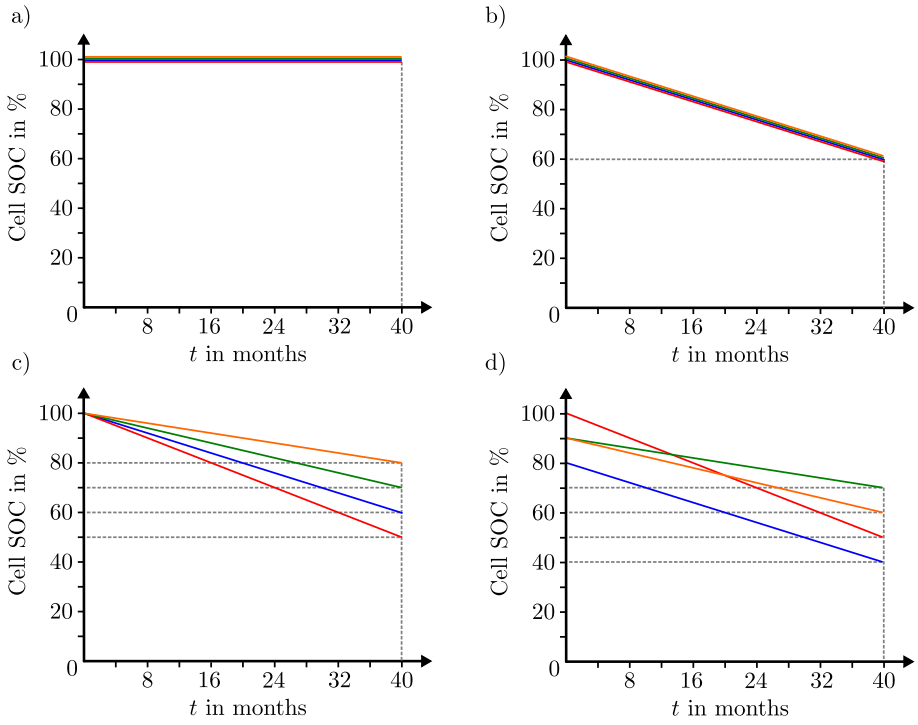

Figure 2.18: Cell SOC depending on different self discharge rates, based on [3].
a) Ideal battery without self discharge. All cells remain constant at 100% SOC.
b) Battery made of identical cells. Cell SOC stays equal during self discharge.
c) Real battery with different self discharge rates becomes unbalanced.
d) Real battery with unbalanced state at the beginning becomes even more unbalanced.

Finally, it is important to consider the effects of different SOCs of the cells on the SOC of the whole battery. During the charging process, the ability of a battery to absorb charge is limited by the cell that is fully charged first. During discharge, the ability of that battery to deliver charge is limited by the cell that is first to be fully discharged. These two points determine the battery capacity. Figure 2.19 shows different scenarios how differences in the Cell-SOC affect the Battery-SOC. In reality, all batteries without BMS behave as shown in Figure 2.19 f). They are not fully balanced and have different parameters such as capacity and internal resistance. The usable capacity of the entire battery is thereby in some cases massively restricted. In the worst case, a strong imbalance in the Cell-SOCs can lead to a completely unusable battery with an effective capacity of 0 Ah, limited by only one single cell.

As a final conclusion, according to [58] it is of great importance that an existing BMS recognizes LICs with deviating parameters and effectively compensates the resulting SOC differences in order to ensure efficient and safe operation of a battery pack.

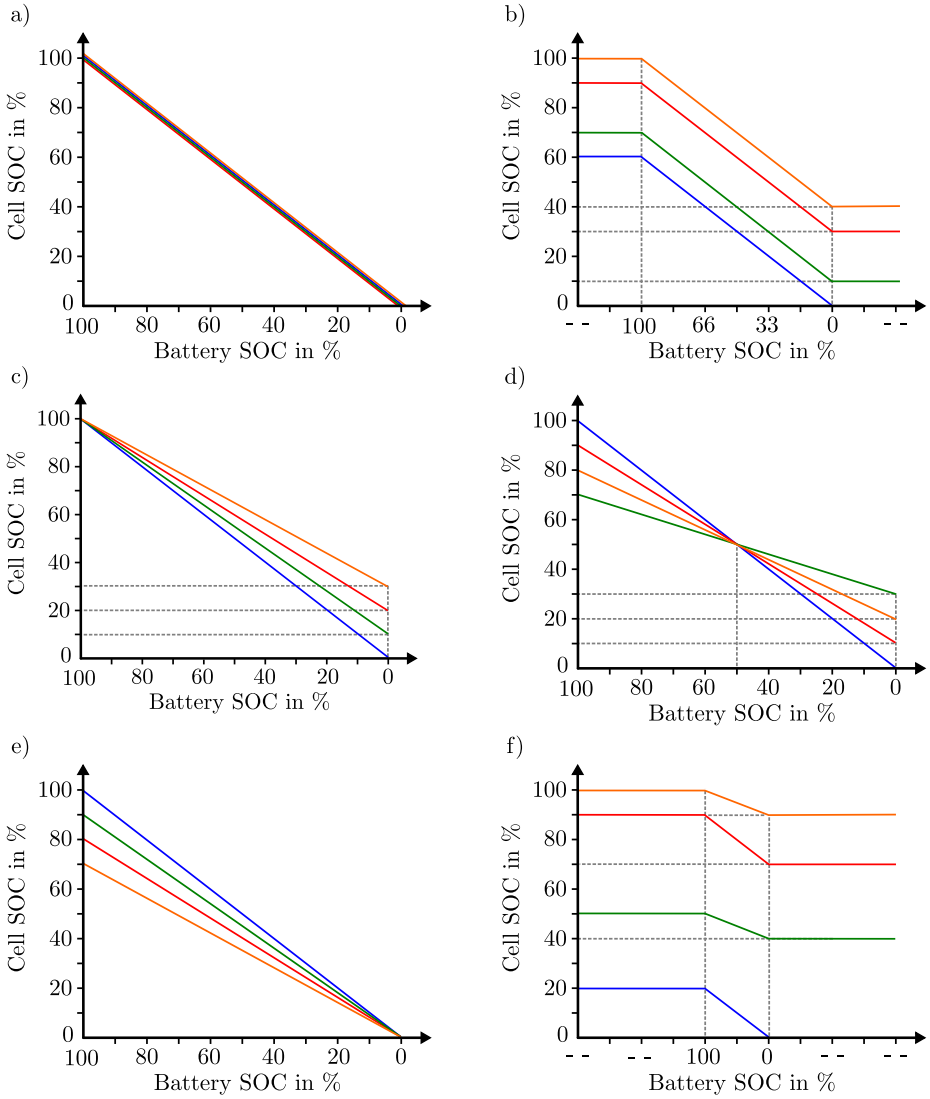

Figure 2.19: Battery SOC depending on different Cell SOCs, based on [3]. Note: The x-axis shows the usable SOC range, deviates between the subplots and is therefore not fully comparable.
a) SOC levels in an ideal, balanced battery. (no self discharge)
b) SOC levels in an ideal, unbalanced battery. Battery capacity is restricted.
c) SOC levels in a real battery balanced at 100% SOC.
d) SOC levels in a real battery balanced at 50% SOC.
e) SOC levels in a real battery balanced at 0% SOC.
f) SOC levels in a real battery, serverly unbalanced. Battery capacity is heavily restricted.

Chapter 3

Battery Management Systems

In the literature, the widely accepted definition is that a BMS is any system that manages the battery. The system may include electronic systems, mechanical systems, or any other device and technology. The connected battery may be a single cell, battery module or battery pack, it may be rechargeable or non-rechargeable. The system can manage the battery by monitoring the battery, estimating the battery condition, protecting the battery, reporting the data, balancing the battery, etc. The BMS in EVs consists of different types of sensors, actuators and controllers that have different algorithms and signal lines. [4]

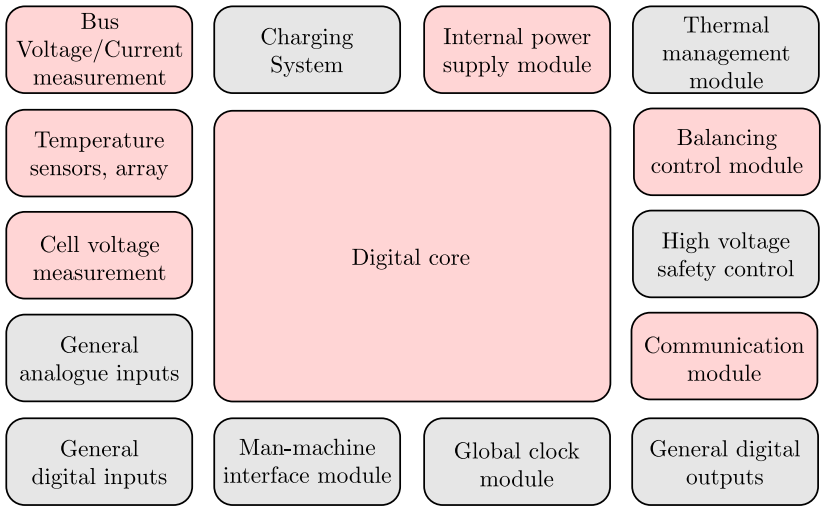

Figure 3.1: Basic framework of software and hardware of BMS in modern EVs, based on [4]. Modules relevant to this thesis are marked in red.

The three main tasks of a BMS are: [60]

1. Protecting the cells and battery pack from damage.
2. Extend the service life of the battery.
3. Maintaining the batteries in a condition in which they can meet the requirements of their application.

In modern EVs, however, the functional scope of a BMS goes far beyond its main tasks. In detail, a BMS uses the following functions to achieve its tasks: [60]

- **Cell Protection:** Protecting the battery from operating conditions outside the cell parameters is essential for all BMS applications. In practice, the BMS must provide complete protection of the cells, covering every conceivable eventuality. Operating a battery outside its specified design limits inevitably leads to battery failure and often to consequential damage, for example, due to fire hazard.
- **Charge Control:** Control over the charging device is an essential feature of the BMS. According to [60] improper charging damages more batteries than any other cause.
- **Demand Management:** The demand management refers to the application in which the battery is used, although it is not directly related to the operation of the battery itself. The aim is to minimize the battery's own consumption of energy, as well as the application's consumption, by integrating energy-saving techniques into the BMS and circuitry of the application.
- **SOC Determination:** Almost all applications request information about the SOC of the battery or the individual cells within the battery. This can simply be used to give the user an indication of the capacity remaining in the battery, or it may be necessary in a control loop, for example to ensure optimum control of the charging process or to balance the charge of individual cells.
- **SOH Determination:** The SOH provides information about the ageing condition of the battery. By determining the SOH, the BMS provides information about whether the battery is still usable for its application or whether it needs to be replaced.
- **Cell Balancing:** In series connection of several cells, small differences between the cells due to manufacturing tolerances or operating conditions tend to increase with each charge or discharge cycle. Weaker

cells will be overstressed during the battery use, causing them to become even weaker until they eventually fail and can cause premature battery failure. Balancing single cells is one way of supporting weaker cells. This can extend the life of the entire battery.

- **History - (Log Book Function):** The monitoring and storage of past measurement data is another possible function of the BMS. This is necessary to estimate the SOH value of the battery. For example, a battery history can also be used to detect incorrect use afterwards. Parameters such as number of cycles, maximum and minimum voltages and temperatures, and maximum charge and discharge currents are recorded.
- **Authentication and Identification:** In the BMS, manufacturer information can be stored, such as the type designation of the manufacturer and the cell chemistry. In case of an error, the presence of batch or serial numbers and the date of manufacture simplify traceability.
- **Communications:** Most BMS systems include communication between the battery and the charger or other connected test equipment. Connections to other systems linked to the battery to monitor its condition or history are also necessary. Communication interfaces are required to allow the user to access the battery to change the BMS control parameters, as well as for diagnostics and testing.

According to Lelie et al., the design of a BMS circuit board is a complex task in which the specific requirements of the application, the system context and the properties of the cells used must be taken into account. A list of system requirements can be derived from these considerations. In general, for the main tasks and functional requirements mentioned above, it is generally important that temperature sensing, voltage sensing (individual cells, stack or whole pack) and battery current sensing operate reliably. Also important is the data communication between the BMS Master Module and BMS Slave Modules (which acquire the above mentioned measurement data), as well as the communication of the battery pack with its application (e.g. car, bike, scooter). Finally, there are the requirements for robustness against Electromagnetic Interference (EMI), redundancy of the system with regard to functional safety, optional galvanic isolation of the functional systems, reliable balancing of the cells, low power consumption, size, weight, etc. [56]

Based on [3], BMS systems in the literature can be divided into four basic topologies, as shown in Figure 3.2:

- **Centralized BMS:** In a central BMS, there is a single circuit board that contains both the logic and the balancing circuit. This is connected to the anode of the first cell and the cathode of each cell to measure or balance all cell voltages. This BMS must be designed for a certain number of cells. The advantage of this structure is the cost of the board, as only one BMS has to be designed/manufactured, which is directly specified for a particular accumulator.
- **Distributed BMS:** In a distributed BMS, each cell has its own circuit board and all boards communicate with the controller. A communication bus must therefore be implemented between individual boards and the controller. The advantage of this structure is its modularity.
- **Modular BMS:** This topology, like the distributed BMS, has several modules with balancing circuits that are managed by a controller. However, unlike the distributed BMS which has a balancing module for each cell, the modular BMS consists of balancing modules that are designed for several cells. This topology is used in EVs, for example, in which several individual battery modules are connected together to form a complete battery.
- **Master/Slave BMS:** A Master/Slave BMS is identical in construction to a modular BMS. However, it differs in that there is an additional master board which is exclusively responsible for data processing. Cell voltages are measured by the slave units and transmitted to the BMS master. In EVs, the slave units of each battery module transmit their data to the BMS master, which communicates with other components via the vehicle's internal communication system.

Within a battery system, every cell must be monitored. The number of necessary measuring channels and the complexity of the balancing circuit depending on the structure of the battery, varies greatly. To achieve a certain voltage range of the battery pack, cells must be connected in series, while parallel connections increase the capacity. In today's systems, one possible variant is to connect several cells with low capacity in parallel to modules with higher total capacity, which are then connected in series to increase the voltage. Another variation is to use high capacity cells connected in series. Both variants are the most sensible in terms of BMS complexity. Connecting several strings of cells in parallel (e.g. for special redundancy requirements)

would increase the effort for monitoring the cell voltage, balancing, etc. by a factor of the number of parallel strings. Example: m cells in series are required to achieve the specified voltage and n cells in parallel to provide the required capacity. Case 1: If m cells were connected in series with n cells in parallel, m measurement/balancing channels would be required. Case 2: If n (e.g. 2) strings were connected in parallel with m (e.g. 3) cells in series, m * n (e.g. 6) measurement/balancing channels would be required. [56]

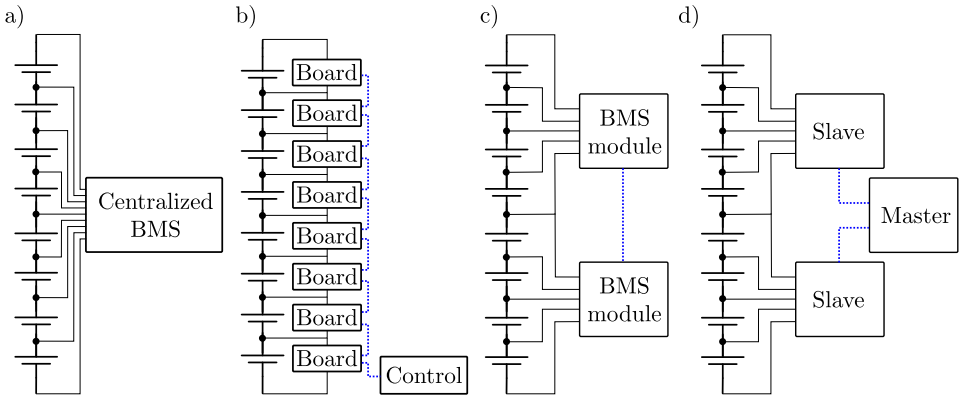

Figure 3.2: Basic BMS topologies. a) Centralized BMS, b) Distributed BMS, c) Modular BMS, d) Master/Slave BMS, based on [3].

In this thesis the focus is on the hardware and software that allows the balancing of the single cells within a battery module. Basically, the marked components shown in Figure 3.1 are necessary for this. In the following, cell balancing topologies known in the literature are presented, balancing methods and the strategies necessary for cell balancing are explained.

3.1 Cell Balancing Topologies

Generally, the literature distinguishes between active and passive cell balancing topologies [6, 61]. According to Ahmad et al. AB was developed to overcome the disadvantages of PB, where capacitors, transformers, converters and inductors are used to transport energy between cells within a battery. Energy is distributed between cells based on their charge quantity to balance all cells without wasting energy through shunt resistors as it appears with PB. The active topology can be used for all cell technologies regardless of their chemical properties. High balancing speed and high efficiency are the main advantages. However, these are associated with high costs and greater complexity. Active topologies are divided into three different types based on the active elements in capacitor-based, transformer/inductor-based and converter-based topologies. An overview of the known topologies is shown in Figure 3.3. [61]

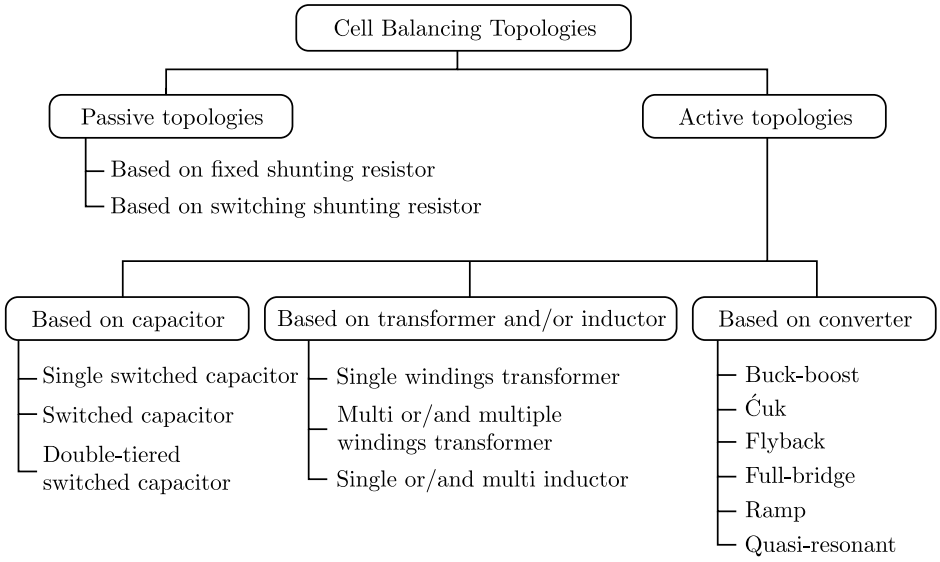

Figure 3.3: Overview of cell balancing topologies, based on [6, 61].

3.1.1 Passive Topologies

The basic principle of PB is the parallel connection of a shunt resistor to each individual cell to discharge the excess energy in the form of heat. The topol-

ogy continuously removes the excess energy until all cell voltages are equal [62]. Little installation space, low cost and simplicity are the advantages of this topology, while the disadvantages are the heat dissipation, energy loss and the long time it takes to reach a balanced state between the cells. Passive cell balancing can be done in two ways: as a fixed shunting resistor and as a switched shunting resistor [61]. The passive topologies are shown in Figure 3.4.

The fixed shunting resistor, was introduced for example in [63]. With this method, the current for all cells is continuously bypassed, and thus energy is permanently dissipated [62]. The resistor is selected to limit the cell voltage of each cell appropriately. This topology can only be used for lead-acid and nickel-based batteries, as these can be brought into overcharge states without damaging the cells. It is characterized by simplicity and low cost, but has a major disadvantage due to the continuous loss of energy as heat [6].

A controlled shunting resistor or switched shunting resistor was presented in [64]. The topology is based on not continuously dissipating the excess energy from the cells, but in a controlled way using switches/relays. Two different methods are known for this. First, in a continuous mode, the topology can control all relays by the same on/off signal. Secondly, in the so-called detection mode, in which the cell voltages are monitored, each resistor can be

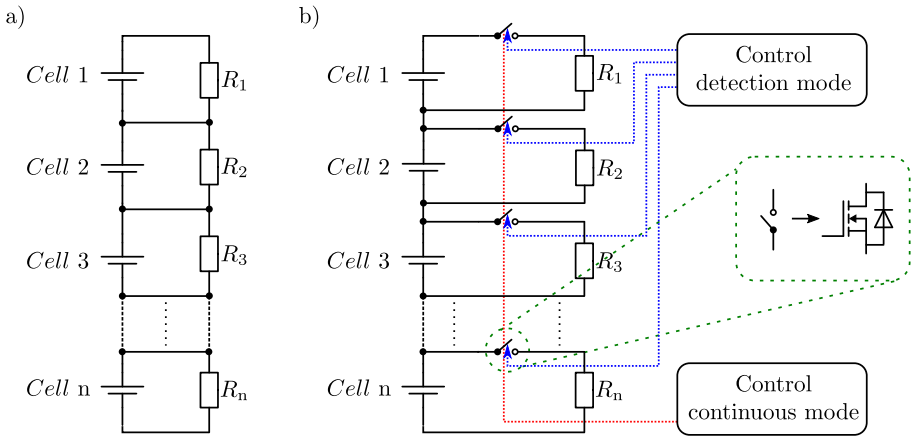

Figure 3.4: Passive cell balancing topologies. a) fixed shunting resistor, b) switched shunting resistor with continuous and detecting mode control, based on [6, 62].

selected and switched individually. After an imbalance has been detected by voltage measurement, the topology decides which resistor should be switched on. Based on [6] this method is more efficient than the fixed shunting resistor topology, simple, reliable and can also be used for LIBs.

3.1.2 Active, Capacitor Based Topologies

Capacitor based cell equalization, also known as "charge shuttling" equalization, uses capacitors as external energy storage devices to distribute the energy between the cells of the pack, thus providing equalization [6]. The main disadvantages are considerable energy losses during capacitor charging and a slow equalization speed. Known topologies are the switched capacitor, the single switched capacitor and the double-tiered switched capacitor [61]. The capacitor based topologies are shown in Figure 3.5.

In the switched-capacitor topology, for example presented in [66], a capacitor is located between each two cells. In the first state each capacitor is connected in parallel to its corresponding upper cell. By connecting the capacitor and the cell in parallel, the capacitor is either charged by the cell, or gives off energy to it. As soon as each capacitor has reached the cell voltage, the state is switched over. In the second state, all capacitors are connected in parallel to their lower cell. Depending on the cell voltage, the

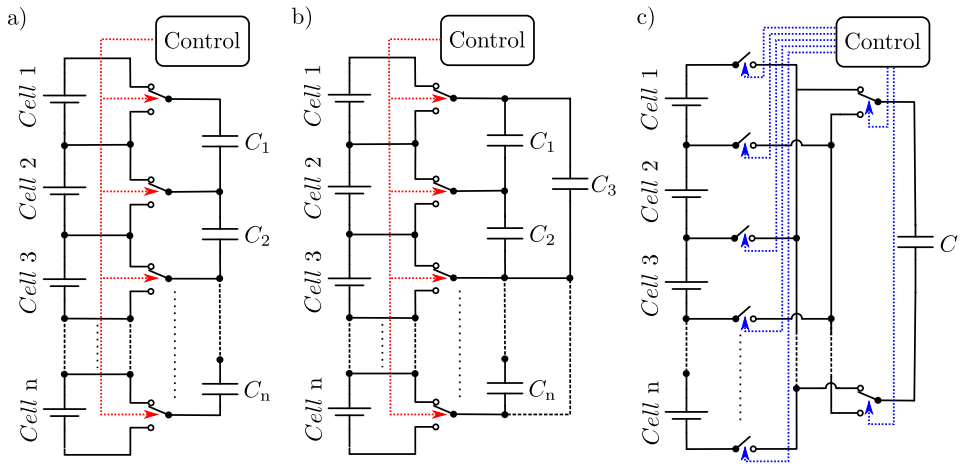

Figure 3.5: Active, capacitor based cell balancing topologies. a) Switched capacitor topology, b) Double tiered switched capacitor topology, c) Single switched capacitor topology, based on [65].

capacitor now transfers energy from the upper cell to the lower cell, or continues to charge itself due to a higher cell voltage of the lower cell. If this process is carried out cyclically, both cells are balanced after some time. According to [62] the main advantages of this method are the efficiency, low complexity and the possibility of low and high power applications. No sensing or closed-loop control are needed. The main disadvantage is the speed, as the lower the voltage difference between adjacent cells is, the lower the balancing current is, and therefore the lower the balancing speed is. The double-tiered switched capacitor topology works in exactly the same way, but the additional capacitor enables a higher balancing current. It was for example introduced in [67] and [68].
The single switched capacitor topology, also called flying capacitor, as it can be derived by its name, has only one single capacitor that can be connected in parallel to each cell within the battery [65]. This topology was introduced in [69] for example. A more advanced control strategy is used, the controller selects the cell with the highest cell voltage and the cell with the lowest cell voltage and compensates the cell charges by cyclically actuating the corresponding switches of the switching matrix [5]. The principle of operation is comparable to the switched capacitor topology.

3.1.3 Active, Transformer/Inductor Based Topologies

Inductors or transformers are used in this topology for balancing by moving energy quickly from one cell pack to another or from cell to cell. However, the high cost of the transformer, magnetic losses and the need to connect a filter capacitor to each cell because of the high frequency are the disadvantages of this topology [61]. Different possibilities of realization are single/multiple-inductors, transformer with single/multiple windings as well as circuits with a single or multiple transformers.

The use of one or more inductors for cell balancing is shown in Figure 3.6. The single inductor balancing system, also called single switched inductor, uses one inductor to transfer energy between the entire module. The control system measures the voltage of the cells and selects two cells to be used for energy transfer. The cell with the highest voltage is connected to the inductor via the switch matrix. When the current in the inductor has reached a certain value, the inductor is switched to the weakest cell. All the energy that is stored in the inductance is used to support the weak cell. As soon as the current in the inductance is zero, the inductor is switched off. The method was for example presented in [70].

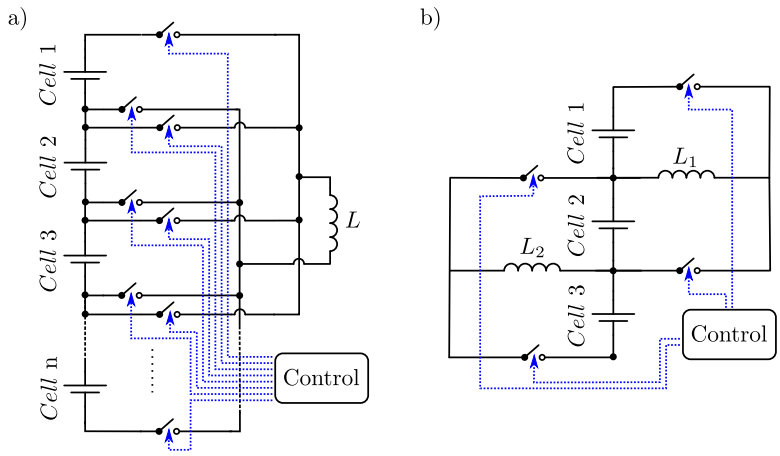

Figure 3.6: Active, inductor based cell balancing topologies. a) Single inductor topology, b) Mulitple inductor topology, based on [65].

The Multiple Switched Inductor balancing system uses $n-1$ inductors to balance n cells and was presented for example in [71]. The controller detects the voltage difference between two adjacent cells and then applies a Pulse-Width Modulation (PWM) with the condition that the higher cell must be switched on first. As a result, when discharging, the average current flow through the lower voltage cell will be lower than that of the high voltage cell [5]. Both topologies are characterized by a fast equalization time. The main disadvantage of multiple switched inductor is the relatively long time required to transfer energy from the first to the last cell, especially in large series connections of cells. Single switched inductor enables a more targeted balancing due to the switching matrix, which is faster for long energy transport paths between two cells [6].

The application of a single windings transformer for cell balancing is shown in Figure 3.7. The topology also called switched transformer was presented for example in [72]. A switched transformer is actually a selectable energy converter. The input of the transformer is connected to the entire battery pack, while the output of the transformer is connected to a series of switches that can be used to select a specific single cell. This topology is actually a pack-to-cell topology, but can also be used in reverse [5]. The controller selects the cell with the lowest voltage and connects this cell to the secondary winding using the switch matrix. Then the switch connects the primary

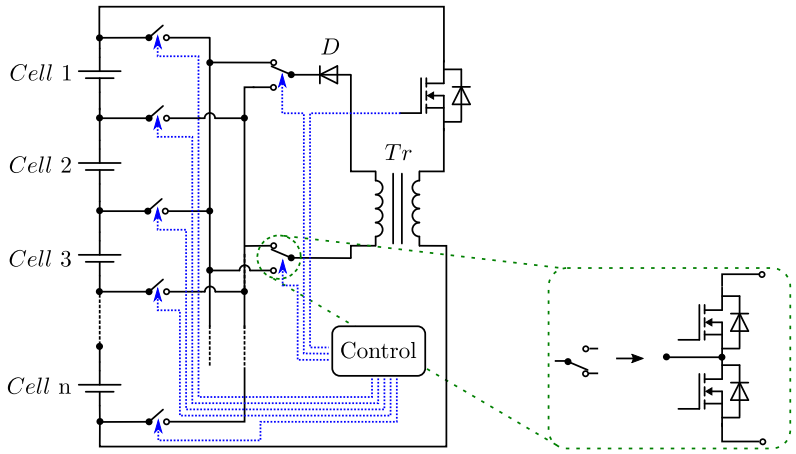

Figure 3.7: Active, single windings transformer cell balancing topology, based on [6, 65]

winding to the entire pack and the current begins to rise in the primary winding. When the current in the winding has reached a certain value, the primary winding is disconnected from the pack and the energy stored in the transformer is used to charge the cell connected to the secondary winding [65].

The balancing topologies of the multiple and/or multi-winding transformer is shown in Figure 3.8. First, the multi-winding transformer, also called shared transformer, which is applied for example in [73], [74] and [75]. Second, the multiple transformer, which is applied for example in [70] and [76]. As its main part, the multi-winding transformer topology uses a shared transformer with a single magnetic core and secondary windings for each cell. This multi-winding transformer must be adapted according to the number of cells, which limits its modularity [5]. The topology has two circuit configurations: Flyback and forward configuration. In the flyback configuration, the switch connected to the primary side is turned on. Part of the energy is thus stored in the transformer. When the switch on the primary side is then switched off, the energy is transferred to the secondary side of the transformer. The secondary winding and thus the battery cell with the lowest reactance has the highest induced current. Due to the galvanic isolation between the individual cells, this circuit ensures a higher safety of the battery pack. In the flyback configuration, the energy exchange is only possible in one direction, from the entire battery into a single cell. In the

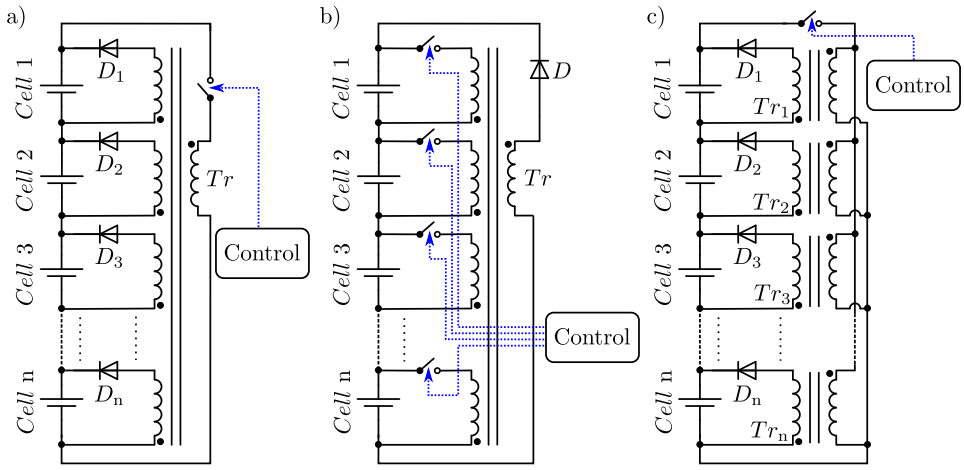

Figure 3.8: Active, multi or/and multiple windings transformer topologies. a) Multiple windings topology in flyback mode, b) Multiple windings topology in forward mode, c) Multiple transformer topology, based on [6, 62, 65].

forward structure, the energy exchange takes place from a single cell to the entire battery. When a voltage difference is detected, the switch connected to the cell with the highest voltage is switched on and the energy is transferred from this cell to other cells via the transformer and the anti-parallel diodes of the switch. The circuit is complex, the cost is high and saturation problems with the transformer have to be avoided [77].
The multiple transformers topology consists of n transformers for n cells. According to the single windings transformer method, the primary winding is connected to all cells of the battery module, the secondary windings are connected to a single cell only [65]. Multiple transformers can be used in the same way as multi-winding transformers by individually coupling the windings with individual magnetic cores instead of coupling them via a shared magnetic core. A central switch connects the primary windings to the whole battery and the current starts to rise. When the current reaches a certain value, the primary windings are disconnected from the entire battery and the energy stored in the transformers is used to charge the cells connected to the secondary windings through the rectifier diodes. Compared to the multi-winding transformers, this method is more suitable for modular design [5]. The modular design can be used to divide the battery pack into groups or modules in which the voltage and/or current load for the circuit components is reduced [6, 77].

3.1.4 Active, Converter Based Topologies

In recent years, interest in converter-based cell balancing has increased due to its attractive features, where it offers complete control of the balancing process. However, the complexity and high costs are still the biggest challenges. The derivation from a standard/modified DC/DC converter has led to the variations for this approach, such as buck-boost, flyback, Ćuk, ramp, full-bridge and quasi-resonant converters [61]. Many of the converter-based topologies are derived from inductor-based circuits and are similar in their functionality [65].

Flyback converters, as for example presented in [78], are used in isolated structures and can be unidirectional or bidirectional. In the unidirectional structure, the energy of a cell with a higher SOC is stored in the transformer when the coupled switch is on and transferred to the pack when it is off. The bidirectional flyback converter in Figure 3.9 a) is more flexible in transferring energy, since the energy can also be transferred from the pack to the cells. Disadvantages are the needed uniformity of the windings and the magnetic losses [77].
The buck/boost converter is similar to the multi-inductor method and requires $n-1$ inductors to transfer energy between n adjacent cells [65]. There are three types of converters for cell balancing in this method also known as buck/boost-shunting. Buck converters can only work unidirectionally, from pack to cell. This means that the energy is transferred from the pack to the weakest cell. Boost converters work in reverse. They draw the excess energy from the strongest cell and push it into the pack. The bidirectional converter or buck-boost converter shown in Figure 3.9 b) was used in [79] for example and can transfer energy in both directions, pack to cell and cell to pack. For balancing, each cell requires its own converter. Therefore the number of converter modules is equal to the number of cells. By using a switch matrix, one converter can be used for several cells (or one cell module). This way a higher modularity of the circuit is achieved and the circuit can be changed easily by removing or adding modules [5, 77].

The topology of ramp converters has the same design as that of multi-winding transformers and represents an improvement of this topology. The ramp converter topology was presented in [80] and requires only one secondary winding for each pair of cells instead of one per cell. During operation, in the first half cycle, the current is used to charge the odd numbered cells with the lowest voltage, while during the other half of the cycle the current is used to charge the even numbered cells at the lowest voltage [5].

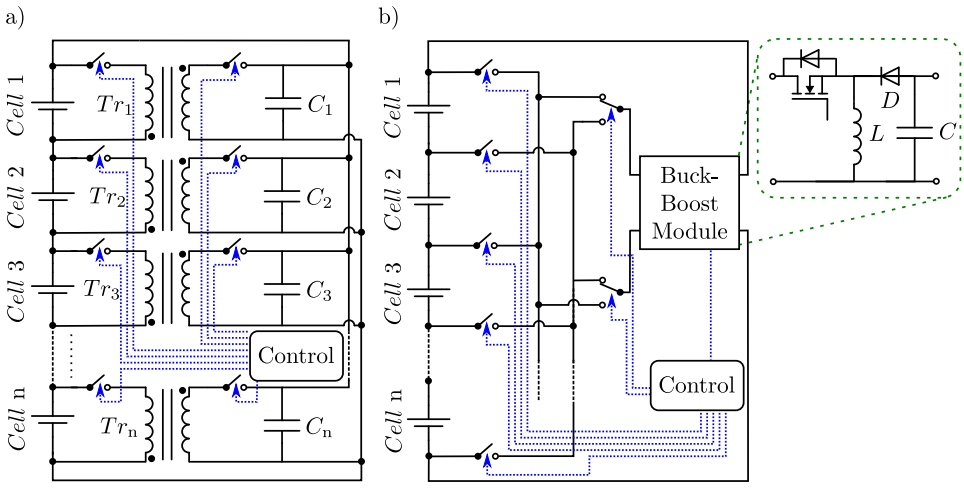

Figure 3.9: Active, converter based topologies, Part I. a) Flyback-converter, b) Buck-Boost-converter, based on [6, 62].

The current rise and fall forms a triangle, so-called "ramp" in each case.
The bidirectional Ćuk-converter can be considered as an individual balancing circuit, and was for example introduced in [81]. As shown in Figure 3.10 a), it consists of two inductors, two switches and a capacitor to balance the minimum amount of cells (two cells). This means that $n-1$ of such circuits are needed to balance the n cells. This is similar to the multiple-inductor topology in Figure 3.6 b). The Ćuk-converter needs the same time for balancing and can also work with large balancing currents, but needs a more complicated control and an accurate measurement system. The disadvantages of this circuit are the higher complexity and the costs due to the large number of components [62].
The quasi-resonant converter was presented for example in [82]. It is a further version of the multiple-inductor method already presented and shown in Figure 3.10 b). Instead of using an intelligent controller to detect and generate a PWM control signal, resonant circuits are used both for power transmission and for driving the MOSFETs. A separate set of resonant circuits is required for each pair of adjacent cells [5]. L_r and C are designed as a resonant tank to provide the zero current switching function for the symmetrical and bi-directional battery equalizer. The main advantage of the resonant converters is that they can reduce the switching losses and thus increase the efficiency of the balancing system. The resonant converters have a complex control, difficult implementation and high converter costs [6].

At last, the full-bridge converter, as presented in [83], can be regarded as a fully controlled energy converter and is shown in Figure 3.10 c). Based on Gallardo-Lozano et al., it can be used in AC/DC mode, which is suitable for the EVs, Plug-In Hybrid Electric Vehicles (PHEVs) or as a DC/DC converter. Both require intelligent control and are superior for modulated battery packs and high power ratings. The main disadvantage of the full-bridge converter is - similar to the other converter topologies - the relatively high cost and complex control. [62]

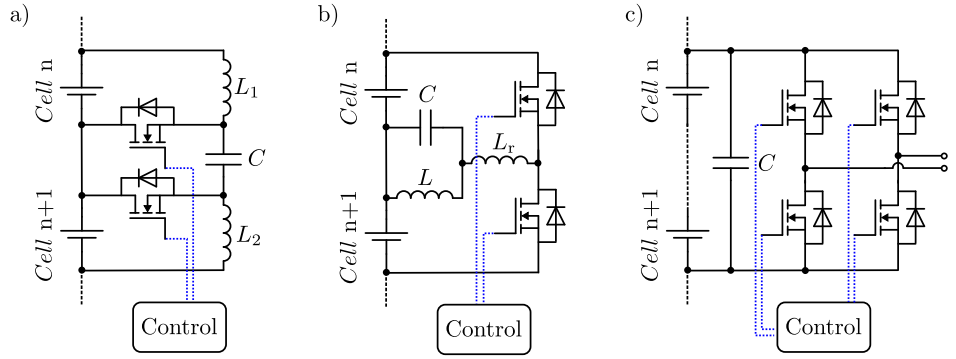

Figure 3.10: Active, converter based topologies, Part II. a) Ćuk-converter, b) Quasi-resonant-converter, c) Full-bridge-converter, based on [6, 62, 65].

3.2 Energy Transport Paths

The presented balancing topologies can be used within different methods which represent different paths for energy transport. According to [82] there are 3 categories for balancing methods, as presented in Figure 3.11:

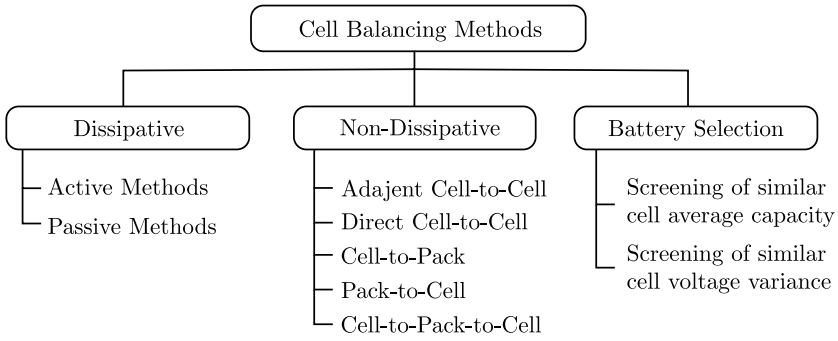

Figure 3.11: Overview of cell balancing methods, based on [56, 82].

The dissipative balancing method, also known as the cell bypass method, uses a dissipative element connected as a shunt to bypass a cell or to draw additional energy from a cell. The dissipative balancing methods can be further divided into two categories, i.e. passive methods (no active control is used for balancing) and active methods (an external circuit with active control is used for balancing). In these methods, cell voltage equalisation is achieved by removing the excess energy from the higher voltage cells. Dissipative balancing is the most cost effective and can be easily modularised and controlled. However, the excess energy is not stored but converted into heat, which leads to energy waste and heat management problems and greatly reduces the available capacity of the battery packs [82]. According to [62], dissipative balancing can be achieved with the topologies fixed shunting resistor and switched-shunting resistor, as presented in Chapter 3.1.1. Optionally, the shunt resistor can be replaced by a shunt transistor.
Non-dissipative balancing methods are realized by AB topologies that use non-dissipative charge-shuttling elements or voltage/current transformers to move energy from one cell to another or from one cell to a pack or from a pack to a cell. The non-dissipative balancing methods can be further divided into five groups according to [82]:

1. **Adjacent Cell-to-Cell Methods:** Charge is transferred between two adjacent cells. In this method, charge is transferred from only one

cell to an adjacent cell. It would take a long time to transfer the charge from the source cell to the target cell, especially if they are located at opposite ends of the pack. The topologies switched capacitor, double tiered switched capacitor, ćuk-converter and quasi-resonant converter are suitable for this purpose.

2. **Direct Cell-to-Cell Methods:** To overcome the disadvantages of the adajent cell-to-cell methods, this method introduces a shared external energy storage. By using a shared energy storage device, such as a capacitor, this method achieves direct charge transport from cell to cell between any two cells in the battery pack. For example, the topologies single capacitor and single inductor topologies are suitable for this purpose.
3. **Cell-to-pack methods:** The charge is transferred from the cell with the highest SOC to the pack. If one cell has a higher voltage than the other cells and furthermore all other cells are balanced at the same voltage level, this method has the best balancing performance. However, if one cell has less voltage than the others while the others are in balance, this is the worst case for the cell to pack method. The topologies suitable for this are single inductor, multiple transformers, switched transformer, multiple windings transformer and converters.
4. **Pack-to-cell methods:** The charge is transferred from the battery pack to cell with lowest SOC in the battery pack. If one cell is less charged than the other cells and furthermore the other cells are balanced at the same voltage level, this method has the best balancing performance. If one cell has a higher voltage than the others while the others are balanced, this is the worst case for this method. The topologies multiple transformers, switched transformer, multiple windings transformer and converters are suitable for this.
5. **Cell-to-pack-to-cell methods:** These method combines cell-to-pack and pack-to-cell equalization. Compared to the other non-dissipative methods, this has a higher balancing speed and higher average efficiency at the expense of control complexity. Topologies that can be designed bidirectionally are suitable for this purpose. For example bidirectional multiple transformers, bidirectional switched transformer, the bidirectional multiple windings transformer and bidirectional converters.

Battery selection, also known as cell matching, in which the battery pack is constructed by selecting suitable cells with similar properties, can be divided into two different screening methods. In the first screening process, cells with similar capacity are selected by discharging at different currents. The second process is used to select the cells from the first process with the similar voltage variance among the pulse discharge/charge currents at different SOC points [84]. Cell matching is not sufficient, because series-connected battery strings do not remain balanced over time [82].

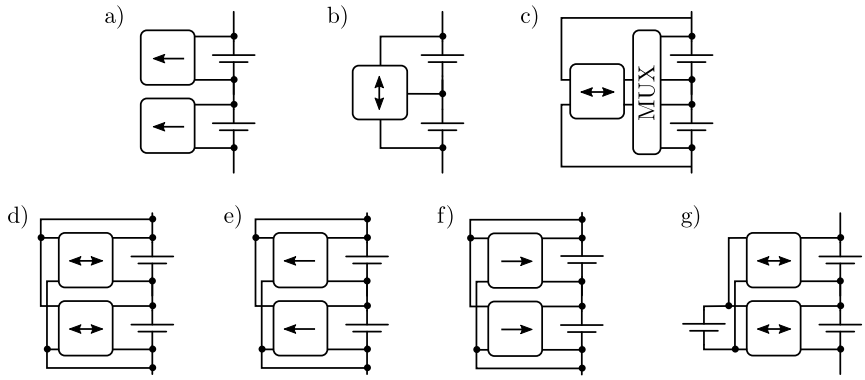

Figure 3.12: Abstracted illustration of energy transport between cells, based on [15]. a) Dissipative Method, b) Cell-to-Cell, c) Cell-to-Pack-to-Cell, d) Cell-to-Pack-to-Cell, e) Cell-to-Pack, f) Pack-to-Cell, g) Cell-to-DC-Bus-to-Cell.

For a simpler overview and to improve the understanding of energy transport between cells which is complex to describe, there are several possibilities of abstraction in the literature, two suitable examples are presented below. Firstly, a schematic representation of the methods is offered in accordance with [15] and [86]. The balancing topologies from Chapter 3.1 are abstracted accordingly. The arrows in the corresponding Figure 3.12 indicate the direction of energy transport. A double arrow symbolizes a bidirectional and a single arrow a unidirectional energy transport. Thus, for the cell-to-cell method b), for example, energy can only be transferred between adjacent cells. The cell-to-pack topology c) is a special case due to the use of the switching matrix in form of a Multiplexer (MUX), in which power transfer between cells and through a single converter is made possible. It is therefore slower than the other balancing topologies at constant converter power.

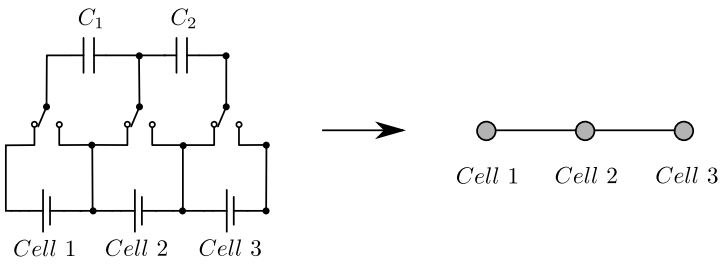

Figure 3.13: Abstract representation of cells and balancing circuit with independence from specific energy storage elements, based on [85].

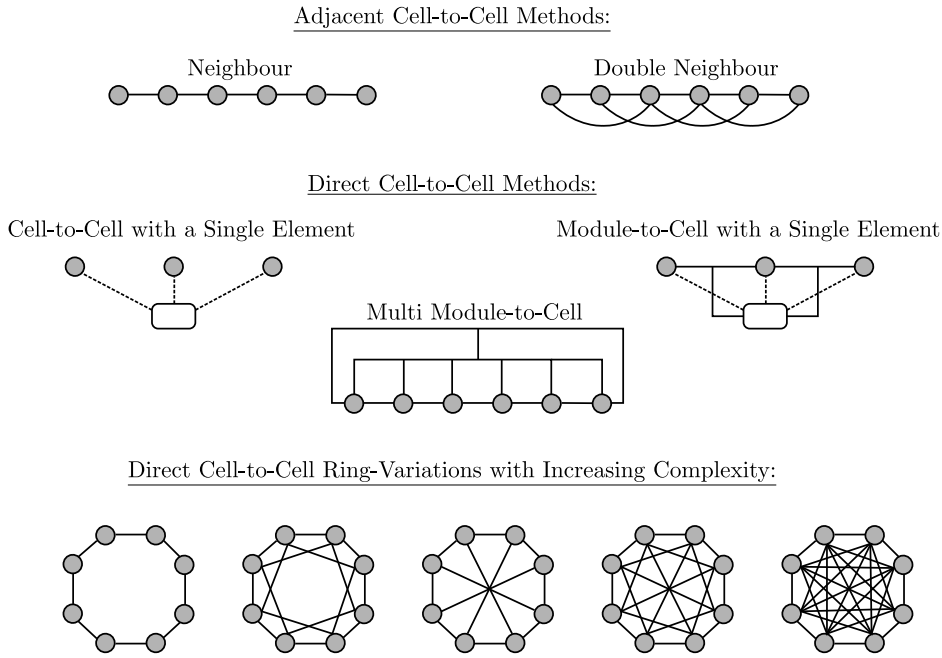

Figure 3.14: Structure overview of abstracted cells and abstracted AB circuits, based on [85].

The cell-to-pack topology d) has a balancing circuit in parallel to each cell, just like the other methods e), f) and g). Method g) is equivalent to the cell-to-pack-to-cell method by using a DC-bus as an energy storage device. The use of a DC-bus was for example presented in [87].
Secondly, in [85] a structural comparison based on the balancing methods

was carried out and the possible energy transport paths between the cells were illustrated. In order to simplify the complexity of a balancing circuits and to symbolize the energy transport between single cells, the cells as well as the transport routes are shown symbolically in Figure 3.13. Some of the presented structures in Figure 3.14 are directly related to the above mentioned adjacent cell-to-cell and direct cell-to-cell methods, others are theoretical possibilities. Especially the ring structures, which realize more and more equal transport paths between the cells in increasing complexity, are worth mentioning as theoretical possibilities.

According to Shang et al. it can be summarized that the non-dissipative balancing methods usually have a higher available battery pack capacity and a higher efficiency than the dissipative balancing methods and cell matching. Nevertheless, a highly efficient battery balancing by matching suitable cells during battery production is necessary to increase the available capacity and lifetime of the battery packs. During operation, dissipative or non-dissipative balancing is required to keep the cells within a uniform operating range over a long period of time. [82]

3.3 Selection of Deviating Cells

There are three known types of balancing strategies/algorithms in the literature to select and balance deviating cells. These include voltage-based balancing, SOC balancing and capacity-based balancing, which is based on the actual remaining capacity of the cells [88].

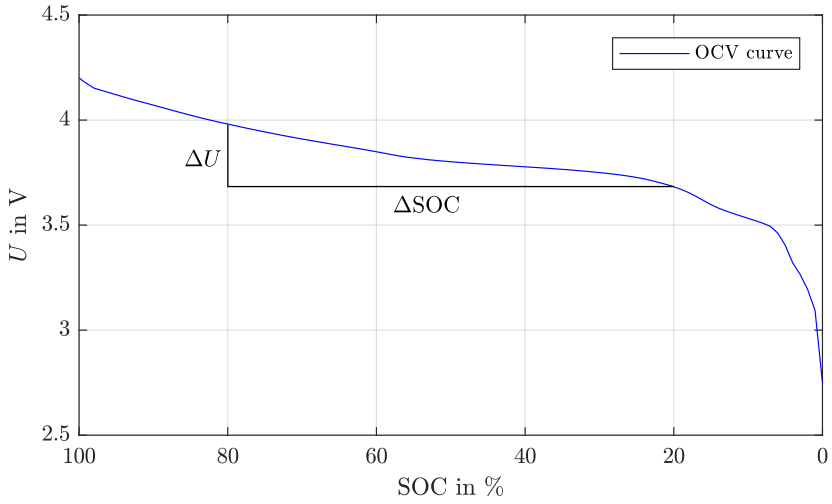

Figure 3.15: Measured OCV-Curve with small $\Delta U/\Delta$SOC ratio in the middle range. Cell-type: ICR18650-26F, current: $I_{bat} = 0.1$C, $T = 25°$C.

Voltage-based balancing is the easiest to realize because of the directly measured cell voltages, but has some disadvantages [88, 89]. It is not suitable for many cell types, including LICs, because the relationship between voltage and charge is not linear. In the middle SOC range the voltage curve is very flat. As shown in Figure 3.15, a large difference in charge can therefore only result in a small difference in voltage [89, 90]. Furthermore, voltage-based balancing, such as in [91], suffers from so-called overbalancing when the cell capacities and internal resistances are different. For example, overbalancing occurs when some cells are charged by the balancer for a while, but later/earlier in the same cycle have to be discharged again. To solve the problem, voltage-based single-point balancing is proposed [92]: When the average cell voltage reaches a certain voltage, the balancer compares the voltages and starts to balance the charge. An example of this is voltage-based balancing of fully discharged or fully charged battery packs, which

ensures that the cells are discharged or charged to the same target voltage [88]. In [93], voltage-based balancing at the end of the charge process is used for cell balancing (so called "top balancing").

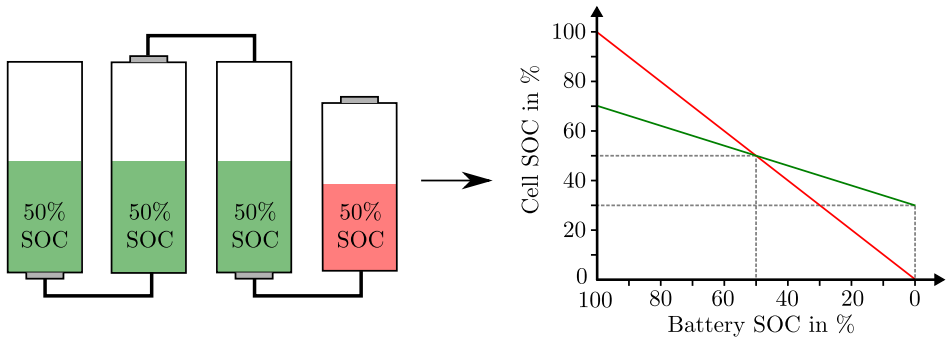

Figure 3.16: Problem with SOC-Balancing of four series connected cells: Different battery charge at same SOC levels leads to restrictions in battery capacity with unequal cells. The different SOH of the cells is symbolized by their height.

The operating principle of SOC based balancing, and thus balancing the average SOC, is to compare the SOC of each cell with the average SOC of the battery pack. A balancing threshold is normally applied to the average SOC to form a balancing tolerance band. If the SOC of a cell is higher than the balancing tolerance band, the cell must be discharged until the SOC falls within the tolerance. On the contrary, if the SOC of a cell is lower than the balancing tolerance band, the cell must be charged until the SOC rises [94]. In SOC based balancing, overbalancing can also occur due to cell capacity variations: The cell with the minimum cell capacity tends to have a higher SOC when the cells are almost fully charged, and it will have a lower SOC when the cells are almost fully discharged. Similar to voltage-based single-point balancing, SOC based single-point balancing is proposed [88]. Another problem is to determine the SOC of each cell at any given time. There are several possibilities to determine the SOC, which are described in Chapter 2.5.2. The simplest way to determine the SOC is to record the OCV curve. However, determining the SOC via the OCV curve has the disadvantage that the battery must remain unloaded for a longer period of time in order to neglect the influence of relaxation. Therefore, no continuous recording is possible [46]. Finally, it must also be mentioned that if the cells have a different SOH or different capacities, the cells do not balance to the

same charge level, but only to the same SOC percentage of each individual cell. This means that each cell can have a SOC of 50% as shown in Figure 3.16 and still not have the same charge. The maximum capacity of the battery can therefore not be used reliably. The SOC balancing is only useful in applications where new cells with the same SOH are used or in applications where the individual cells are to be kept mostly in the medium SOC range in order to achieve a longer life [88, 90, 46].

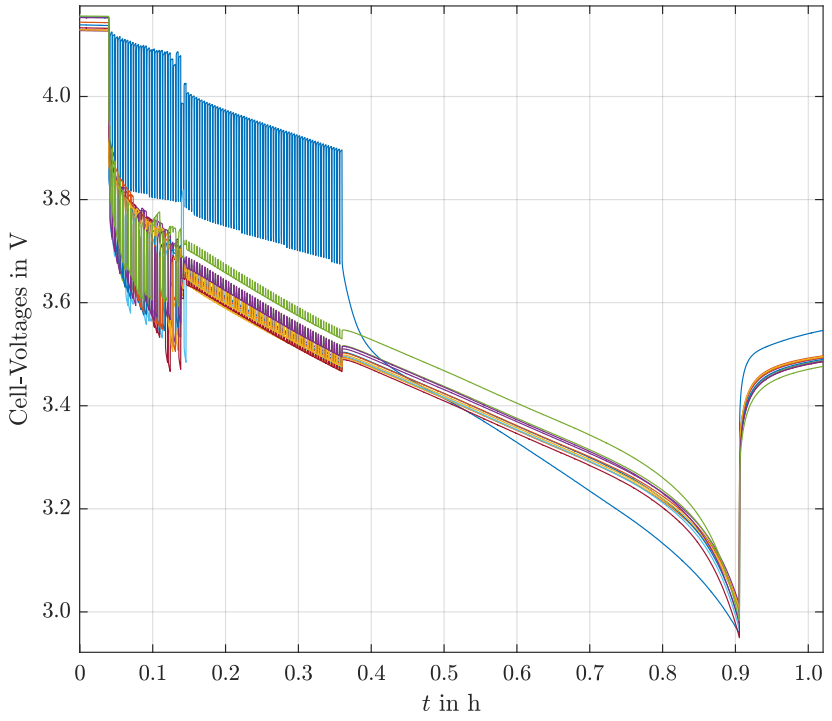

Figure 3.17: Example measurement with a capacity-based balancing method of 12 cells in series connection. With capacity-based equalization during discharge, all cells reach their EOD-voltage at the same time. Cell-type: ICR18650-26F, current: $I_{bat} = 2.4$ A, $T = 25$°C.

In the literature there are several approaches (e.g. [95]) to overcome the disadvantages of voltage-based balancing by SOC based balancing, as well as by intelligent combination of the two methods.

Since voltage and SOC based balancing cannot directly achieve the overall purpose of balancing (maximizing battery capacity), capacity-based balancing was developed [88]. Unlike conventional voltage-based balancing methods, which require cell voltages in a battery pack, the method also known as residual charge-based balancing uses the SOC, capacity and impedance information of each cell to calculate the charge differences and the equalization processes [96]. This balancing strategy, unlike SOC balancing, can also be usefully applied to aged cells with different SOC, SOH and internal resistance. Furthermore, this strategy prevents over-balancing of the cells. The overall goal of the method is, as shown in Figure 3.17, that all cell voltages reach their EOC or EOD voltage simultaneously [88, 89, 90].

Chapter 4

The Applied Active Battery Management

This chapter explains reasons for using a specific converter-based balancing system in this thesis as one of many possible AB topologies. The chosen topology and its universal possibilities of energy transfer are described. Software with balancing algorithm is introduced and explained.

4.1 Balancing Topology

The claim of this work is to use an modular AB system with a wide range of functions that can be used universally for a variety of different batteries. By using a topology without restrictions on energy transfer possibilities between cells, it is possible to evaluate the general advantages and disadvantages of AB topologies.

4.1.1 Topology Selection Based on Important Characteristics

The evaluation criteria for selecting a balancing topology include the balancing speed, the complexity of the control, the simplicity of the design, size, costs, possible energy transport paths, possible applications, efficiency and the number of components required. An optimal system for this thesis requires a fast balancing speed, flexible energy transport paths, efficiency and universal applicability. These criteria are considered for identifying a suitable topology step by step, without considering size or costs.
Bidirectional flow of energy is the first mandatory feature. Bidirectional means that energy can be added to a specific cell in order to support it, or extracted from it. Some active topologies from Chapter 3.1 can be excluded due to missing bidirectionality. These topologies are using multiple wind-

ings transformer and multiple-transformer topologies from Figure 3.8. All circuits with multiple or shared capacitors and inductors are considered to be bidirectional, as well as all converter-based approaches.
Bidirectional topologies should be able to transfer energy from each cell to any other for optimal balancing. For reasons of efficiency, this makes most sense if the transport takes place as directly as possible and not via additional battery cells as intermediate storage. From literature it can be seen that the longer the transport route, the greater the losses [85]. This excludes topologies, such as switched capacitor, double tiered switched capacitor and multiple switched inductor topologies (see Figure 3.5 a), b) and Figure 3.6 b)), which transfer energy via neighbouring cells. Depending on the design, flexible and direct energy transfer is possible with converter-based circuits or circuits with a shared energy storage (inductance, capacity, transformer) connected by a switch matrix. Unfortunately, some converters are designed for energy transfer with adjacent cells only. These include the Ćuk- and quasi-resonant-converter from Figure 3.10 a) and b). Both topologies could theoretically be designed such that each cell is connected to each other (ring structure from Figure 3.14). For balancing e.g. 4 cells a number of 6 converters is required. For 6 cells, already 15 converters are needed (as shown in Figure 4.1) and for a real life battery application with e.g. 12 cells in series a total amount of 64 converters would be necessary. This effort is usually unacceptable.

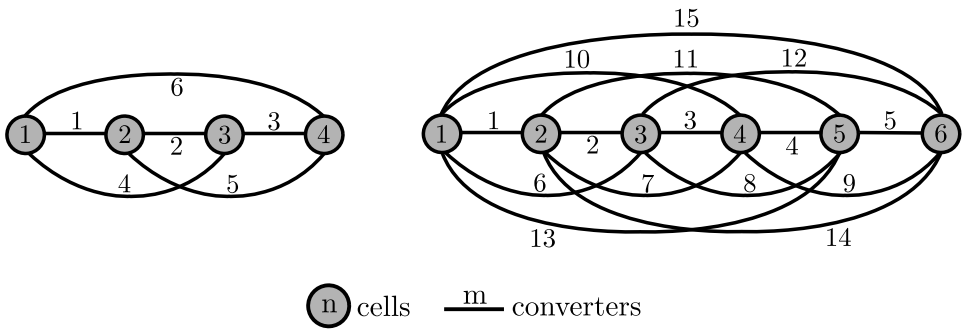

Figure 4.1: Number of necessary converters. n cells need m converters to connect them to each other.

The required balancing time is another important factor. It should be short in each operating point, and can be achieved by balancing all cells

simultaneously. Topologies using a shared energy store or a shared converter via a switch matrix can only balance the two connected cells at once. Therefore they are described as slow, which excludes circuits such as single switched capacitor from Figure 3.5 c), single inductor from Figure 3.6 a), single transformer from Figure 3.7, single converter (such as e.g. Buck-Boost) from Figure 3.9 b) and other converters with shared energy storage (such as Buck-Boost converter topology with shared inductance from [70]). Converter-based topologies without a switching matrix are able to balance several up to all cells simultaneously and reach high balancing speeds, however depending on the converter type and its power rating [65].

A promising approach is the bidirectional flyback converter shown in Figure 3.9 a). n cells are connected to n flyback converters, each of which is controlled separately. All flyback converters together require a number of $2n$ switches. A second possible topology is the full bridge converter topology shown in Figure 3.10 c). This topology also uses n converters for n cells, but requires twice the number of switches, $4n$ switches in total. Since all converters in both topologies can be coupled on the secondary side, direct energy transport between any selected cells can be realised simultaneously. According to [6], the flyback topology can transfer energy from one cell to the pack and vice versa.
Various sources attest both topologies, a high balancing speed as well as a high efficiency [62]. However magnetic losses are a disadvantage of the flyback converter [77]. Because practical feasibility, universality and speed are considered to be most important, some magnetic losses can be accepted. Due to additional benefits like less switches and the more versatile energy transfer possibilities, which are decisive for this PhD thesis, the multiple flyback converter topology will be used in this work.

4.1.2 Multiple Bidirectional Flyback Converter Topology

The flyback converter is a galvanically isolated DC voltage converter. Energy is transferred via a two windings inductor (often also referred to as transformer) between the input and output side, whereby the converter can be operated in both directions (bidirectional). It is used as a step-up and step-down converter which is beneficial for use in balancing systems. Within a BMS, each battery cell is equipped with a separate flyback converter, whose primary side is connected to a single battery cell. The secondary side is connected to a parallel bus system. Optionally, this bus system can be connected directly to the battery terminals. The structure can be simplified as

shown in Figure 4.2.

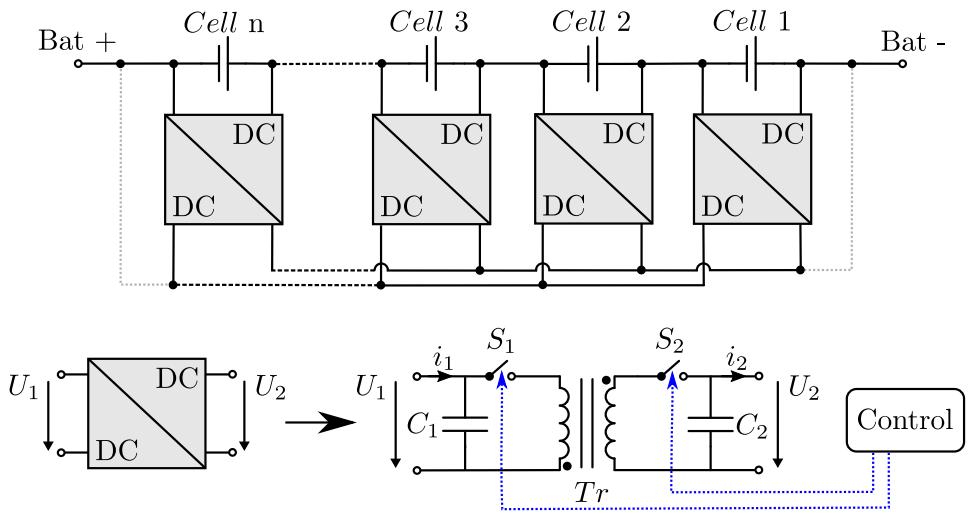

Figure 4.2: Schematic illustration of the multiple converter topology, using bidirectional flybacks as DC/DC converters.

Functional Principle

To generate a flow of energy, the two switches S_1 and S_2 in Figure 4.2 (implemented in practice as MOSFETs) are switched on alternately. The transformer is magnetised e.g. from the input side by closing switch S_1. The ramp-like increasing current i_1 is switched off by opening S_1 at a predefined current maximum. Energy stored in the core is transferred to the output side by switching on S_2, causing a positive current i_2. The currents vary depending on the voltage level and the permitted switch-on times of the switches. By setting a current maximum, the flyback converter can be operated with a constant current independent of the voltage. This ensures a constant balancing current even if the voltage of the battery cells changes. For this purpose the currents i_1 and i_2 are measured by shunt resistors in the current paths. Since the transformer acts as a single energy storage device, a storage transformer with an air gap in its magnetic core must be used. The flyback converter is well known in a variety of literature sources, e.g. [78, 97, 98, 99] and needs no further analysis in this thesis.

Energy Transfer

In this paragraph the energy transfer between cells is described idealised and is therefore considered to be lossless. Due to the voltage dependency of the converter power, the energy exchange is not considered directly. When all voltages are constant at a static operating point, the charge transfer by flowing balancing currents can be used to explain the energy transfer. The relevant currents are shown in Figure 4.3 and are only drawn for the positive branch (high-side). A load current at the battery terminals is not taken into account. The converters used are abstracted similarly to Figure 3.12. The presented topology can exchange energy between any two or more cells (cell-to-cell), furthermore also between a cell and the battery pack (cell-to-pack) as well as vice versa (pack-to-cell). It is therefore called a *cell-to-pack-to-cell* topology with arbitrary energy transfer possibilities.
i_{cn} represents the current through cell n. i_{b} represents the equalising current between the bus system and the battery. i_{c} and i_{b} are designed accordingly to the definition in Chapter 2.2 as charging currents. i_{bn} corresponds to the balancing currents from the individual cells that enter the bus system via the converters. Like i_{b}, i_{bn} has a positive sign if a single cell is charged. Due to the idealised approach with no losses the balancing power before and after the converters is identical, but the current i_{bn} differs from i_{bn0} due to the voltage difference between the primary voltage U_1 and secondary voltage U_2:

$$U_1 \cdot i_{\mathrm{bn0}} = U_2 \cdot i_{\mathrm{bn}} \;\Rightarrow\; i_{\mathrm{bn}} = \frac{U_1}{U_2} \cdot i_{\mathrm{bn0}} \tag{4.1}$$

All currents i_{bn0} are set by hardware configuration, constant and known. During operation, balancing currents flow the bus system between the individual converter connections. The following conditions basically do apply in the balancing system:

$$i_{\mathrm{b12}} = -i_{\mathrm{b1}}\ ,\quad i_{\mathrm{b23}} = i_{\mathrm{b12}} - i_{\mathrm{b2}}\ ,\quad i_{\mathrm{b3n}} = i_{\mathrm{b23}} - i_{\mathrm{b3}} \tag{4.2}$$

$$i_{\mathrm{b}} = i_{\mathrm{b3n}} - i_{\mathrm{bn}} \tag{4.3}$$

$$\Rightarrow i_{\mathrm{b}} = -\sum_{j=1}^{n} i_{\mathrm{bj}} \tag{4.4}$$

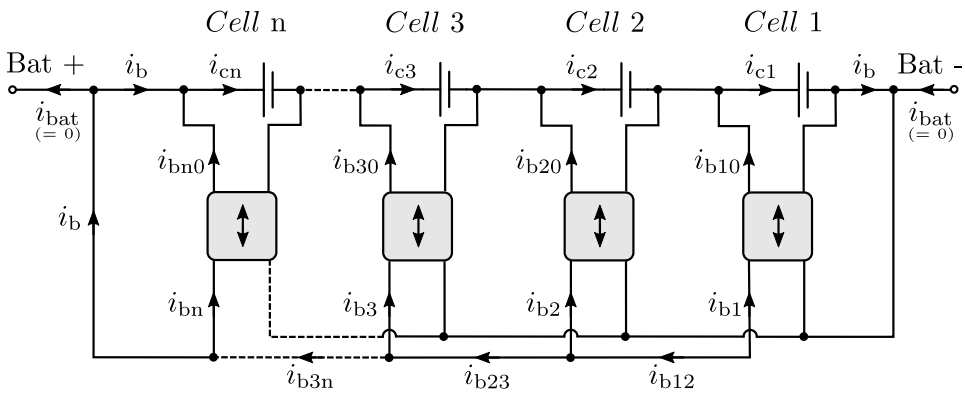

Figure 4.3: Abstracted multiple converter topology with idealized balancing currents.

A positive equalising current i_b into the battery can only flow when the sum of the balancing currents of the cells is negative, meaning that energy is being removed from them.

In cell-to-cell operation, energy can be exchanged directly between cells 1 and 2, for example. Ideally, it is assumed here that the values of the balancing currents i_{b1} and i_{b2} are equal but with a different sign. Thus, the following conditions apply to this operating state:

$$i_{b1} = -i_{b2} \quad \text{and} \quad i_{c1} = -i_{c2} \tag{4.5}$$

$$i_{b12} = i_{b2} - i_{b1} \tag{4.6}$$

$$i_{b3} = i_{bn} = 0 \quad \text{and accordingly} \quad i_b = i_{b3n} = i_{b23} = 0 \tag{4.7}$$

In pack-to-cell and cell-to-pack operation, the energy is exchanged between the cells and the battery. Here, the conditions in operation are more complex. If energy is taken from a cell and supplied to the battery, this cell itself IS a part of the battery and gets back part of the energy taken from it. This means that the balancing current i_{b10} set by the converter is never equal to the cell current i_{c1}. If, for example, cell 1 is balanced individually in this mode, it supplies energy to the battery pack or takes energy from the pack:

$$i_b = -i_{b1} \tag{4.8}$$

$$i_{c1} = i_b + i_{b10} \quad \Rightarrow \quad i_{c1} = i_{b10} - i_{b1} \tag{4.9}$$

If the pack consists of n cells, the voltages and currents of the primary and secondary sides of the converters differ by a factor of n:

$$i_{\mathrm{b1}} = \frac{i_{\mathrm{b10}}}{n} \tag{4.10}$$

following:

$$i_{\mathrm{c1}} = i_{\mathrm{b10}} - \frac{i_{\mathrm{b10}}}{n} \quad \Rightarrow \quad i_{\mathrm{c1}} = \frac{n-1}{n} \cdot i_{\mathrm{b10}} \tag{4.11}$$

With this condition, a proportion of the balancing current extracted, which depends on the number of cells in the battery, also reaches the cell itself. However, the current i_{c1} flowing through the balanced cell itself is a result of the withdrawn balancing current i_{b10} and the re-supplied current i_{b}, and is therefore reduced by $\frac{1}{n}$.
Numerical example: The battery consists of 12 cells ($n = 12$)

$$i_{\mathrm{c1}} = \frac{n-1}{n} \cdot i_{\mathrm{b10}} \quad \Rightarrow \quad i_{\mathrm{c1}} = \frac{11}{12} \cdot i_{\mathrm{b10}} \tag{4.12}$$

In reality, a mixed operation often takes place. In this case, the number of balanced cells can be odd, so there is not only balancing between the cells, but via the battery as well. Furthermore, the balancing currents i_{bn} are not completely identical. It therefore always has to apply for all cells j:

$$\sum_{j=1}^{n} i_{\mathrm{bj}} \neq 0 \quad \Rightarrow \quad i_{\mathrm{b}} \neq 0 \tag{4.13}$$

And for all cells j whose converters are active:

$$i_{\mathrm{cj}} \neq i_{\mathrm{b}} \tag{4.14}$$

Summary in general notation:
During cell-to-cell operation of cell x and cell y $i_{\mathrm{b}} = 0$ with $i_{\mathrm{bx}} = -i_{\mathrm{by}}$ and $i_{\mathrm{cx}} = -i_{\mathrm{cy}}$.
During cell-to-pack or pack-to-cell operation of cell x and a pack consisting of n cells $i_{\mathrm{b}} = -i_{\mathrm{bx}}$ and $i_{\mathrm{cx}} = \frac{n-1}{n} \cdot i_{\mathrm{bx0}}$.

Balancing Current

Several factors have to be taken into consideration in order to make a statement about the necessary balancing currents. In addition to the available

balancing time, these also include the cell capacities and their dispersion. The key question is therefore how much charge has to be balanced between the cells in a certain amount of time. In the following, a generally valid correlation is to be found.
This correlation has already been considered in general by Davide Andrea in his book *Battery Management Systems* [3]. He assumes so-called *grossly disbalanced packs*, in other words batteries in which cells have either 100% or 0% of their possible SOC value and thus deviate from each other to the maximum. In this case, the capacity to be balanced corresponds to the battery capacity. This type of imbalance can not occur in practice. However, his considerations make clear that there are essentially two questions to be answered separate from each other for dimensioning the balancing current:

1. How big is the maximal possible imbalance in the battery?
2. In what amount of time should the battery be balanced?

With regard to the possible imbalance studies of new cells, i.e. their BOL, can be found in the literature. For example, in [100] 20,000 cells were measured and a capacity dispersion of 1.3% was detected. However, it is not the initial imbalance that is decisive for balancing, but the imbalance during operation or at the EOL of the battery. In [101], own investigations show a deviation depending on the load and temperature of 1.73% (0.5C, 40°C) up to 8.61% (1.0C, 30°C) already at 80% SOH.
The time available for balancing t_b results from the battery capacity C_cap and the load current I_bat. This is also equivalent to the C-rate of the battery from Chapter 2.2. The time t_b thus corresponds to the maximum discharge time of the battery, but can also be defined shorter depending on the application:

$$t_\mathrm{b} = \frac{C_\mathrm{cap}}{I_\mathrm{bat}} \tag{4.15}$$

The charge Q_b to be balanced is calculated from the difference between the maximum $C_\mathrm{c,max}$ and minimum $C_\mathrm{c,min}$ single cell capacity. Since a balancing system is often not able to keep a constant balancing current over the entire time, its average value must be determined. The following formula then results for the minimum required averaged balancing current $\overline{I}_\mathrm{b}$:

$$\overline{I}_\mathrm{b} = \frac{Q_\mathrm{b}}{t_\mathrm{b}} \tag{4.16}$$

The above-mentioned relationship is shown in Figure 4.4. Necessary balancing currents can be derived directly from the y-axis as a function of the dispersion and the load.

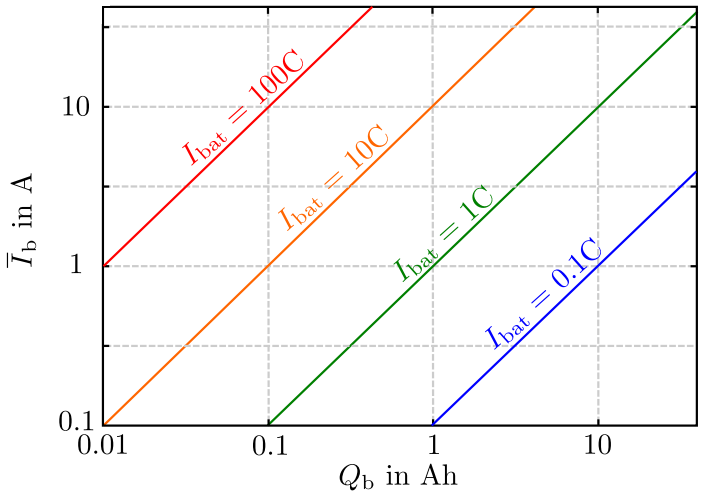

Figure 4.4: Balancing current $\overline{I}_{\mathrm{b}}$ as function of charge to be balanced Q_{b} and battery load I_{bat} in a double logarithmic plot.

Figure 4.4 can be used to determine whether the balancing system can deal with the particular battery in its given use case. Similarly, a BMS can be designed or configured according to the necessary balancing current. If the maximum balancing current of the system is smaller than the calculated necessary balancing current of the battery, the balancing process will not be completed by the end of the discharge cycle and the battery will not be operated optimally.

4.2 Balancing Algorithm

This section describes the strategy of the balancing system and its algorithms. A software basis is responsible for acquisition of voltage and current measurement data from the battery in fixed programmed intervals and the issuing of commands necessary for balancing. Thus, depending on the decision of the balancer algorithm, commands for balancing battery cells are sent to the hardware controllers via software interfaces. The mentioned software basis is a functional environment for the algorithm, which includes all necessary communication options with the hardware and the operator (user) of the BMS. Essentially, the algorithm contains all the functions necessary for cell balancing and thus provides the core of this chapter. In addition to the separation of the algorithm into different sub-functions, methods for data acquisition, cell diagnosis and calculation of other important parameters are explained.

4.2.1 Determine Battery Status

The core of the algorithm is a function called *balancing manager* whose activity diagram can be seen in Figure 4.5. This function determines the status of the battery on the basis of measured voltage and current values, which are recorded in a fixed measurement interval t_{meas}.
The battery status is the first important parameter to be determined. In addition to the battery current I_{bat}, the voltages $U_{\mathrm{c,i}}$ of all connected cells i are measured. Only if all parameters are within specified operating limits the battery status is OK. The following must apply:

$$U_{\mathrm{c,EOD}} < U_{\mathrm{c,i}} < U_{\mathrm{c,EOC}} \ \wedge \ |I_{\mathrm{bat}}| < |I_{\mathrm{bat,max}}| \tag{4.17}$$

The limit values are taken from the data sheet of the cells. $U_{\mathrm{c,EOD}}$ and $U_{\mathrm{c,EOC}}$ can be read off directly. $I_{\mathrm{bat,max}}$ is calculated from the number of cells connected in parallel in the battery and can be different for charging and discharging depending on the battery cell.
Once the battery status has been successfully checked to be ok a distinction is made between two different balancing methods according to predefined limit values:

- Voltage-based balancing, in this work also referred to as *top balancing*, is carried out at the end of the charging process to equalise possible remaining voltage differences of the battery cells. The voltage limit

for top balancing is referred to as U_{tb}. Voltage-based balancing is activated as soon as a battery cell exceeds the voltage U_{tb}.

- Capacity-based balancing is carried out during the charging and discharging process to equalise the capacity differences of the cells. The voltage limit for capacity-based balancing is U_{cb}. If a cell falls below the voltage U_{cb}, balancing is no longer carried out. Capacity-based balancing therefore only takes place between the voltages U_{tb} and U_{cb}.

For both voltage-based and capacity-based balancing, the measured current value I_{bat} is relevant as the second variable to be checked. Since voltage-based balancing only takes place while the battery is being charged, the measured charge current must be larger than or equal to zero. For capacity-based balancing, which can be carried out when charging and discharging, the measured current value must differ from zero. When the battery is in rest, capacity-based balancing will not be active due to efficiency reasons.

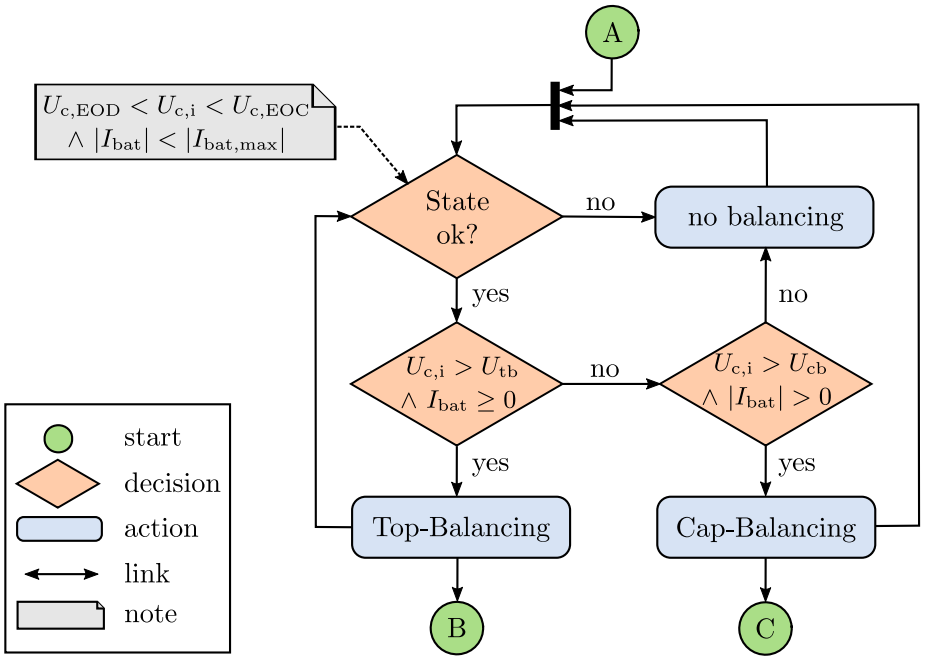

Figure 4.5: *Balancing manager* routine to choose balancing action. Cell voltage $U_{\mathrm{c,i}}$ is checked simultaneously for all connected cells i. This routine is executed in loop.

In conclusion, the two balancing strategies mentioned above are selected as follows. Voltage-based balancing is chosen if it applies:

$$U_{\mathrm{c,i}} > U_{\mathrm{tb}} \ \wedge \ I_{\mathrm{bat}} \geq 0 \tag{4.18}$$

Capacity-based balancing is chosen if it applies:

$$U_{\mathrm{c,i}} > U_{\mathrm{cb}} \ \wedge \ |I_{\mathrm{bat}}| > 0 \tag{4.19}$$

If neither of the two strategies can be selected based on the measured parameters, the battery condition check starts again. The routine *balancing manager* is thus executed in an endless loop.

4.2.2 Voltage-Based Balancing

This method is a classic voltage-based balancing (literature according to Chapter 3.1.1 and 3.3) and decides exclusively based on the cell voltages which cells have to be balanced. Since the voltages in the range of 50% SOC do not contain any precise information about the charge of the cells due to the flat OCV curve of lithium-ion cells (see Chapter 3.3) top balancing is only carried out in the upper voltage range of the cells. Here, the OCV characteristic curve is much steeper and charge differences between cells can be detected more clearly on the basis of the cell voltage. Top balancing performs similar to PB, but has, decisive advantages if carried out with an AB system. Excess energy of one cell is not converted into heat, but is transferred to other cells. Also significantly higher currents are available for balancing.
Voltages of all individual cells $U_{\mathrm{c,i}}$ are first recorded and then sorted according to their values. The mean value of the measured voltages $U_{\mathrm{c,avg}}$ is calculated, which forms the centre of a tolerance band, also referred to as *voltage band*:

$$U_{\mathrm{c,avg}} = \frac{1}{n} \sum_{i=1}^{n} U_{\mathrm{c,i}} \tag{4.20}$$

This tolerance band is described by the voltage U_{lim}, which forms both the upper and lower voltage limits. Thus, if a cell voltage U_{c} is more than U_{lim} above or below the mean voltage $U_{\mathrm{c,avg}}$, the affected cells are selected for balancing, as shown in Figure 4.6. In this example, $U_{\mathrm{c,max}}$ exceeds the voltage U_{tb} at time t_1, whereupon the top balancing routine is activated by the *balancing manager*. From this point on, $U_{\mathrm{c,avg}}$ is calculated and the tolerance band is created using U_{lim}. Cells can be selected for balancing,

even if the battery charge does not change from CC to CV phase until time t_2. Balancing the cells is thus also possible before the CV phase is reached. Depending on how the voltage U_{tb} is defined, the voltage-based balancing can also be limited to the constant voltage phase or, in oppose, be activated significantly earlier. If activated earlier, U_{tb} is defined in a way that balancing is activated before the CV phase is reached, so that cells with increased internal resistance and thus higher cell voltage are discharged and cannot prevent entry into the CV phase in the charging process by an overvoltage. In the example shown in Figure 4.6, the cell voltages would exceed the tolerance band at time t_3 within the CV phase and are balanced. The balancing is carried out several times as soon as the cells reach the limit of the tolerance band again after previous balancing. This results in a cyclically visible repetition with 3 balancing steps in this case.

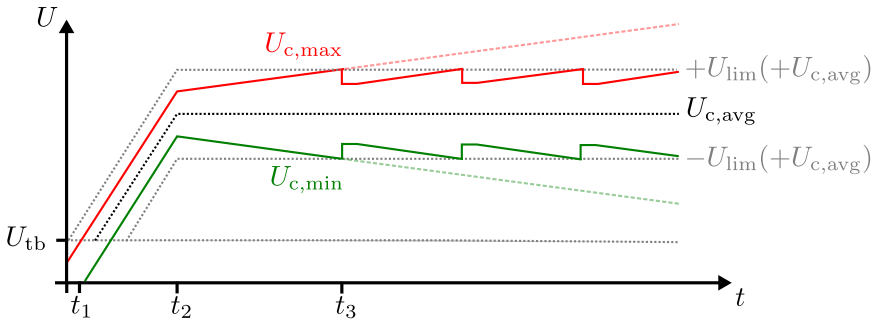

Figure 4.6: Illustration of voltage-based balancing. Maximum cell voltage $U_{\mathrm{c,max}}$ and minimum cell voltage $U_{\mathrm{c,min}}$ have to be balanced as soon as they leave the tolerance band.

The process of the top balancing routine can also be viewed in more detail in the activity diagram in Figure 4.7. If a cell exceeds/falls below the tolerance band, the balancing is activated for the duration of t_{step}. For this purpose, all cell voltages $U_{\mathrm{c,i}}$ are evaluated simultaneously. The following conditions, here represented by the highest and lowest cell voltage, must be checked:

$$[U_{\mathrm{c,i}} - U_{\mathrm{c,avg}}] > U_{\mathrm{lim}} \longrightarrow \text{Discharge cell.} \tag{4.21}$$

$$[U_{\mathrm{c,avg}} - U_{\mathrm{c,i}}] > U_{\mathrm{lim}} \longrightarrow \text{Charge cell.} \tag{4.22}$$

The value t_{step} is variable and pre set in the balancing system. This means that each balancing process maintains the balancing current of the selected cell for a duration of t_{step} after activation. Afterwards the battery status

checked again by the balancing manager. The diagram also shows that after each check of the cell voltages against the tolerance band, regardless of whether balancing actually takes place or not, the routine hands over to the balancing manager again to check the battery status. If no cell is selected for balancing, the handover to the balancing manager takes place immediately.

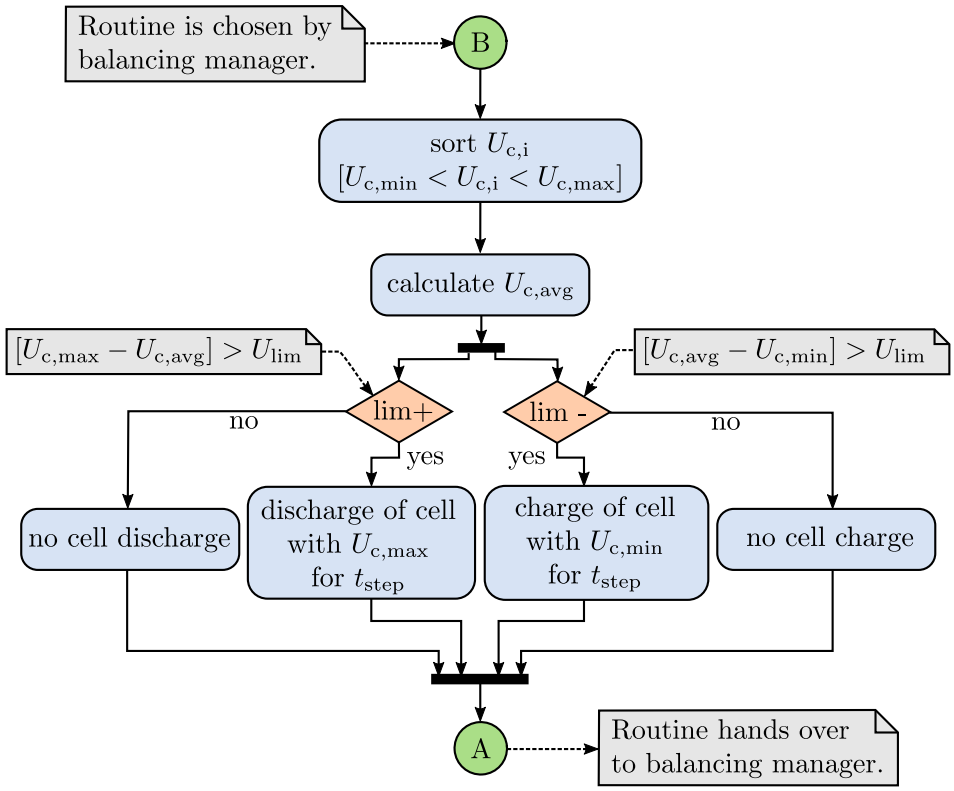

Figure 4.7: Activity diagram of voltage-based balancing. Cell voltage U_c is checked simultaneously for all connected cells i and therefore referred to as $U_{c,i}$. This routine is executed together with *balancing manager* from Figure 4.5.

The voltage-based balancing algorithm can also be displayed as control loop (Figure 4.8). For this purpose, the value U_{lim} is defined as the set-point, which defines the permissible voltage band and thus the maximum permissible distance between the cell voltages $U_{\mathrm{c,i}}$. U_{lim} itself is a fixed value as described above. The value of ΔU_{c} for each individual cell is referred to as $\Delta U_{\mathrm{c,i}}$ and is calculated after voltage measurement at the battery. The following applies here:

$$\Delta U_{\mathrm{c,i}} = U_{\mathrm{c,avg}} - U_{\mathrm{c,i}} \tag{4.23}$$

The aim within the control loop is to regulate the value $\Delta U_{\mathrm{c,i}}$ of each individual cell, i.e. the difference between the cell voltage and the mean value U_{avg}, to be less than the value U_{lim}. For this purpose, balancing currents for each cell $i_{\mathrm{b,i}}$ are set by the controller, referred to here as *Voltage-based balancing*. The controlled system generates the cell voltages of the battery as measured values, from which the deviations $\Delta U_{\mathrm{c,i}}$ are determined. The sign of the balancing current $i_{\mathrm{b,i}}$ is equal to that of the voltage difference $\Delta U_{\mathrm{c,i}}$. If $\Delta U_{\mathrm{c,i}}$ is a positive value, the cell voltage is below the average and the affected cell must be additionally charged by a positive balancing current. The disturbance variables of the controlled system are the parameter variation of the cells and the battery current.

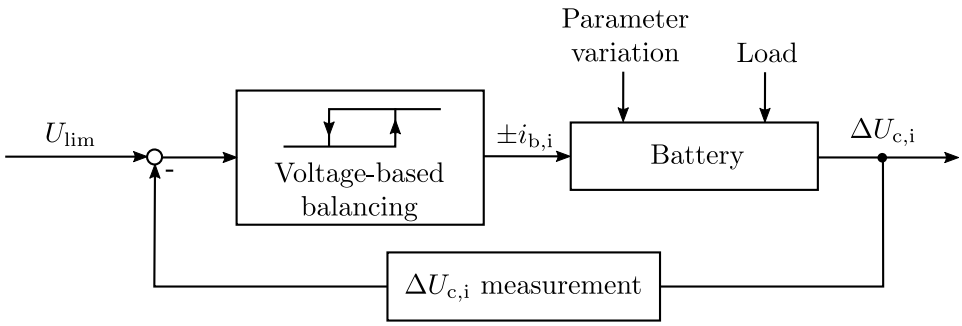

Figure 4.8: Control-loop of voltage-based balancing.

4.2.3 Capacity-Based Balancing

The capacity-based balancing method (literature from Chapter 3.3) aims to achieve the end-of-charge voltage or the end-of-discharge voltage for all cells at the same time, so that the entire capacity of all cells within the battery can be used. In contrast to top balancing, the cells are not balanced based

on their voltage, but on a calculated charge difference ΔQ_{c}. Since the charge of a single cell cannot be measured directly it is determined/calculated iteratively.
The activity diagram in Figure 4.12 can be used to summarize the process. Once the capacity-based balancing is activated by the *balancing manager* it is decided whether the balancing charges of the cells (ΔQ_c) are within a defined tolerance band. The balancing charge of a cell indicates how much charge must be added or removed from that cell. If no balancing charges have yet been determined for the battery (e.g. on its BOL, or after first connection of the AB system to a used battery), balancing it not performed during the first discharge cycle. Once the first battery cycle has been completed, the so-called learning phase is terminated and the capacity-based balancing is performed. The measured values at EOD of the learning cycle are used as starting values for all calculations. If the battery is *full*, no balancing must be performed and the routine hands over to the *balancing manger* again under the following condition:

$$U_{\mathrm{c,i}} = U_{\mathrm{c,EOC}} \ \wedge \ I_{\mathrm{bat}} = 0 \tag{4.24}$$

In contrast, the following condition is used to check whether the battery is completely discharged:

$$U_{\mathrm{c,i}} = U_{\mathrm{c,EOD}} \ \wedge \ I_{\mathrm{bat}} = 0 \tag{4.25}$$

The *empty* condition is fulfilled as soon as one cell reaches the final discharge voltage and thus ends the discharge cycle. At this point, cell voltages and the charge taken from the battery (Q_{disch}) are stored and used for calculating the necessary balancing charges ($\Delta Q_{c,i}$) of the cells. The charge (Q_{disch}) is determined by integrating the current during the complete discharge process (Equation 2.1). The relative state of charge of each cell ($SOC_{c,i}$) is determined using the cell voltages and the stored state of charge characteristic. For this purpose, an OCV characteristic curve, which gives the ratio of the voltage and the charge at no load, is used. In this work, the characteristic curve of a Samsung ICR 18650 26F cell is determined analogously to the Chronopotentiometry procedure presented in Chapter 2.5.2 and stored in the software as a cell model in the form of an equivalent electric circuit diagram analogous to Chapter 2.4, Figure 2.7. The cell model is then used to determine the state of charge. Figure 4.9 shows symbolically how the end-of-discharge voltage of the individual cells in conjunction with the stored state of charge curve can represent a SOC difference. However, because of the

influence of the internal resistance, the marked voltage points cannot simply be transferred by identical voltage values from the measured discharge curve (left plot) to the marked SOC points in the stored characteristic curve (right plot).

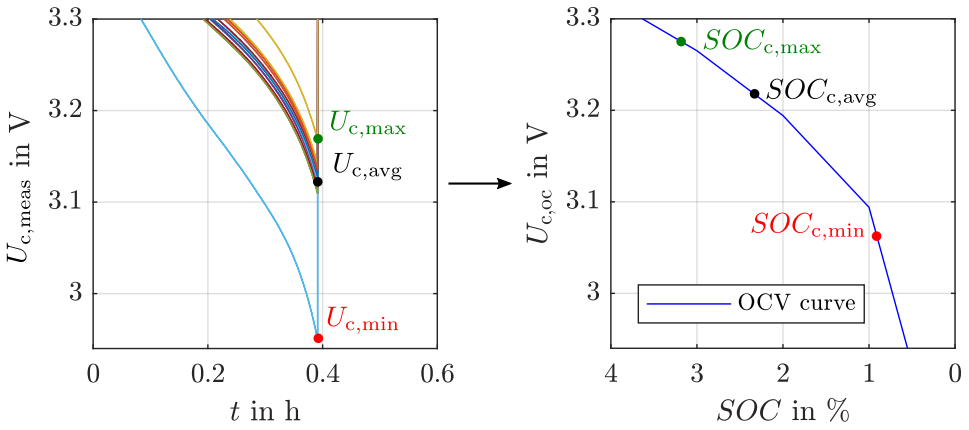

Figure 4.9: Transfer of the measured end of discharge voltage (left) to the OCV characteristic curve (right). $U_{c,oc}$ is calculated from $U_{c,meas}$ in Equation 4.26. In this specific example, cell level internal resistance is 10 mΩ and I_{bat} = 10 A, which equals to $U_{c,oc} = U_{c,meas}$ + 0.1 V. SOC-values are read from the x-axis of the right plot.

The internal resistance R_{DC} is determined for each cell at the beginning of the discharge using the current pulse method from Chapter 2.5.1. For simplification, it is assumed that the internal resistance of the cells does not change during the discharge. In order to calculate the reference voltage $U_{c,oc}$ for transfer to the OCV characteristic curve based on the measured voltage of the cells $U_{c,meas}$, the following equation is used:

$$U_{c,oc} = U_{c,meas} + (I_{bat} \cdot R_{DC}) \tag{4.26}$$

With the SOC values of the individual cells now available, the mean value of the states of charge (SOC_{avg}) and the deviation of the state of charge of each cell ($\Delta SOC_{c,i}$) from the mean value can be determined, taking into

account the number of cells n_{c}:

$$SOC_{\mathrm{avg}} = \frac{\sum_{i=1}^{n} SOC_{\mathrm{c,i}}}{n_{\mathrm{c}}} \tag{4.27}$$

$$\Delta SOC_{\mathrm{c,i}} = SOC_{\mathrm{avg}} - SOC_{\mathrm{c,i}} \tag{4.28}$$

Then, the required balancing charge ($\Delta Q_{\mathrm{c,i}}$) can be determined for each individual cell from Figure 4.9. The balancing charge of a cell is calculated with the deviation of the state of charge of the cell ($\Delta SOC_{\mathrm{c,i}}$) and the charge taken from the battery (Q_{disch}):

$$\Delta Q_{\mathrm{c,i}} = \Delta Q_{\mathrm{c,prev}} + (\Delta SOC_{\mathrm{c,i}} \cdot \frac{|Q_{\mathrm{disch}}|}{100}) \tag{4.29}$$

The value $\Delta Q_{\mathrm{c,prev}}$ required to calculate the balancing charge $\Delta Q_{\mathrm{c,i}}$ is the calculated balancing charge from the previous cycle. By including $\Delta Q_{\mathrm{c,prev}}$ the algorithm can iteratively approach the optimal values of the charges to be balanced after each cycle. Since assumptions have to be made in order to calculate relevant variables, it makes sense to increase the accuracy by iterating the measured/calculated parameters from cycle to cycle. This method thus becomes more accurate with increasing amout of cycles and can adapt in the event of a change in the parameters of the cells during operation.
Cells with a negative value of ΔQ_{c} are called strong cells because their states of charge are above the mean value. Cells with a positive value of ΔQ_{c} are called weak cells because their states of charge are below the mean value. During the discharge cycle, charge is removed from strong cells and added to weak cells. In the charge cycle, this process is reversed, the identical charges are returned for this purpose. In this case, the weak cells (less capacity) are additionally discharged, since they can take up less charge and would reach the end of charge voltage significantly faster. Strong cells (more capacity) are additionally charged in the same way, so that they receive enough charge during the charging process and are not limited by weak cells. In the activity diagram from Figure 4.12, the distinction between charging and discharging processes with the correspondingly adapted cell balancing is visible in the right branch of the diagram.
As the last step before balancing, the cells are sorted by their balancing charge values. If ΔQ_{c} of the strongest or weakest cells are outside the tolerance band Q_{lim}, these cells are charged or discharged by a balancing pulse with time t_{step} and current I_{b}. I_{b} depends on the used balancing hardware

and is predefined. After each balancing pulse, the charge (Q_{step}) added to or removed from the cells during the balancing pulse is calculated. Q_{step} in units of mAh is calculated from the balancing current (in unit mA) and the time (in unit s) the cells were charged or discharged:

$$Q_{\text{step}} = \frac{t_{\text{step}} \cdot I_{\text{b}}}{3600\ \frac{s}{h}} \tag{4.30}$$

Using Q_{step} it is possible to recalculate ΔQ_{c}, of the balanced cells, after each balancing pulse. Thus, after each pulse, it is checked whether $\Delta Q_{\text{c,i}}$ is now in the tolerance band or the cell needs to be balanced further. After that, the cells are sorted again. The balancing is repeated until ΔQ_{c} of each cell is inside the tolerance band or if the discharge cycle (limit voltage U_{cb}) or the charge cycle (limit voltage U_{tb}) has ended. The tolerance band is defined by Q_{lim} as follows:

$$\pm\, Q_{\text{lim}} = |Q_{\text{step}}| \tag{4.31}$$

An example of how to select cells for balancing in a high dispersed battery based on their $\Delta Q_{\text{c,i}}$ is shown in Figure 4.10. Here it is assumed, that the difference in SOH-values equals the difference in cell charge. Balancing charges are calculated as soon as the $\Delta Q_{\text{c,i}}$ of one cell leaves the tolerance band given by $\pm Q_{\text{lim}}$ (shown on the left). In this balancing operation, the sum of all balancing charges $\Delta Q_{\text{c,i}}$ equals zero.

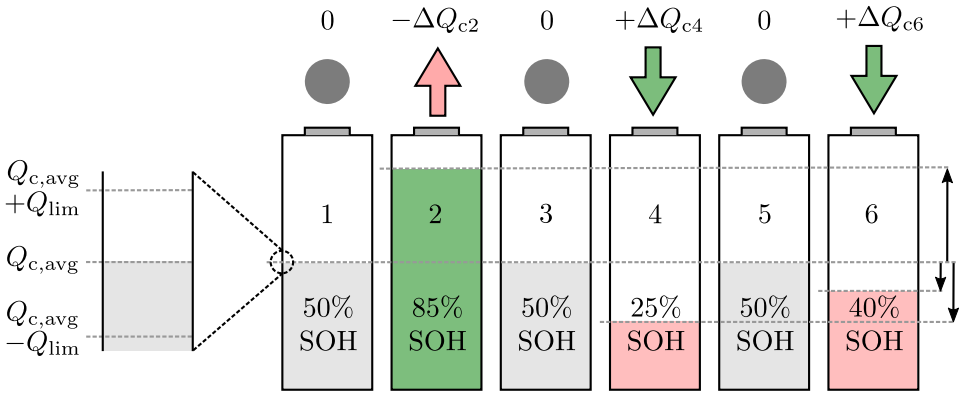

Figure 4.10: Illustration of capacity-based balancing. Cell with maximum capacity needs to be discharged by $-\Delta Q_{c2}$ and cells with less capacity need to be charged by $+\Delta Q_{c2}$ and $+\Delta Q_{c6}$.

Capacity-based balancing algorithm can be presented as a closed control loop (Figure 4.11) analogue to voltage-based balancing. For this purpose, the value Q_{lim} is defined as the set-point, which defines the permissible ΔQ_{c} band and thus the maximum permissible distance between the cell capacities. Q_{lim} itself is a calculated and fixed value as described above. The value of $\Delta Q_{\mathrm{c,i}}$ for each individual cell is calculated as described above after each complete discharge cycle by Equation 4.29. The aim within the control loop is to regulate the value $\Delta Q_{\mathrm{c,i}}$ of each individual cell, i.e. the difference between the cell charge and the mean value $\Delta Q_{\mathrm{c,avg}}$, to be less than the value Q_{lim}. For this purpose, balancing currents for each cell $i_{\mathrm{b,i}}$ are set by the controller, referred to here as *capacity-based balancing*, and impressed into the controlled system *Battery*. The controlled system generates the cell charges of the battery as calculated values, from which the deviations $\Delta Q_{\mathrm{c,i}}$ are determined. The sign of the balancing current $i_{\mathrm{b,i}}$ is equal to that of the voltage difference $\Delta Q_{\mathrm{c,i}}$. If $\Delta Q_{\mathrm{c,i}}$ is a positive value, the cell charge is below the average and the affected cell must be additionally charged by a positive balancing current. The disturbance variables of the controlled system are again the parameter variation of the cells and the battery current.

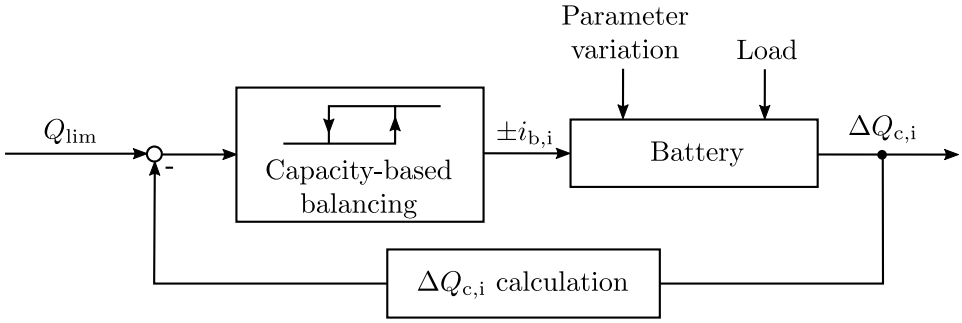

Figure 4.11: Control-loop of capacity-based balancing.

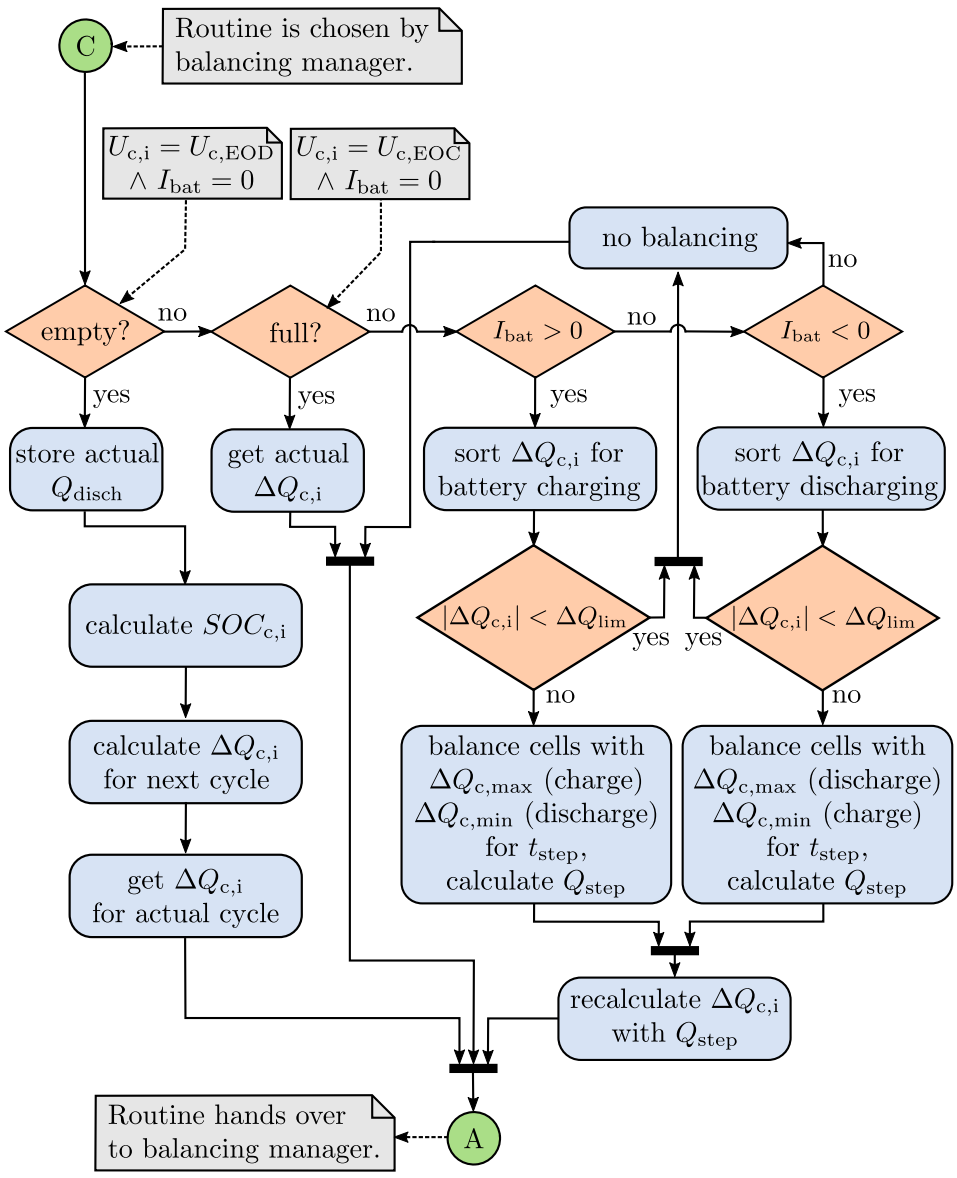

Figure 4.12: Activity diagram of capacity-based balancing. All cell charges Q_c are checked simultaneously for all connected cells i and therefore referred to as $Q_{c,i}$. This routine is executed together with *balancing manager* from Figure 4.5.

Chapter 5

Ageing Analysis of Battery Packs

This chapter describes the long-term ageing of several batteries using active and passive BMSs. First, findings from the literature show a relevant gap that is to be filled with this new test approach. Then, the experimental setup and the test procedure with all important parameters are explained. Finally, the test results are presented and discussed.

5.1 Insights from Literature

This first section provides an insight into the literature to find some kind of comparison between active and passive balancing systems. Known similarities to this work are found, but also a gap in the literature is identified that this work aims to fill. The following list shows summaries of the respective results.

5.1.1 Theoretical Consideration and Simulation

1. **Battery Balancing Methods: A Comprehensive Review** [5]
   In this paper, Cao et al. present a complete review of the balancing methods and corresponding hardware topologies. The balancing methods are grouped into 3 categories according to their balancing methods. Operation principles of each method are explained. Finally, a comparative analysis is given in order to find proper balancing methods for different applications.

2. **Comparison of Passive Cell Balancing and Active Cell Balancing for Automotive Batteries** [102]
   This paper presents a quantitative performance analysis of a conventional passive cell balancing method and a proposed active cell balanc-

ing method for automotive batteries by Lee et al. An experimentally validated battery model was used to simulate the balancing process of both balancing circuits for a high capacity battery module. The results suggest that the proposed AB method can improve the power loss and extend the discharge time of a battery module.

3. **A Review of Passive and Active Battery Balancing based on MATLAB-Simulink** [6]
   In this work, Daowd et al. present a review and comparisons between the different balancing topologies based on MATLAB/Simulink simulation. The comparison has been carried out according to circuit design, balancing simulation, voltage/current stress, practical implementations, application, balancing speed, complexity, balancing system efficiency, size, cost etc.

4. **Simulative Comparison of Balancing Algorithmms for Active and Passive Cell Balancing Systems for Lithium-Ion Batteries** [103]
   Fleischer et al. implement and compare different balancing algorithms using active and passive systems. The voltage-based method is the least complicated method to implement and therefore state of the art technique in electrical vehicles. The improvement of this method is based on the OCV of the individual cells. This implies the knowledge of all internal resistances, which - as postulated in the paper - should not be a challenge for intelligent BMS algorithms. The best balancing method according to this work is based on the SOC estimation of each cell.

5. **Comparison of Active Battery Balancing Systems** [65]
   A quantitative model-based comparison of 10 AB circuits is presented by Caspar et al. for equalizing imbalanced cell energies of lithium-ion batteries. A modelling approach and mean current calculations have been outlined for comparing all relevant different AB circuits with PB. As a result an improvement of 3% for new cells and an improvement of 8.4% for aged cells are shown for the best AB methods.

6. **Battery equalization active methods** [62]
   In this work, Gallardo-Lozano et al. present a summary, comparison and evaluation of the different active battery equalization methods, providing a table that compares them, which is helpful to select the

suitable equalization method depending on the application. Advantages and disadvantages of each presented method are identified.

7. **Performance comparison of active balancing techniques for lithium-ion batteries** [104]
   Starting from the simple passive technique, in which extra energy is dissipated on a shunt resistor, active techniques, aiming at an efficient energy transfer between cells, are investigated by Baronti et al. The different topologies are compared by means of statistical simulations. They clearly show that the cell to cell topology is the quickest and most efficient one. Moreover, the pack to cell topology is the least effective one and surprisingly dissipates more energy than the passive technique, if the converter efficiency is below 50%.

8. **Comparison of Li-ion active cell balancing methods replacing passive cell balancer** [105]
   This article from Valda et al. describes possible proposals of the active battery cell balancers from literature, which could be used as a replacement for the common passive cell balancer in the existing BMS. Many types of the balancers were proposed, described and implemented. But the requirements of high number of switches, inductors, transformers or multi-winding transformers and other key and expensive components as well as the complex control methods are leading to a significant design difficulty, poor modularity and high cost.

9. **Structural Comparison of Battery Balancing Architectures with Optimal Control** [85]
   In this paper Caspar et al present a systematic comparison of AB circuit architectures on battery module level which counteracts the multiple influences of cells and circuit properties on AB results. A time-optimal and an energy loss-optimal approach for AB control enables a systematic and clean comparison of different balancing architectures by ruling out the influence of heuristic control algorithms and differences of circuit parameters on AB results.

10. **Synthesis of Active Cell Balancing Architectures for Battery Packs** [106]
    As a remedy, Lukasiewycz et al. present an automatic synthesis of balancing circuits and their corresponding control, optimizing the number of required MOSFETs and necessary control signals. The proposed

synthesis combines a mathematical solver to explore the search space with a graph-based verification that iteratively excludes infeasible solutions until the optimal architectures are obtained.

11. **A Comparative Study of Battery Balancing Strategies for Different Battery Operation Processes** [89]
    Zheng et al. present a comparative study of four battery balancing strategies for different battery operation processes. These balancing strategies are developed from the state of the art battery balancing circuits and algorithms reported in recent literature. The performance of balancing strategies is evaluated and compared by battery pack maximum available capacity, SOC variances at the EOC and EOD.

12. **Comparison on cell balancing methods for energy storage applications** [107]
    This paper by Lee et al. investigates the advantages and disadvantages of passive and active cell balancing methods. First, a categorization of cell balancing circuits as passive or active cell balancing methods based on the usage of resistors is carried out. By comparing the advantages and disadvantages of cell balancing methods, a guide for selecting a proper cell balancing method for energy storage applications is presented.

13. **Comparative survey on modular cell-equalizing circuits for battery management systems** [108]
    Bui et al. present a comparison survey study among different modular cell balancing approaches that are used to balance battery cell voltages. In particular, the cell equalizing methods that are considered in this paper have a modular structure. The authors provide guidelines for selecting a suitable topology during the design process of modular cell balancers.

14. **Battery Management System Hardware Concepts: An Overview** [56]
    In this article, Lelie et al. focus on the hardware aspects of BMSs for EVs and stationary applications. The paper is giving an overview on existing concepts in state of the art systems and enabling the reader to estimate what has to be considered when designing a BMS for a given application.

15. **Cell Balancing Topologies in Battery Energy Storage Systems: A Review** [61]
    Several cell balancing topologies have been proposed by the researchers in the last decade. Ahmad et al. present a review of the proposed cell balancing topologies for energy storage systems. Comparison among the topologies is performed for four categories: balancing speed, charge-discharge capability, main elements required to balance n cells, and application types.

16. **A comprehensive review on inconsistency and equalization technology of lithium-ion battery for electric vehicles** [109]
    This review from Hua et al. summarizes the origin of inconsistencies within lithium-ion batteries from production to usage process, and introduces classification methods and application scenarios of the battery management system in detail. Compared with the passive topologies, the active topologies have advantages of high equalization efficiency and high speed which can effectively improve the consistency of pack but with high cost and complex control strategy as extended burden.

5.1.2 Measurements and Test Results

1. **Comparison and Evaluation of Charge Equalization Technique for Series Connected Batteries** [77]
    Various circuits for charge/discharge equalization are proposed. But so far there is no criterion for comparison and evaluation. In this paper Kong et al. divide all the circuits into four groups according to structure, and each of them is qualitatively analysed. In a specific test, equalization among four cells in a string is performed.

2. **Charge balancing of serially connected lithium-ion battery cells in electric vehicles** [93]
    The advantage of active charge balancing is shown by Einhorn et al. using a prototype with twelve serially connected LICs. Moreover, the influence of the cell capacity variance and the influence of the balancing current on the discharging energy is investigated. For a specific battery stack the usable energy was increased by 13% with active cell balancing. The discharging energy in a battery stack can already be increased significantly with a small balancing current especially for large capacity variations.

3. **Experimental Validation of an Efficient Charge Equalization System for Lithium-Ion Batteries** [86]
   Charge equalization among the series connected cells is achieved with a cell to cell balancing topology. In this work of Baronti et al. found, that battery equalization lasts around 25 h and wastes 1% of the battery energy, if one of the cells is 17.7% imbalanced. AB allows the recovery of the full battery charge, otherwise limited to 82.3%, with an energy saving factor of 6, if compared with PB.

4. **Effectiveness of active balancing on high dispersion batteries** [110]
   In this own work investigations examine the benefit of an AB system based on an LTC-3300 IC with help of an arbitrarily configurable battery. The usable capacity of the cell-combinations is compared with and without balancing during discharge. In all three tests, the capacity could be significantly increased and stabilized with help of the AB system.

5. **Comparison of active and passive balancing by a long term test including a post-mortem analysis of all single battery cells** [111]
   In this own work, one battery with an active and one with a PB system are aged by full cycles. After about 2600 cycles test is stopped to start with further investigations. Capacity decrease and the increase of internal resistance of the two used battery packs and its cells are presented. Active balancing increases the usable capacity by a maximum of 2% compared to PB and reduces the cell to cell deviation of capacity and internal resistance.

5.1.3 Summary

A large number of comparisons between different balancing options can be found in the literature, which can be basically divided into comparison by simulation and comparison by measurement.
At first glance, it becomes clear that there seems to be sufficient literature available in the area of theoretical comparisons. There are many reasons to compare these systems in a simulation. Examples are the low costs for a necessary test environment and test equipment, the avoidance of dangers when handling LICs and the enormous time savings. Due to the large num-

ber of simulation approaches chosen, it is difficult to compare them with each other in order to obtain consistent statements.

However, some consistent and important statements can be derived:

1. AB has considerable (various, not always precisely described) advantages over conventional PB such as
   - balancing speed,
   - efficiency,
   - increase in usable capacity.
2. The control of an AB circuit is generally described as complex and computationally demanding.
3. Active balancing is described as expensive.

A large number of articles attempt to select the most suitable balancing circuits for a specific application by means of appropriate comparison. Further, especially younger articles, refer to literature research and then compare various other aspects by means of reviews and overviews of existing solutions. These articles seem to avoid data collection or own new simulation approaches. The literature research reveals that many authors assume battery models can sufficiently reproduce the electrochemical behaviour in the battery cycle. However, they quickly reach their limits when approximating the complex ageing processes.
When searching for comparisons by measurement, only very few examples could be found in literature beside the own measurements presented in the past. It is clear that existing comparisons of measurements can only be performed with a low number of cells and only stressing them with small numbers of cycles. The processes in cell groups are known to be complex and can therefore not be adequately covered by the presented approaches with small numbers of cells in series and partially missing parallel circuits. The effects of tolerances in cell production and design related effects within the battery might not come into effect. A statistically significant statement regarding the effects of AB on real cells could not be achieved by the researched literature nor by own measurements presented.

5.2 Objectives of the Chapter

The above described gap in the literature which is caused by measurements with low statistic significance, shall be addressed in this chapter. For this purpose, a series of measurements with uniform test conditions is to be carried out which represent the behaviour of batteries with AB and PB over their entire lifetime. Statistical significance is to be achieved by using more than one identical battery per test. Consistent and controversial statements from the existing literature can thus be validated.

The following objectives are to be achieved in this chapter:

- Investigation of the ageing process of identical batteries under the same charge-discharge conditions, but different BMS systems.
- Identify performance variations (e.g. capacity, service-life, efficiency) caused by the application of AB, compared to PB.
- Examine the influence of different battery configurations and battery loads on the ageing behaviour the batteries with their battery management systems.
- Observe and interpret the development of battery internal cell parameter variation over the complete service life.
- Elaboration of statements on potential battery applications for AB, depending on battery type and load.

5.3 Experimental Study Design

For ageing battery packs, there is an almost unlimited variety of operating modes and load types. This needs to be limited in this experiment, but still contain a minimum amount of variance in order to achieve the objectives described above. Furthermore, limitations arise from the presumed long test duration for battery ageing in combination with the limited number of test benches. A few essential findings from the literature are motivating to design the experiment as follows. Firstly, the type and amount of the load on the battery directly influences the ageing rate [112, 113]. Further, several sources show that the ageing is affected by or leads to a parameter variation of the individual cells [114, 115, 116, 117]. Lastly, it can be derived from [118], that the behaviour of the individual cells and battery lifetime can be affected by the amount of cells connected in parallel. Including the literature insights of this work, all mentioned parameters are likely to have a direct effect on the operating behaviour of the BMS.
Thus, the battery load and the battery configurations (cells in parallel) are varied in the experiment, as can be seen in Figure 5.1. Each marked point represents a long term comparison test between an actively balanced and a passively balanced battery with identical test conditions.

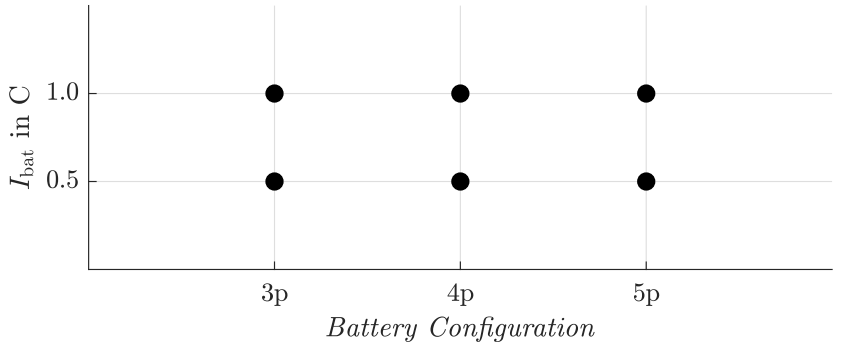

Figure 5.1: Test matrix of performed ageing experiments. Each test is a comparative long-term measurement of two 12s battery packs.

5.3.1 Test Conditions

The overall experiment is carried out with 12 battery packs, of which two identical batteries are operated together in a comparison test. The main dif-

ference here is the connected BMS system. One battery is operated with the active BMS presented in Chapter 4, the other with a conventional passive BMS as described in Chapter 3.1.1. As described above, the configuration of the battery (number of parallel cells) and the battery load are chosen accordingly to Figure 5.1. More detailed information on other selected components and test conditions are explained in the following paragraphs.

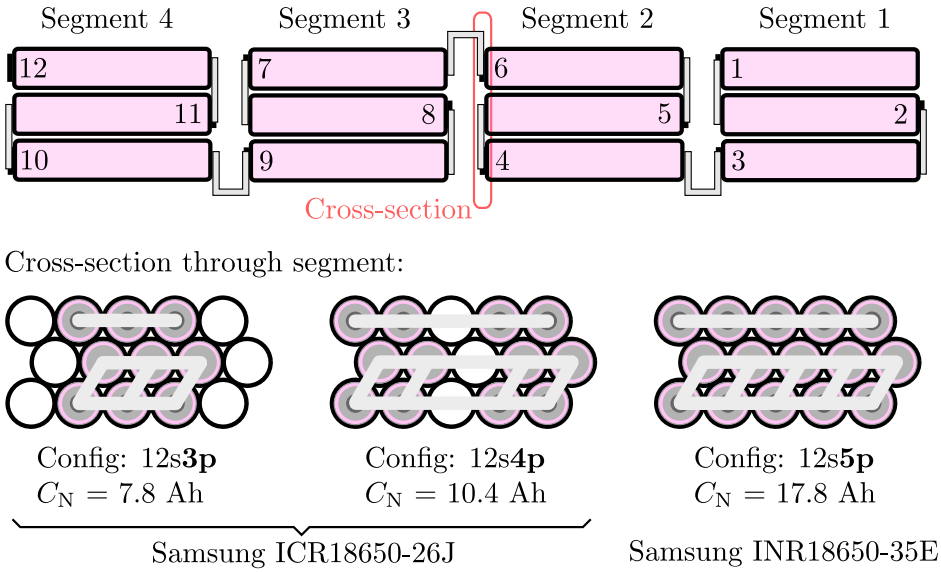

Figure 5.2: Overview of the modular battery design and technical data. 12 cell levels in series connection are separated into 4 segments, which are constructed depending on the configuration.

Battery Pack

Commercial batteries are purchased for the experiment as it is not possible to produce identical batteries of sufficient quality within the given circumstances. In the selection process, the focus has been on a modular battery type with high-energy cells that is already available on the market. After a market research, the choice fell on the manufacturer "Bafang", which supplies e-bike batteries of the same type, but with different nominal capacities. The nominal voltage is specified identically with 43 V (12 cells in series). The different nominal capacity results from the different number of parallel cells (e.g. 3p, 4p, 5p), although the design of the battery does not change.

The manufacturer uses two different cell types, which is acceptable in view of the planned comparative tests of two identical batteries (same cell type). As can be seen in Figure 5.2 the positioning of the battery cells in the battery housing changes.

Battery Management Systems

For the active balanced batteries, the system described in Chapter 4 is used. Variable parameters, as explained in Chapter 4, are predefined according to test conditions and the cell chemistry. They are configured according to Table 5.1. For more information and technical data also see Appendix A.1 The PB is carried out by a laboratory system. This system is constructed according to Figure 3.4 b). Balancing is activated as soon as the cell voltage exceeds 4.175 V and remains active until it falls below this value again. Balancing takes place in intervals of 10 s with a subsequent pause of 1 s for voltage measurement. The balancing current is 100 mA.

Parameter	Value	Description
t_{meas}	100 ms	Voltage/Current measurement interval.
I_{b}	1.7 A	Balancing current.
t_{step}	10 s	Duration of balancing intervals.
U_{tb}	4.1 V	Start of voltage based balancing.
U_{lim}	15 mV	Tolerance for voltage based balancing.
U_{cb}	3.1 V	End of capacity based balancing.
Q_{lim}	4.7 mAh	Tolerance for capacity based balancing.

Table 5.1: Preconfigured parameters in the AB system.

Ageing Cycle

In order to not extend the duration of the experiment, full cycles are used and thus the voltage limits of the battery cells are almost completely exploited. In [119] it is shown that the conservative adjustment of the voltage limits or the use of partial cycles in a smaller, medium SOC window considerably extends the service life of the battery cell. The single cells are operated between 2.95 V and 4.175 V, resulting in voltage limits of 35.5 V and 50.1 V for the packs. The lower voltage limit of the pack is usually not

reached, as the discharge is stopped as soon as one single cell's voltage falls below the allowed minimum voltage. According to the cell data sheet, the absolute maximum voltage ratings are not reached for greater test safety reasons by protecting the packs against overcharging and deep discharging. The load currents for the battery are taken from the cell data sheets. Here, 0.5C (for standard charging) and 1.0C (for fast charging) are given. To avoid further variations, the discharge currents in this experiment are chosen to be identical to the charge currents. The batteries are thus charged and discharged with a constant current of 0.5C / 0.5C and 1.0C / 1.0C respectively. The reason for this is the self-built AB system, which in its current configuration within this first long-term application can only achieve sufficient accuracy at constant charging and discharging currents. The constant voltage phase of the charging process is stopped when the current drops below 0.05C. A complete ageing cycle is shown in Figure 5.3.

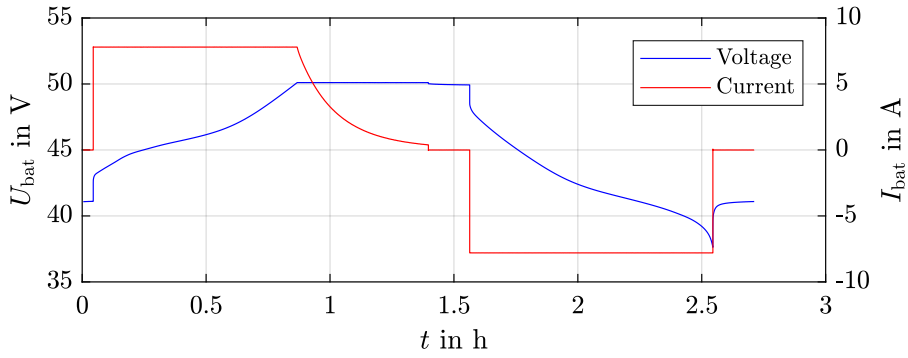

Figure 5.3: Full ageing cycle with $I_{\mathrm{bat}} = \pm 1.0\mathrm{C}$ (± 7.8 A) using a 3p ($C_{\mathrm{N}} = 7.8$ Ah) battery pack.

Ambient Temperature

Literature has already shown that the variation of ambient temperature can have a major impact on battery ageing [120]. In this work, the ambient temperature should not cause any additional influence on the experiment. In order to neither accelerate nor slow down battery ageing, an average room temperature of 25°C is chosen as the ambient temperature.

5.3.2 Test Procedure

After the arrival of the batteries, their batch number is checked to ensure that the two batteries for the comparison test are identically built and have the same age. Then the battery case is opened and all cell voltages are measured. In the next step, the standard BMS is removed and the connections required for the active and passive BMS as well as current measurement and the safety temperature sensors of the battery tester are installed. From now on, the BMS is located outside the battery. All necessary connections are routed out of the battery housing by a cable duct. The battery is then closed again and positioned in the climate chamber for cycle ageing. The internal resistances of all cells are calculated using the current pulse method during the first battery cycle. Afterwards, the described ageing cycle is repeated by a battery test system until the battery reaches a residual capacity of 60% or less. During this test duration, the parameters mentioned below are recorded for later evaluation. The test duration itself is variable and depends on the ageing behaviour of the batteries. Once the ageing process is complete, the battery is disconnected from the test system and the BMS is removed again. Finally, the battery gets completely disassembled in order to be able to examine the individual cells separately, explained in a separate chapter. The test procedure for each battery is shown in Figure 5.4. For more information and technical data about the test bench see Appendix A.2.

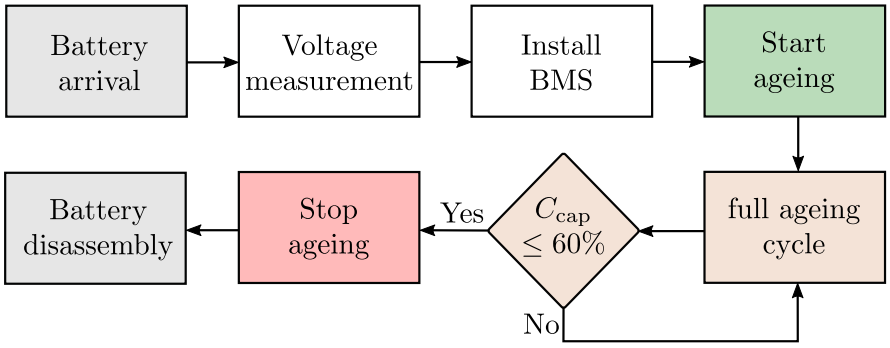

Figure 5.4: Test procedure for all battery packs.

Measured and Calculated Parameters

This subsection lists measured and calculated parameters by the battery test system that are necessary for generating the test results.

Voltage and Current:
The battery test system continuously records the battery voltage and current as well as all cell voltages during the measurement. The measurement interval is set to 1 s.

Capacity:
The capacity of the battery is recorded during each battery charge and discharge. The measured current is integrated for this purpose analogously to Equation 2.1 during the charging/discharging.

Internal Resistance:
The internal resistance is determined using the current-pulse method presented in Chapter 2.5.1. The time difference between the two voltage measurement points is defined as 1 s. This is done in accordance with various published literature in which the measurement interval is defined between 0 s and 10 s and in particular in the range of 1 s in comparison to impedance spectroscopy [115]. In order to make the measurement comparable in each cycle, it is performed at a SOC of 100%.

Equivalent Full Cycles:
In addition to the term cycle, equivaltent full cycles EFC (both defined in Chapter 2.2) is mainly used for evaluation. For this purpose, the total amout of charge removed in the service life of the battery is divided by its nominal capacity:

$$EFC = \frac{\Sigma Q_{\text{disch}}}{C_{\text{cap,N}}} \tag{5.1}$$

Energy Efficiency:
To calculate the energy efficiency η_{bat} (in percent) of the battery, the amount of energy extracted by the battery test system during the discharging process is divided by the energy added during the charging process:

$$\eta_{\text{bat}} = \frac{E_{\text{disch}}}{E_{\text{ch}}} * 100 \tag{5.2}$$

Voltage Spread:
The voltage spread is determined at the switch-off point at the end of the discharge process. For this purpose, all cell voltages are measured and the maximum difference inside the pack is determined:

$$\Delta U_c = U_{\mathrm{c,max}} - U_{\mathrm{c,min}} \tag{5.3}$$

Further Evaluation Methods

This subsection describes calculation methods that are necessary for generating the test results from the measurement data.

Calculation of balanced charge per cell:
In order to obtain the charges balanced by the active BMS in each cycle, an automated algorithm is used for calculation. In a prior investigation, it was found that the balanced charge amounts cannot be taken directly from the data calculated by the BMS. Individual balancing pulses (e.g. between directly adjacent cells) can influence each other, which means that the charge values stored in the BMS may not be equal to the actual balanced charge quantity. Furthermore, the balancing process of a cell inevitably leads to current flows and thus charge transfers in other cells, which cannot yet be recorded by the BMS. A calculation of the actually balanced charge is therefore only possible by looking at each balancing process individually.
The first step of the calculation is to detect the voltage pulses of the balancing processes in the voltage curves of the cell levels within the battery pack. To detect an edge, two adjacent points on the voltage curve are compared. If their difference is greater than a positive threshold value, the algorithm counts this as a rising edge, but if the difference is less than the negative threshold value, it is a falling edge. In order to recognise which pair of edges generates a balancing pulse, the time duration t_{step} defined above is used. The algorithm now compares the appearance of the edges over time and identifies the individual balancing processes from this. Figure 5.5 shows the detection of the edges and their marking.

The calculation itself is done in three steps. First, Equation 4.30 is used to determine the amount of charge that is theoretically balanced by a balancing pulse. In approximation, the algorithm now assumes that this leads to the average pulse height $V_{\mathrm{p,avg}}$, which corresponds to a kind of standard pulse.

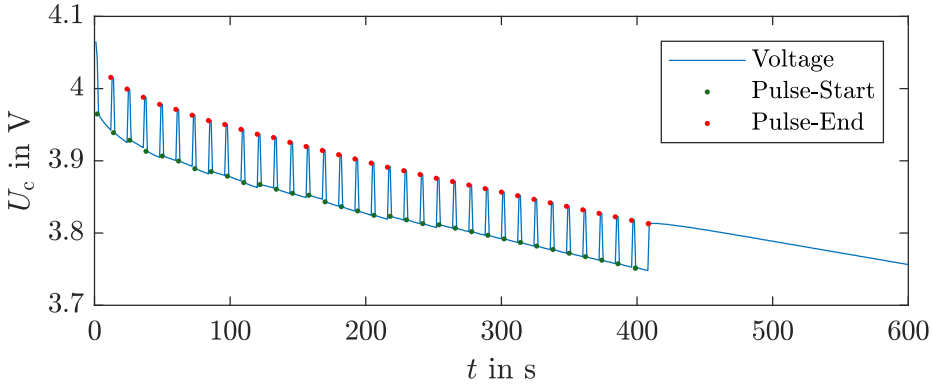

Figure 5.5: Detection of balancing pulses for balanced charge calculation on a single cell. In this specific output of the matlab script, a single cell gets additionally discharged by the active balancer during full battery discharge.

To determine how often this standard pulse occurs during the discharge, the pulse heights (voltage difference V_p) of all detected pulses are determined in the second step. This is done using the voltage difference immediately after the start/end of the pulse. In the third step, the actual balanced charge is calculated using the ratio between the sum of all pulses $V_\mathrm{p,sum}$ and the standard pulse $V_\mathrm{p,avg}$:

$$Q_\mathrm{b} = \frac{V_\mathrm{p,sum} \cdot Q_\mathrm{step}}{V_\mathrm{p,avg}} \tag{5.4}$$

Capacity Spread:
The balanced capacity Q_b is determined separately for each cell, as shown in Figure 5.6. This results in the value $Q_\mathrm{b,max}$ with a positive sign for the cell that receives the most energy from the balancer and the value $Q_\mathrm{b,min}$ with a negative sign for the cell from which the most energy is removed. The balanced charge Q_b thus also corresponds to the capacity deviation of each cell from the average of all cells. The capacity spread of all cell levels ΔQ_c is thus determined from the two extrema of Q_b:

$$\Delta Q_c = Q_\mathrm{b,max} - Q_\mathrm{b,min}\ , \quad Q_\mathrm{b,min} < 0 \tag{5.5}$$

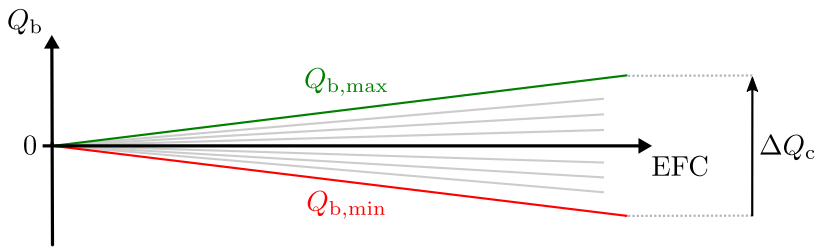

Figure 5.6: Schematic illustration of Q_b development and ΔQ_c calculation.

Determination of capacity and service life gain:
To illustrate the differences in the ageing behaviour of two batteries, the capacity gain and the service life gain are analysed. To determine the gain in capacity the capacity of both batteries is compared for the same number of completed EFC and the difference is calculated, such as at EFC_1 in Figure 5.7. This results in a capacity difference in percent, for each completed EFC. The capacity difference can be determined until one of the two batteries reaches the end of the test at a residual capacity of 60%. To determine the service life gain, the number of EFC is compared at a constant relative capacity, such as at 80% in Figure 5.7.

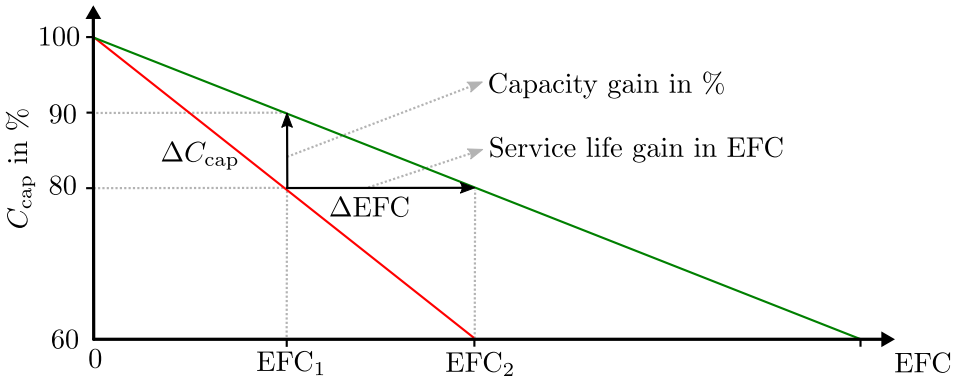

Figure 5.7: Schematic illustration of capacity and service life variation between the ageing curves of two batteries.

5.4 Results and Discussion

In this section, the measurement results generated during the ageing of the packs are presented and discussed.

5.4.1 Initial State of Battery Packs

Before starting the test, all cell voltages within the battery packs were measured using a multimeter and the internal resistances of the individual cell levels were determined using the current pulse method. It is expected, that an industrial, well-assembled battery has only small tolerances in these measured values. It is also important for this test approach that the two batteries within the comparison tests have similar values. The measurement data are presented in Table 5.2. As expected, it becomes clear that depending on the battery configuration, the internal resistance of the cell levels decreases with a higher number of parallel cells. All cells voltages are in the range of their nominal voltage of 3.6 V.

Battery-ID	$V_{c,min}$	$V_{c,max}$	ΔV_c	$R_{DC,min}$	$R_{DC,max}$	ΔR_{DC}
3p 1.0C AB	3.586 V	3.596 V	10 mV	16.5 mΩ	18.5 mΩ	2.0 mΩ
3p 1.0C PB	3.589 V	3.590 V	1 mV	17.0 mΩ	18.9 mΩ	1.9 mΩ
3p 0.5C AB	3.580 V	3.590 V	10 mV	17.5 mΩ	19.4 mΩ	1.9 mΩ
3p 0.5C PB	3.580 V	3.590 V	10 mV	17.4 mΩ	19.4 mΩ	2.0 mΩ
4p 0.5C AB	3.590 V	3.590 V	0 mV	12.4 mΩ	14.4 mΩ	2.0 mΩ
4p 0.5C PB	3.580 V	3.590 V	10 mV	12.6 mΩ	14.7 mΩ	2.1 mΩ
4p 1.0C AB	3.636 V	3.637 V	1 mV	11.9 mΩ	12.6 mΩ	0.7 mΩ
4p 1.0C PB	3.631 V	3.632 V	1 mV	12.0 mΩ	13.0 mΩ	1.0 mΩ
5p 1.0C AB	3.655 V	3.656 V	1 mV	5.9 mΩ	6.9 mΩ	1.0 mΩ
5p 1.0C PB	3.635 V	3.647 V	12 mV	6.1 mΩ	7.0 mΩ	0.9 mΩ
5p 0.5C AB	3.522 V	3.533 V	11 mV	4.9 mΩ	6.3 mΩ	1.4 mΩ
5p 0.5C PB	3.540 V	3.541 V	1 mV	4.9 mΩ	6.4 mΩ	1.5 mΩ

Table 5.2: Measured initial battery pack parameters.

The age of the battery packs is compared by their serial number before the start of the test. However, this serial number cannot be decoded for a production date. But a slight numerical deviation might indicate that the batteries were produced at approximately the same time. The production date of the cells in the battery can only be determined after the end of the test when the batteries are disassembled. Then it is possible to read the pro-

duction stamp affixed to the cells. From this, in contrast to the packs, the age can be decoded. Looking at Table 5.3 it becomes clear that the 5p 0.5C test has inconstancies in its cell age and has to be considered separately.
In conclusion, with the help of both tables, it can be stated that the measured input parameters at the beginning of the ageing do not contain clear indications of a different battery age or any other inconstancies, which is why it was not possible to prevent the invalid test before starting the test.

Battery-ID	Prod.-Stamp	Decoded-Date	Descripion
3p 1.0C AB	TIW3	08.2018	same age,
3p 1.0C PB	TIW3	08.2018	test valid
3p 0.5C AB	TJR3	04.2019	same age,
3p 0.5C PB	TJR4	04.2019	test valid
4p 0.5C AB	TJR4	04.2019	same age,
4p 0.5C PB	TJR4	04.2019	test valid
4p 1.0C AB	KM1T	—*	same age,
4p 1.0C PB	KM1T	—*	test valid
5p 1.0C AB	IH2T	02.2017	same age,
5p 1.0C PB	IH1T	01.2017	test valid
5p 0.5C AB	JF4T	04.2015	different age,
5p 0.5C PB	2JB3	11.2019	test invalid

*decoding not possible

Table 5.3: Comparison of cell age in battery packs.

5.4.2 Capacity and Internal Resistance Development

The ageing curve of capacity and internal resistance of the tested batteries is described below and can be found in Figure 5.8. The figure is divided into 3 rows and 2 columns, each row corresponding to one of the 3 battery configurations 3p, 4p and 5p. The columns show separately capacities and internal resistances. When comparing the plots, it should be noted that the axis scaling of all x- and y-axes was set identically for easier comparison. An exception exists for plots e) and f), where the x-axis limits had to be chosen larger due to the significantly longer service life of the 5p batteries. The explanations of individual ageing effects are based on literature from the Chapters 2.1 and 2.3.

On the y-axes of plots a), c) and e) the capacity is displayed in relative values. The relative capacity refers to the averaged capacity of the batteries

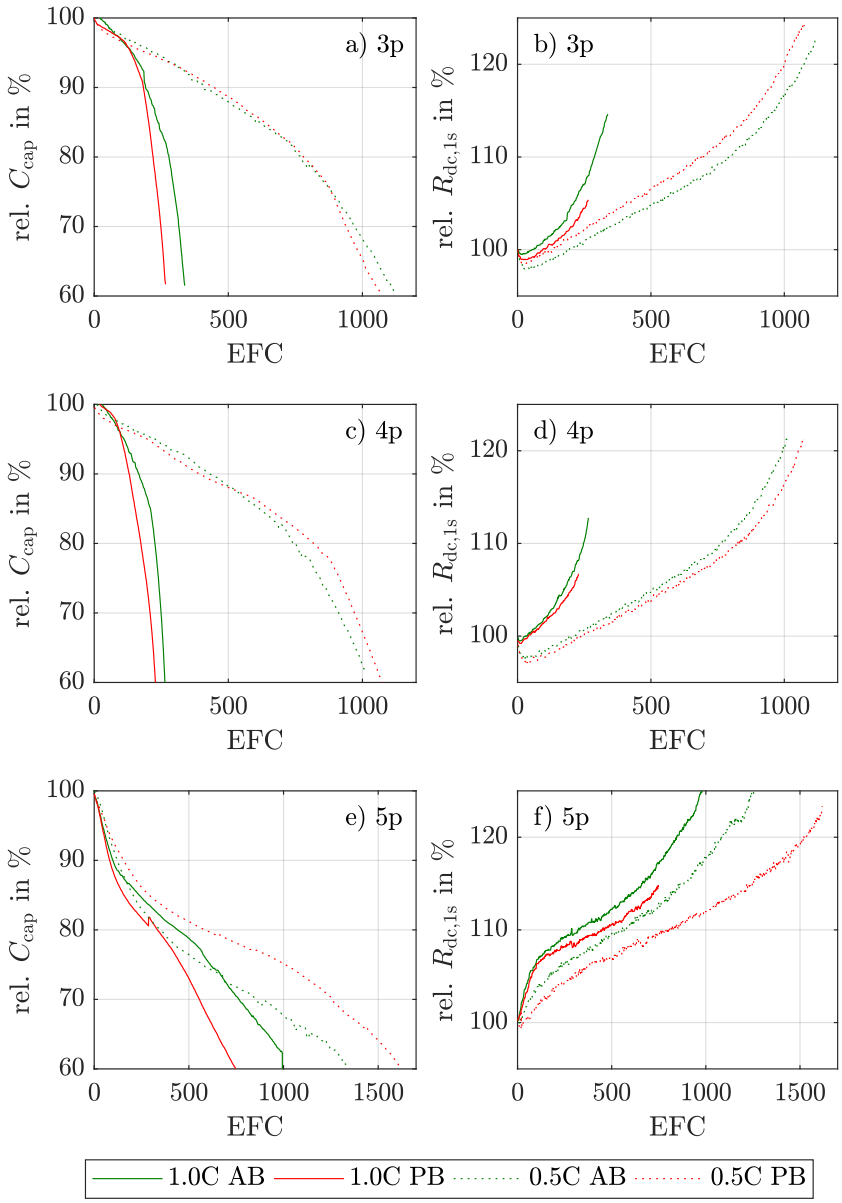

Figure 5.8: Capacity and Internal Resistance during ageing process. Figures a) and b) show 3p batteries, c) and d) show 4p batteries and e) and f) show 5p batteries.

measured within the first 5 cycles. Plots b), d) and f) show the internal resistance of the batteries in relative values, also related to the averaged resistance within the first 5 cycles. Relative values were chosen to make it easier to see the differences that occur during ageing, and are considered to be common in the literature. The different absolute starting values can be taken from Table 5.2. Significant differences at the beginning of the measurement do not exist. Due to a calculation error of the relative capacity, the ageing of the two packs exposed to 1.0C in plot a) ended slightly too early.
Looking at the ageing behaviour of all capacities from plots a), c) and e) in general, the transition from a more or less linear (no lithium plating) to exponential ageing (with lithium plating) is clearly recognisable in a) and c). What is different, however, is the starting point of exponential ageing. In all batteries aged with 1.0C, this happens earlier than with 0.5C. Linear ageing is almost not visible here, which leads to the impression that lithium plating is the main cause of ageing. In contrast, all packs with 0.5C load have a more linear ageing start suggesting that only the SEI film in the cells grows before lithium plating finally sets in. The internal resistances shown in plots b), d) and f) behave similarly. Decreasing battery capacity is associated with an increase in internal resistance.
When looking at the service life it becomes visible that the battery load is mainly responsible for differences in the ageing rate. In this experiment, halving the charging and discharging currents leads to an approximated increase in service life by a factor of 3. In contrast to plots a) and c), a different result becomes visible in e). Here, the batteries with a lower load also last longer, but only by about 50% of the service life. The main reason for this is the changed ageing behaviour of the 5p batteries, which age significantly slower than the 3p and 4p packs. Several reasons for this could be identified in the context of this work. Firstly, the lower internal resistances known for NCA chemistry compared to NMC ensure lower thermal losses within the battery, as well as the permissible discharge current of the NCA cells used in e) is higher than that of the NMC cells in a) and c). Furthermore, the test evaluation shows that the 5p1.0C tests only reached the intended battery load of 1.0C during discharging but not during charging due to a power limitation of the battery tester. The affected packs were only charged with an average of about 0.6C, which indicates slower cell ageing. Finally, a chemical-dependent characteristic can be taken from the ageing curves. While the capacity curves for NMC always start with a low but increasing gradient, NCA initially shows a high but decreasing gradient. However, the gradient increases again at a later stage.

The development of the internal resistance also depends on the cell chemistry. While the 3p and 4p packs in plots b) and d) start with a low but increasing gradient, the internal resistance increase of the 5p batteries in plot f) show a high but decreasing gradient behaviour, which changes into an increasing gradient after a turning point with increasing age. While the capacities always end at 60% according to the test approach, the internal resistance curves have different end values. At a battery load of 1.0C, the actively balanced batteries often run a little longer. Therefore they show higher internal resistances. The actively balanced packs also show a slightly faster increase in internal resistance. The permanent charge transfer between the cells is associated with a permanently higher charge throughput in the cells and therefore seems to have a negative effect on the internal resistance. If AB is used, the internal resistance increases faster except for the 0.5C test in plot b).
For all packs with a load of 0.5C, the longer service life also results in higher internal resistances. Here it can be concluded that the internal resistance can increase further because less active lithium is lost in the cells during slower ageing. The cell thus simply has more time to develop higher internal resistances, for example through thicker passivation layers

Focusing on the different BMS, it can be observed in a), c) and e) that AB at 1.0C load leads to slower ageing behaviour compared to PB, whereas at a lower load of 0.5C, this trend can be seen at plot a), but not in c). Various reasons for this are explaind in the following sections. The ageing behaviour of the 0.5C batteries in e) differs due to the different battery age as the significantly older actively balanced battery ages significantly faster.

Finally, the curves allow the general conclusion that a variation of the battery load in the range of 0.75C, i.e. exactly between the loads selected in this test approach, would also lead to an intermediate ageing behaviour. Loads below 0.5C would further extend battery life, loads beyond 1.0C would accordingly shorten it even further. According to initial findings, AB seems to show significant positive effects especially at high loads. At lower loads, the results are inconsistent.

5.4.3 Voltage Spread

The voltage spreads at the end of the discharge process shown in Figure 5.9 provide insights and explanations about the loss the battery capacity and the effects of the BMS used. The calculated voltage differences ΔU_c of the packs are plotted in the same y-axis scaling over EFC.

Plot a) shows all batteries with a 1.0C load. It can be seen that the voltage difference of all actively balanced batteries is below that of the comparable passively balanced batteries. While the AB already adjusts the voltage difference to a stable level within the first cycles, the PB needs more than 100 equivalent full cycles to balance/optimise the battery. In this case, the PB reaches a minimum voltage difference between the cells after some time, but can no longer have a reducing effect on the voltage difference as the number of cycles increases. In case of the 5p batteries, the voltage deviation is initially even smaller than the BMS could influence within the scope of its accuracy. However, the deviation increases with increasing number of cycles and reaches the influence range of the BMS after approx. 100 EFC. A reason why the voltage spread of the 4p batteries increases earlier than the 3p batteries cannot be provided in this work, but indications can be found, for example, in the battery structure shown in Figure 5.2. While in the 3p and 5p configuration the cells are arranged directly next to each other, the cells of the 4p battery are further apart, which could cause a more inhomogeneous parameter variation due to possible temperature differences. Corresponding temperature measurements of all individual cells were not implemented. The homogeneity of the batteries, which is assumed in the experimental study design to increase with an increasing number of parallel cells, cannot be confirmed in this experiment.

Active balancing aims to ensure that all cells reach their final discharge voltage at the same time. Thus, as a direct effect of AB, keeps the voltage difference constant on average. While the voltage difference of passive batteries begins to rise with increasing cycles, AB manages to stabilise the voltage differences in the range of 100 mV to 120 mV with only a slight upward tendency. In general, an increasing voltage difference is a direct indication that the parameter dispersion of the individual cell levels in the battery pack increases with increasing number of cycles. The associated capacity difference is compensated by AB as long as the available balancing current and available balancing time shown in Chapter 4.1.2 are given. If the active balancer reaches its power limit or doesn't have sufficient time to finish balancing, the voltage difference suddenly rises sharply. A few cycles

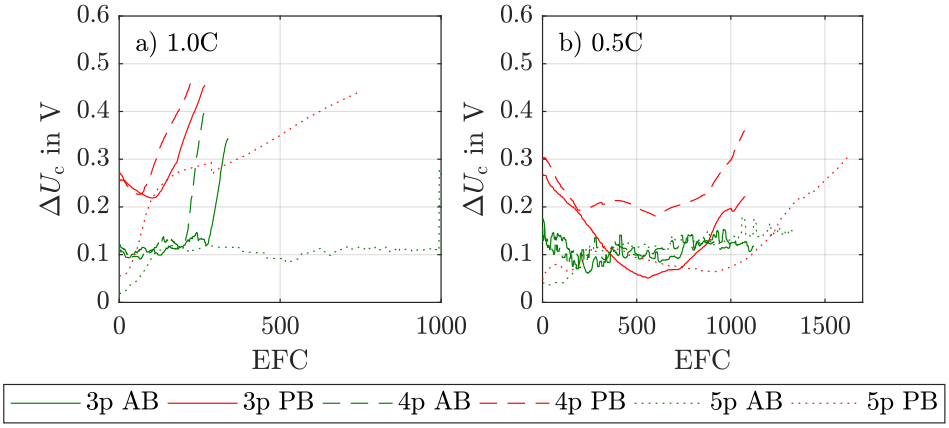

Figure 5.9: Battery voltage spread at end of discharge during ageing process. Figure a) shows all batteries with $I_{\text{bat}} = 1.0\text{C}$ and Figure b) all batteries with $I_{\text{bat}} = 0.5\text{C}$.

later, the battery reaches its end of life. It can be stated that the available balancing current of 1.7 A was not sufficient any more for the battery load of 1.0C. If a higher balancing current is selected or is increased during ageing, the voltage spread can be kept constant for a longer time and the service life of the batteries is further extended.

Plot b) shows all batteries subjected to a load of 0.5C. Due to the lower load, lower voltage differences are achieved, which is also due to the lower influence of the internal resistances. For example, the highest measured voltage difference at 1.0C is 473 mV and at 0.5C only 359 mV, which corresponds to a decrease of almost 25%. The voltage difference and thus the parameter variation of the cell levels is lower over the entire lifetime.
Basically, the progress of the ΔU_c values is similar to plot a), but the development takes place much more slowly and reaches lower end values. The passive BMS can prevent an increase of the voltage difference up to approx. 500 EFC (3p, 4p) or approx. 900 EFC (5p), the active BMS achieves this over the complete duration of the test. A sudden increase as in plot a) is not visible here. Due to the seemingly smaller deviation of the cell parameters in connection with the longer discharge time due to lower load, the set balancing current seems to be sufficient here.

Shown in this experiment, the increasing voltage differences between the cells are equivalent to an increasing switch-off voltage of the entire battery.

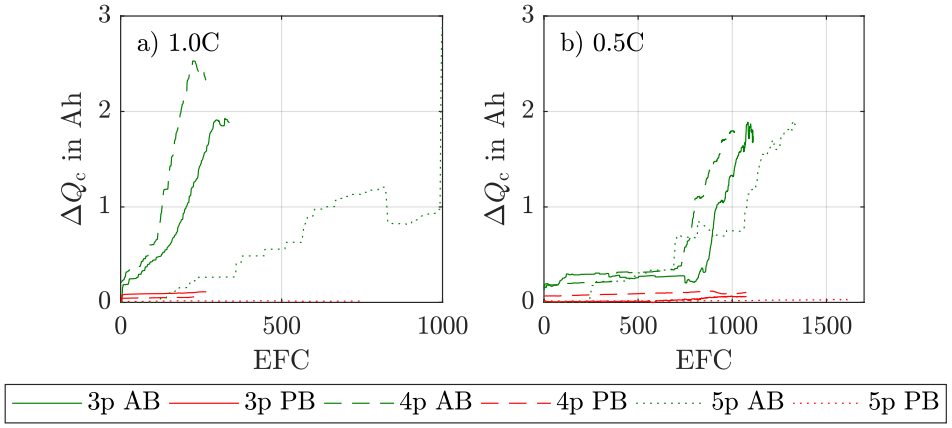

Figure 5.10: Balanced charge spread of internal cells during ageing process. Figure a) shows all batteries with $I_{bat} = 1.0C$ and Figure b) all batteries with $I_{bat} = 0.5C$.

The greater the voltage difference and the parameter variation of the cells, the earlier the entire battery must be switched off, as shown in Chapter 2.6. The usable amount of energy is thereby reduced further and further.

5.4.4 Balanced Charge and Capacity Spread

The balanced charge by the BMSs is calculated as explained in the evaluation methods section. The resulting balanced charge Q_b for each cell level is converted into a capacity spread ΔQ_c. The complete calculated curves of Q_b for all cell levels are shown in the Appendix B for better understanding. The resulting values of ΔQ_c are plotted on the y-axis of the plots in Figure 5.10 over EFC. The y-axes are scaled equally, the x-axes are adapted to the different lifetimes depending on the battery load.

The comparison between all actively balanced batteries and all passive batteries in plots a) and b) shows the most significant difference right at the beginning. While the balanced charge difference of the passive BMS is very small over the entire ageing process and only increases slightly, clear differences and a sharp increase in ΔQ_c are visible with AB. This demonstrates the design-related differences of the various topologies and their possibilities explained in Chapter 3.1.

In plot a), the values for ΔQ_c increase steeply for the actively balanced 3p and 4p batteries, which indicates a rapidly developing parameter variation. A sudden reduction of the balanced charge after reaching the maxima is also visible. This happens when the active balancer does not have enough time to finish balancing. In practical terms, the discharge of the battery is completed before the balancer has fully balanced the capacity differences of all cells, which inevitably leads to a decrease in the balanced charge amount. From this point on a kind of chain reaction starts as the shortening discharge time means that less charge can be balanced. However, the incomplete balancing leads to a higher deviation of the cells and thus to a shorter discharge time again. In summary, as already observed with the voltage spread, this results in a rapid end of the service life of the affected battery.
The 5p battery shows a slower increase of ΔQ_c, which indicates a slower developing parameter variation. The obvious jumps in the curve could be attributed to calculation problems of the balancing algorithm but can in general also indicate sudden parameter changes of the cells within the battery. As main reason the lower internal resistances of the NCA cells are responsible for the calculation problems. Since the balancing algorithm is based primarily on the measurement of voltage and current, the effects of the parameter changes must have a significant effect particularly on the measured values of the cell voltages in order to be detected. The voltage changes caused by parameter variation of the individual cells are mainly dependent on the influence of the internal resistances in addition to the cell capacity. However, these were so low in the scope of the test that they remained within the tolerance band of the balancing algorithm presented in Chapter 4.2.3 over longer periods of time. Only when the tolerance band was left after several cycles a sudden change in the balanced charge occurred.
Towards the end, this kind of sudden increase in ΔQ_c (again in analogy to ΔU_c) also marks the end of life. In this case, the analysis revealed that a single cell had actually failed and was no longer functional after the battery had been disassembled. Important indications for the failure of the individual cell could thus be revealed while the battery was still in operation by the calculation methods of the active balancer.

In plot b), the values of ΔQ_c initially remain relatively constant. Due to the low battery load of 0.5C, there are only minor parameter variations at first, which remain constant on average over a longer period of time. After 700 to 850 EFC, a characteristic steep increase of the values of ΔQ_c appears in analogy to plot a). In the period before this, the active balancer thus has little to no influence on the ageing behaviour of the battery due to the

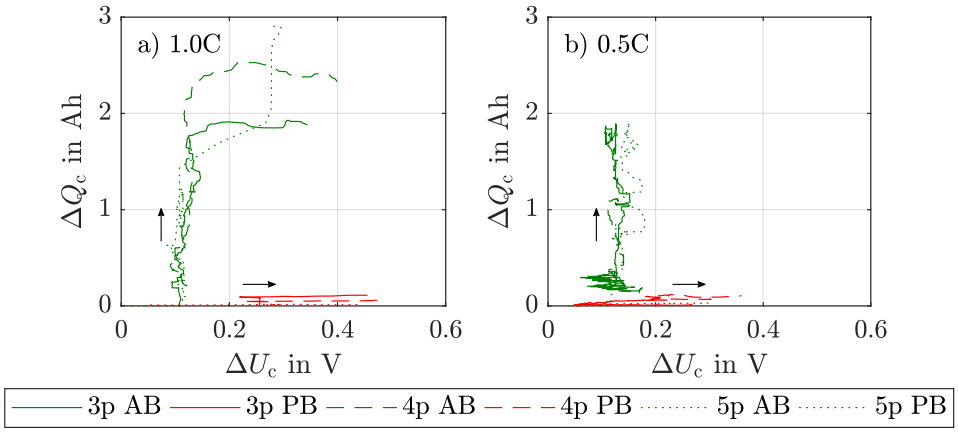

Figure 5.11: Correlation between balanced charge spread ΔQ_c and voltage spread ΔU_c. Figure a) shows all batteries with $I_{bat} = 1.0C$ and Figure b) all batteries with $I_{bat} = 0.5C$. Arrows indicate the increasing cycle number.

low balancing charge, similar to the passive balancer. For instance, the experiment shows with the 0.5C batteries in Figure 5.8 a) and c) that the batteries develop differently during this period without much impact from the balancer.

In order to provide a better understanding of the correlations between the measured values and the BMSs used, a comparison with the voltage spread from Figure 5.9 seems to be useful here. The voltage difference of the passive packs increases significantly during ageing, while the balanced charge quantity does not change. In contrast, the voltage difference of the active packs remains approximately constant, while ΔQ_c is further increasing. The effect of AB thus becomes clearly visible, as well as the obvious disadvantages of PB with regard to the possible charge redistribution between the cells. A combined illustration of voltage spread and capacity spread is suitable to show cell deviation during the test, as this can only be visible using the value changes of ΔQ_c for AB and ΔU_c for PB. In Figure 5.11, the values of ΔQ_c on the y-axis are plotted against those of ΔU_c on the x-axis to visualize the relationships mentioned above. It becomes evident that the parameters of the individual cells deviate more and more from each other with increasing numbers of cycles regardless of the BMS used.

In summary it can be stated that the occurrence of parameter variation and thus the values of ΔQ_c are mainly dependent on the battery load. The ac-

tive balancer intervenes significantly earlier at high battery load than at low load. If the parameter deviation of the cells is small or difficult to detect within the measurement tolerance, the balancer cannot reliably influence the ageing process of the battery in a positive way.

5.4.5 Energy Efficiency

The energy efficiency is plotted over EFC in Figure 5.12. Plots a) and b) again separate the batteries with a load of 1.0C and those with a load of 0.5C. The scaling of the y-axis was chosen identically as in previous chapters. The x-axis is adjusted to the different lifetimes of the batteries.

Regardless of the test conditions, the energy efficiency depends on the internal resistance of the batteries. The internal resistance affects the battery as a further consumer within the equivalent circuit (see Figure 2.5 a)) from an electrical point of view. The energetic losses at the internal resistances are therefore linearly dependent on its absolute value and quadratically dependent on the selected battery current. Plot a) shows that the 5p batteries have a generally higher efficiency due to the lower internal resistance. Comparing plot a) to b), it becomes visible that the lower load of the batteries from plot b) leads to lower losses at the internal resistance and thus to a higher efficiency.

In both plots it can be seen that with increasing number of cycles, the efficiency of the actively balanced packs is always lower than that of the comparable passive packs. This is due to the energy efficiency of the balancing itself. While the amount of energy balanced in PB is equivalent to a loss of energy, in AB the energy is not directly lost. However, the efficiency of the power electronics required for AB is certainly not ideal. If the amount of energy to be balanced continues to increase during the duration of the test, AB can produce higher losses than PB. Comparing Figure 5.12 with Figure 5.10, as described above, shows the correlation between the amount of charge balanced and the energy efficiency. If the charge difference ΔQ_c between the cells rises sharply, the energy efficiency of the battery drops due to the energy losses of the power electronics. This can be observed consistently in all tested batteries.

The expected increased efficiency through AB described at the beginning of the chapter must therefore be considered in a very differentiated manner. Of course, an increased capacity of the battery through AB can improve

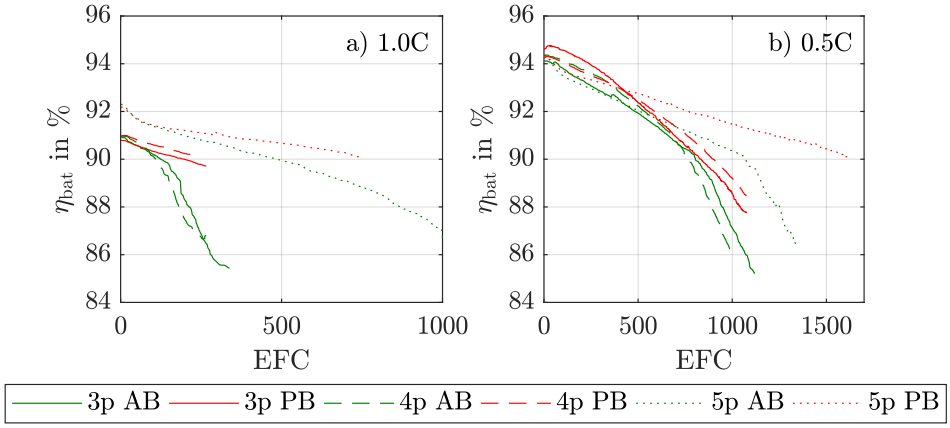

Figure 5.12: Battery energy efficiency during ageing process. Figure a) shows all batteries with $I_{bat} = 1.0C$ and Figure b) all batteries with $I_{bat} = 0.5C$.

its utilisation and therefore contribute to resource savings in the long term due to a longer service life. However, this happens at the expense of the energy efficiency of the overall system. Due to the energetically non-ideal power electronics of the active balancer, an additional amount of energy has to be applied by the battery test system during charging to compensate the energy losses of the BMS until all cells within the battery have been completely balanced. Furthermore the subsequent balancing processes during discharging cause additional losses.

5.4.6 Capacity and Service Life Gain

The results described so far result in two key questions about the capacity gain and the service life extension due to AB, which are answered in this section. For this purpose, as explained in Chapter 5.3.2, the calculated differences in capacity development and service life are presented in Figure 5.13 for each comparative test (AB vs. PB). In this direct comparison, only the valid tests shown in Table 5.3 are presented for reasons of better presentation and easier comparability. The test of the 5p batteries with a load of 0.5C is not shown, but is listed in the numerical results in Table 5.4.

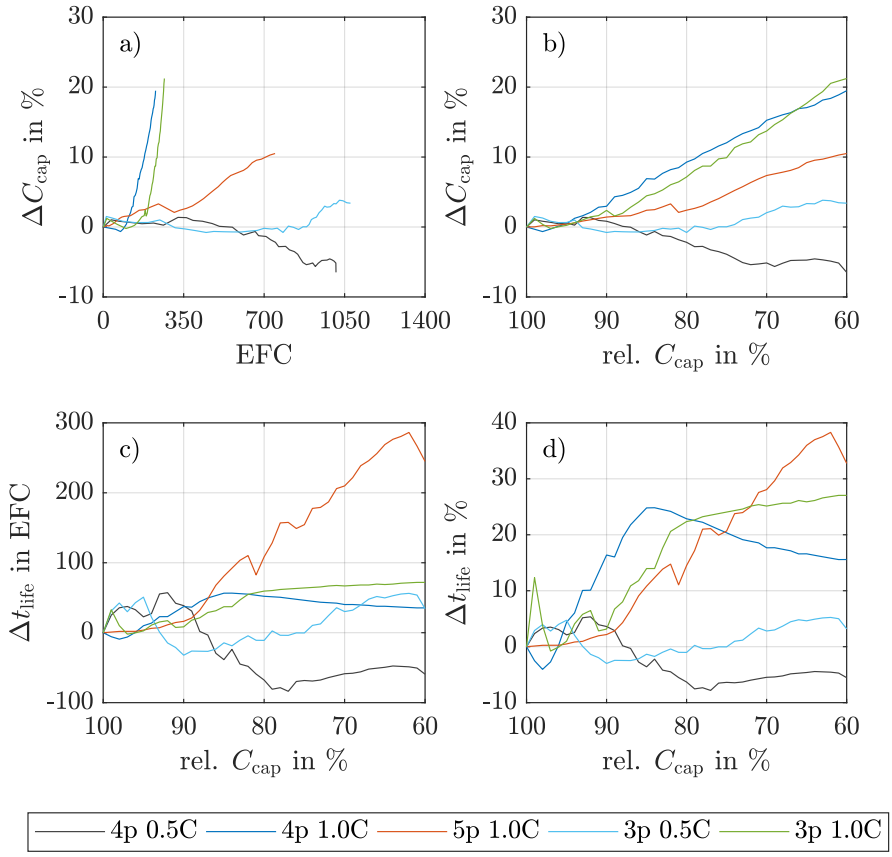

Figure 5.13: Gain in capacity and service life due to AB. Figure a) and b) show the capacity gain in relative values over EFC and relative capacity. Figures c) and d) show the gain in service life in absolute and relative values over relative Capacity.

Plots a) and b) show the capacity gain of the actively balanced batteries on the y-axis, in plot a) over EFC and in plot b) over relative capacity. The illustration in relative values improves the comparison of the value development over service life. If the values are negative, the passive battery is better than the active battery at this point.
When looking at plot a) in detail, the very different lifetimes of the individual tests and, above all, the steepness of the curves are noticeable. All batteries with 1.0C load show a clear increase, particularly in the 3p and 4p test. All batteries with 0.5C load show a clearly flatter curve which ends in

a negative values for the 4p and 5p test. Plot b) shows that all tests behave similarly at the beginning and only start to develop differently from 95% relative capacity.

Plot c) and d) show the service life variation of the batteries. Plot c) contains the increase in service life of the actively balanced batteries in EFC over relative capacity. In order to be able to show the differences and their development more clearly, plot d) shows the service life extension in relative values. If the values of plots c) and d) are negative, the passive battery has a longer service life than the active one, similar to plots a) and b).
With batteries subjected to a load of 1.0C, AB can further increase the service life over the entire test. While the values of the 3p and 5p tests increase continuously, the 4p test shows a maximum at approx. 85% relative capacity. The service life variation of packs with 0.5C load develop analogously to the difference in capacity and only show an increase in service life at the 3p test. The 4p and 5p batteries end with negative values, which clearly shows a disadvantage of the actively balanced packs.

Test	Capacity Gain	Service Life Gain
3p 1.0C	+ 21.2%	+ 27.0%
4p 1.0C	+ 19.5%	+ 15.6%
5p 1.0C	+ 10.5%	+ 32.8%
3p 0.5C	+ 3.4%	+ 3.2%
4p 0.5C	- 6.5%	- 5.5%
5p 0.5C	- 7.2%	- 16.8%

Table 5.4: Numerical overview of the test results at EOL.

5.5 Conclusion

In this chapter, a suitable empirical test approach was developed and described in detail based on insights from literature. The test results showed significant differences in the ageing behaviour of the battery packs. These are mainly dependent on the selected load, less on the selected configuration of the batteries or their construction. Direct effects of the AB could also be shown. The following statements and findings are derived from the measurements:

- **Capacity and Internal Resistance:**
  At a battery load of 1.0C, the capacity of the batteries decreases significantly faster than at 0.5C; analogously, the internal resistance increases more slowly at 0.5C, but reaches higher absolute values towards the end of ageing. The AB system helps to reduce the ageing rate, especially at the higher battery load. However, the internal resistance of the actively balanced packs increases slightly faster. At low battery loads, the influences of AB are inconclusive.

- **Voltage Spread:**
  The voltage spread between cells that occurs during ageing is mainly dependent on the selected load. A lower load also results in a lower voltage difference. In general, the voltage spread increases with the number of cycles, whereby a decrease can be observed in the first few cycles, especially with PB batteries, followed by a sharp increase. As long as the balancing power of the active balancer is high enough, the voltage difference can be kept constant on average, which is a clear advantage compared to PB. Once the power limit of the active BMS is reached, the voltage spread rises sharply and the batteries reach their end of life shortly afterwards.

- **Balanced Charge and Capacity Spread:**
  In contrast to the passive balancer, the active balancer can detect and compensate significant parameter variations depending on its technical design. While the amount of charge balanced by the passive balancer hardly changes over the entire test period and is generally low, the values of the active balancer show a clear increase with increasing number of cycles. Especially in comparison with the voltage spread, the disadvantages of the PB become visible, since in contrast to the AB, it cannot compensate the increasing voltage spread with an in-

creasing charge transfer. The resulting parameter variation in this experiment is primarily load-dependent and must be reliably detected by the balancing algorithm. If the parameter variation is too small at low battery load or remains within the tolerance band for a longer period of time, the active balancer cannot influence the ageing behaviour of the battery.

- **Energy Efficiency:**
  Due to losses of the power electronics used for AB, the energy efficiency of actively balanced batteries is worse than that of passively balanced batteries with their losses in the resistors used for PB. The effect of the internal resistance of the batteries and the correlation between efficiency and balanced capacity becomes clear. The higher the internal resistance of the battery and the higher the amount of charge balanced by the active balancer, the worse the energy efficiency of the battery.

- **Capacity and Service Life Gain:**
  Active balancing has a positive influence on the battery capacity and service life in every test at 1.0C load. The positive influence can be maintained over the entire test duration. In case of batteries subjected to a load of 0.5C, only the 3p test shows a positive development. While an increase in capacity and service life is achieved in the test with 3p batteries, negative effects are visible with 4p and 5p. Therefore an obvious advantage due to AB is not visible with low load current.

Chapter 6

Parameter Determination of Single Cells

In this chapter, the single cells of the previous pack ageing are investigated in more detail. First, the objectives are introduced and the study design is explained. After the description of the test conditions and procedure, the results of the parameter determination are presented. Finally the measured single cell parameters are compared with the results of the pack measurement.

6.1 Objectives of the Chapter

The results of the previous chapter supplemented by the examination of the individual cells. The following objectives are to be achieved in this chapter:

- Determine whether correlations between pack tests and single cell tests can be identified.
- Identification and interpretation of cell parameter and their deviations.
- Find significant differences in cell dispersion of the packs investigated in the previous Chapter.
- Identification of correlations between cell parameter dispersion and previous battery ageing conditions.
- Identification of correlations between cell parameter dispersion and BMS used.
- Investigate the further benefits of AB.

6.2 Experimental Study Design

The aim of this experiment is to determine the parameters capacity and internal resistance of all single cells that were tested in battery packs of Chapter 5. It is intended to analyse the influences of the selected test conditions of the pack ageing on the individual cells. In the following, the selected test conditions and the test procedure are explained in more detail.

6.2.1 Test Conditions

Two different types of single cells from the manufacturer Samsung SDI are available for this experiment. The batteries with 3p and 4p configuration are equipped with cells of the type INR18650-26J with NMC chemistry, batteries in the 5p configuration consist of cells of the type INR18650-35E with NCA chemistry. Cell data from the data sheets is summarized in Table 6.1.

Type	INR18650-26J	INR18650-35E
Nominal Voltage	3.63 V	3.60V
Nominal Capacity	2.550 mAh	3.350 mAh
Standard Charge	0.5C	0.5C
Fast Charge	1.0C	2 A
Initial R_{DC}	100 mΩ	35 mΩ

Table 6.1: Relevant values from single cell data sheets.

The specification of the internal resistance is usually made very generously by the manufacturers, the cells usually have much lower resistances and only reach the specified value in a clearly aged state. The internal resistance is the main difference between the two cell characteristics besides the capacity. Because of relevant differences between the cells, only cells of the same type can be compared with each other. This becomes clear when looking at the basic differences in cell chemistry described in Chapter 2.1. For example, Figure 2.2 shows that the NMC chemistry has similar energy densities compared to the NCA chemistry, but the NCA chemistry can deliver higher power (indicates lower internal resistance).

Since batteries are disassembled and thus their structure described in Chapter 5.3.1 is not retained, the individual cells are individually numbered in

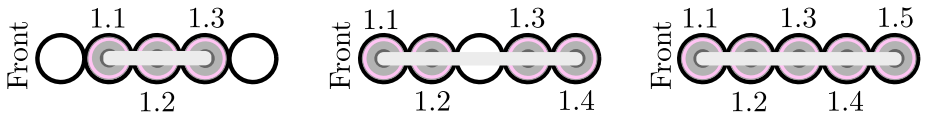

Config: 12s**3p** Config: 12s**4p** Config: 12s**5p**

Figure 6.1: Numbering of the extracted cells as a addition to Figure 5.2. Numbering example depends on the battery configuration and based on cell level 1. The cell on the left in the illustration is the foremost cell in the side view of the battery.

this experiment. For this purpose, the battery structure from Figure 5.2 is extended by the numbering concept shown in Figure 6.1. This allows the measured cells to be assigned to the original battery pack and the mounting position of the cell in the pack. The first number of the numbering describes the cell level and the second number the position of the cell within the level. Cell "3p 1.0C AB 1.2", was thus aged in a battery with the configuration 3p at a load of 1.0C and furthermore operated with an AB system. It was located in cell level 1 in the centre position.

The ambient temperature of the experiment is set to 25 °C, similar to the pack tests in order not to cause any deviation between the battery parameters and the single cell parameters.

6.2.2 Test Procedure

The experiment described in this chapter starts after the ageing tests of the battery packs. After the pack ageing is finished the batteries are disassembled and the cells are individually numbered. The cells are stored for a few days at room temperature, while a sufficient number of test channels are prepared for the simultaneous parameter determination of all cells. Before the actual measurements begin, the cells are tempered homogeneously in a temperature chamber for at least two hours in order to exclude a temperature difference between the cells as well as a temperature difference within the cells. During this time, the cells are already mounted in individual, electrically, mechanically and thermally independent cell holders within the temperature chamber. They ensure electrical four-point contacting for correct voltage measurements. The actual Reference-Parameter-Test (RPT) for parameter determination then starts with determining the capacity of

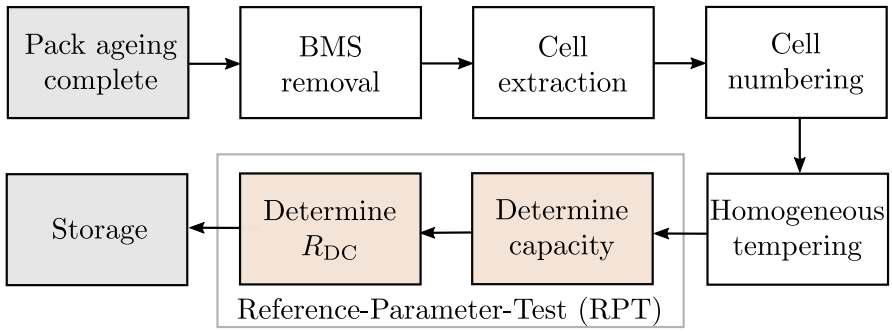

Figure 6.2: Test procedure for all single cells.

the cells followed by the measurement of the internal resistance. After the measurements are completed, the cells are stored permanently at room temperature in battery storage cabinets as the conclusion of the experiment. This enables measuring individual or all cells again if necessary.

The complete test procedure of the cells is shown in Figure 6.2.2. More information about the battery test system used and the temperature chamber can be found in Appendix A.3.

Measured and Calculated Parameters

To determine the individual cell capacities and internal resistances, the RPT, which has already been mentioned above, is carried out for each cell. This test procedure is standardized at the institute where this experiment is conducted and uses the measurement methods for parameter determination already presented in Chapter 2.5.1. The test procedure described below and its voltage and current curves are shown in Figure 6.3.

Before testing, a pause of 2 h ensures correct cell tempering. The cell test system records the cell voltage and cell current in a constant measurement interval of 1 s. The test sequence shown in Figure 6.3 starts after the described pause.
In the first part of the test sequence, the cell capacity is determined. For this purpose, the cell, which can have different charge states at the beginning of the test, is first completely discharged with a current of 0.2C to a voltage of 2.75 V. After a 10-minute pause, the cell is fully charged. The charging current for this process is 0.5C in the CC phase and is reduced to a minimum of 20 mA at a voltage of 4.2 V in the subsequent CV phase.

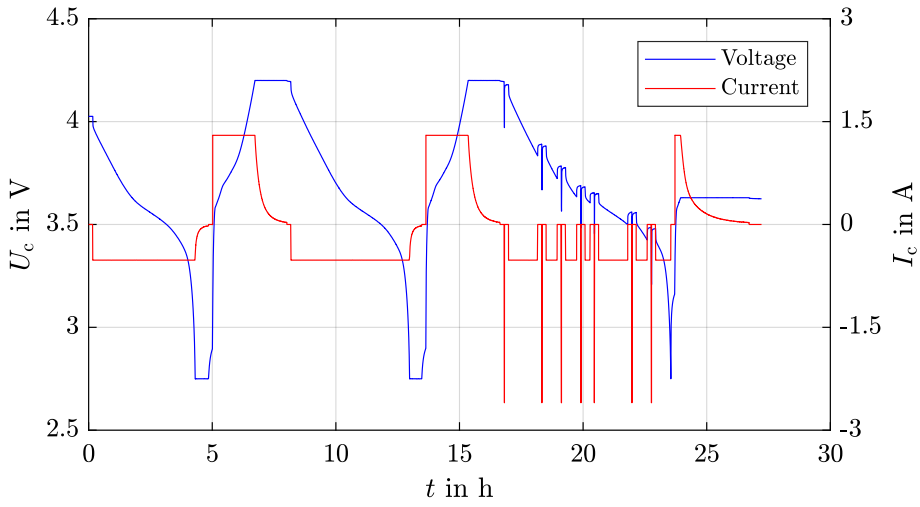

Figure 6.3: Example RPT measurement with cell '3p 1.0C AB 3.1' at $T = 25$ °C.

The charging process is terminated according to the data sheet either by reaching the mentioned lower current limit or by the expiration of a charging time of 3 h. After a further pause of 10 min, the discharge for capacity determination begins with a constant current of 0.2C. If the cell reaches the final discharge voltage of 2.75 V, an additional constant voltage phase follows during which the discharge current is reduced to a minimum value of 20 mA. The constant voltage phase during discharging serves the same purpose as the constant voltage phase during the charge, which is to reduce the influence of the internal resistance on the determination of the discharge capacity. The integrated current $\int I_c dt$ during CC and CV discharge results to the cell capacity.

The second part of the test starts after a further pause of 10 min with a further complete charging of the cell to 4.2 V using the identical conditions mentioned above. Then the internal resistance of the cells is first determined at 100% SOC by a discharge current pulse test of 1.0C applied for a total of 30 s. The internal resistances are evaluated/calculated after a time interval of 1 s. Before and after each current pulse, the cell can relax in a pause of 10 min.
Once the measurement is completed at 100% SOC. The internal resistance is determined analogously at various other predefined SOCs of 75%, 65%,

55%, 50%, 25% and 15%. The previously determined cell capacity is used to precisely calculate the discharge steps in advance and ensure that these are excactly achieved through intermediate discharges with 0.2C. Both the amount of charge removed during the current pulses and the amount of charge removed during the intermediate discharge are recorded and the necessary discharge capacity for the desired state of charge is calculated in advance.
In order to be able to compare the measured values of the single cells with those of the packs, the measured values at a SOC of 100% are subjected to detailed evaluation in this experiment. The other measured values can be neglected, as their distribution is very similar in each case and therefore no significant additional information is obtained. At the end of the RPT, the cell is charged to 3.6 V and thus into the range of its nominal voltage for subsequent permanent storage.

Further Evaluation Methods

Colour-Map:
In order to display the measured cell parameters and make their distribution visible, colour-maps are used in this work. Also areal correlations are made visible. The colour-map itself is a 2D representation, which means that the three-dimensional arrangement of the battery cells in the pack must be transferred to a single level. For this purpose, the cell levels are plotted next to each other in the horizontal axis, with their numbering in ascending order. In the vertical axis, the actual cell number is plotted in ascending order. This results in a division into rows and columns, where each value can be assigned to a specific single cell.

High capacities are shown in green, which symbolizes the adjective "good". Low residual capacities are shown in red, which symbolizes the adjective "bad". Values between the best and the worst capacity are displayed in the colour spectrum between red and green.
When displaying the internal resistances, the highest value corresponds to the adjective "bad" and the lowest to the adjective "good". The colour assignment in this case is therefore exactly the opposite.
Figure 6.4 shows an example of a colour-map for capacities of the fictive values 2.15 Ah to 2.60 Ah. In this example, the numerical value 10.00 can be assigned to cell 4.2 according to the numbering scheme presented.

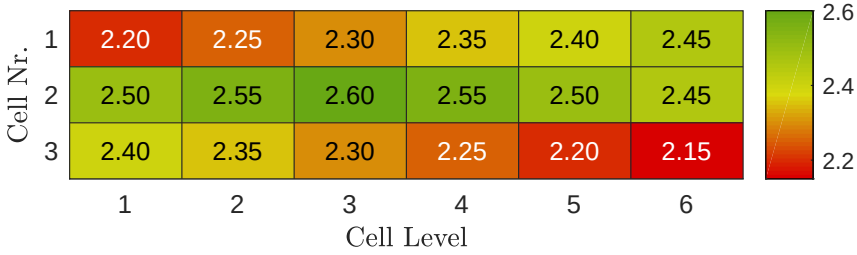

Figure 6.4: Colour-map fictive example plot for cell capacity with the different cell levels on the horizontal axis and the cell numbers on the vertical axis.

Box-Plot:
The box plot is used in this work to present the measured cell parameters as a group of values in a compact and well-arranged way. The box plot enables comparing several data sets directly with each other and displaying statistical distributions over a defined range.
In Figure 6.5 such a box plot is shown schematically and its different elements are labelled. The plot deliberately omits x- and y-axis as well as a representation of concrete numerical values. The individual elements of the box plot are explained below:

- Box: 50% of the measured data are within the visible box.
- Upper/lower quartile: These values define the boundaries of the box. They mark the upper and the lower 25% of all measured values, respectively. Thus, 25% of all values are larger than the upper quartile and 25% of the measured values are smaller than the lower quartile.
- Median value: The median value is exactly in the middle of the data set. It divides the entire data set in the middle, regardless of the box. One half of the measured values is larger than the median, the other half is smaller.
- Upper/lower whisker: The whiskers of the box-plot are two vertical lines outside the box with a horizontal end marker. They represent data that are outside the box, but still within a defined dispersion range. In this work, as is common practice, the length of the whiskers can be a maximum of 1.5 times the length of the box.

- Outliers: All data points that are neither in the range of the box nor in the extended dispersion range of the whiskers are called outliers and are displayed as red crosses. Outliers are especially relevant in the context of this work because they can significantly limit the usable battery capacity.

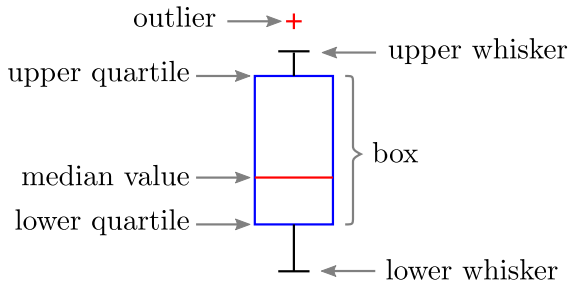

Figure 6.5: Schematic box plot example with labelled elements, without axis assignment.

6.3 Results and Discussion

In this section, the measurement results generated during the RPTs of all cells are presented and discussed. Initially, the data sets are displayed independently of each other in colour-maps. Subsequently, the individual data sets are compared with each other using box-plots. Finally, the results are summarized and concluded.

6.3.1 Measured Cell Data

All measured parameters for capacity and internal resistance are shown within colour-maps. The following plots are all structured in the same way for easier understanding. The upper two plots show the capacities in units of Ah, first those of the actively balanced battery in plot a) and then those of the passively balanced battery in plot b). The lower two plots show the measured internal resistances at 100% SOC and after 1 s in units of mΩ. Plot c) shows the internal resistances of the actively balanced battery, plot d) those of the passively balanced battery. The colour scaling within each figure is identical for plots a) and b), as well as c) and d). The comparability within a figure is therefore already given in this form of illustration.
In Figure 6.6 the measured values of all cells aged in a 3p pack configuration and with 1.0C load are displayed. Figure 6.7 shows 3p batteries with a load of 0.5C. Since the space required for the plots is very large, the colour-maps for all batteries with 4p and 5p configurations are shown in Appendix C. Cells that cannot be measured in this experiment after extraction from the batteries are labelled "NaN". These either failed during operation or were damaged during/after disassembly of the packs. For cells of the 5p0.5C AB pack, the higher calendar age is to be considered.

Results of Cells Aged with 1.0C

The measured capacity values of all actively balanced batteries in the respective sub-plots a) are distributed quite homogeneously within cell levels 1 to 8. However, levels 9 to 12 show locally lower residual capacities. The measured capacities in these levels show a very strong capacity loss compared to the initial capacity according to the data sheet. Individual cells show residual capacities of only about 62% (1.59 Ah), which also corresponds to the residual capacity of the entire battery at shut-down. A possible cause for the local minimum capacities is the proximity of these cells to the cable duct

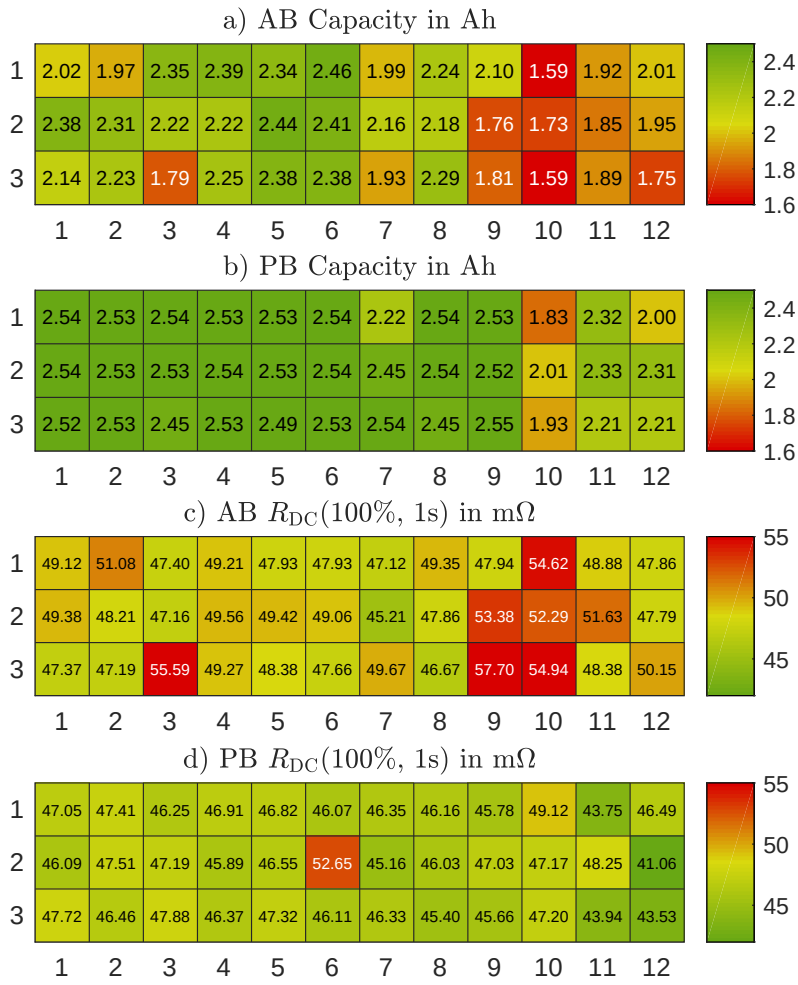

Figure 6.6: Single cell data colour-maps of 3p1.0C packs. AB pack completed 338 EFC, PB pack 266 EFC.

inside the battery, which represents a heat source at high load. This can be confirmed by measurement results of the 4p packs. The actively balanced battery with the 5p configuration does not show this behaviour and seems to be completely homogeneous, which is probably again due to the slightly

lower charge current already described in Chapter 5.4.2.
The passively balanced packs in sub-plots b) generally show higher values for the residual capacities. In some cases, these are only slightly below the original design capacity of the cells. Within the passively balanced packs, individual cells have aged only very little. However, it is significant that the data sets contain individual weak cells. These are mostly located within one cell level, and will significantly limit the battery capacity of the passively balanced battery. This directly confirms the results from Chapter 5. The significant poor cell levels are 10 (3p) and 11 (4p, 5p). At closer examination, a slight capacity loss of cell levels 9 to 12 can also be seen in the passively balanced batteries, which, analogous to the actively balanced packs, suggests design-related thermal reasons.

The measured internal resistances in all sub-plots c) and d) behave like the capacities. Cells with poorer capacitance show an increased internal resistance. The described differences between active and passive balancing can also be observed here. Comparing plots a) with c), and b) with d), similar patterns can be seen. However, the differences of the measured internal resistances are not as significant as those of the capacities. The variations of the absolute values are smaller. In general, it can be seen that the internal resistances after ageing are still well below the values specified in the data sheet (see Chapter 6.2).

Results of Cells Aged with 0.5C

The measured residual capacities of the cells are lower than those of the cells at a load of 1.0C. Since the visual impression of the colour-map can be mistaken here, a look at the value range of the legend helps. While the residual capacities of the 1.0C packs are still over 2.4 Ah (3p, 4p) and 3 Ah (5p), the 0.5C packs show maximum values of approx. 2.1 Ah (3p, 4p) and 2.7 Ah (5p). The distribution of values also deviates,. For for the 0.5C packs the worst cells are better distributed within the packs (3p, 4p), or are located in the centre (5p). Increased thermal stress in the centre of the battery seems logical as a cause here. Cells inside the pack, can not deheat as good as cells on the outside, thus they experience higher temperature over their complete lifetime. Individual outliers or individual bad cell levels cannot be identified here. In general, the lower residual capacities and the better distribution of the parameters within the packs, in direct comparison with the 1.0C batteries, suggest a more homogeneous ageing and thus a better utilization of the 0.5C batteries.

Again, the internal resistances behave analogously to the capacities. The absolute values measured for batteries subjected to a load of 0.5C are higher. This is also due to the higher number of cycles as already described in Chapter 5.

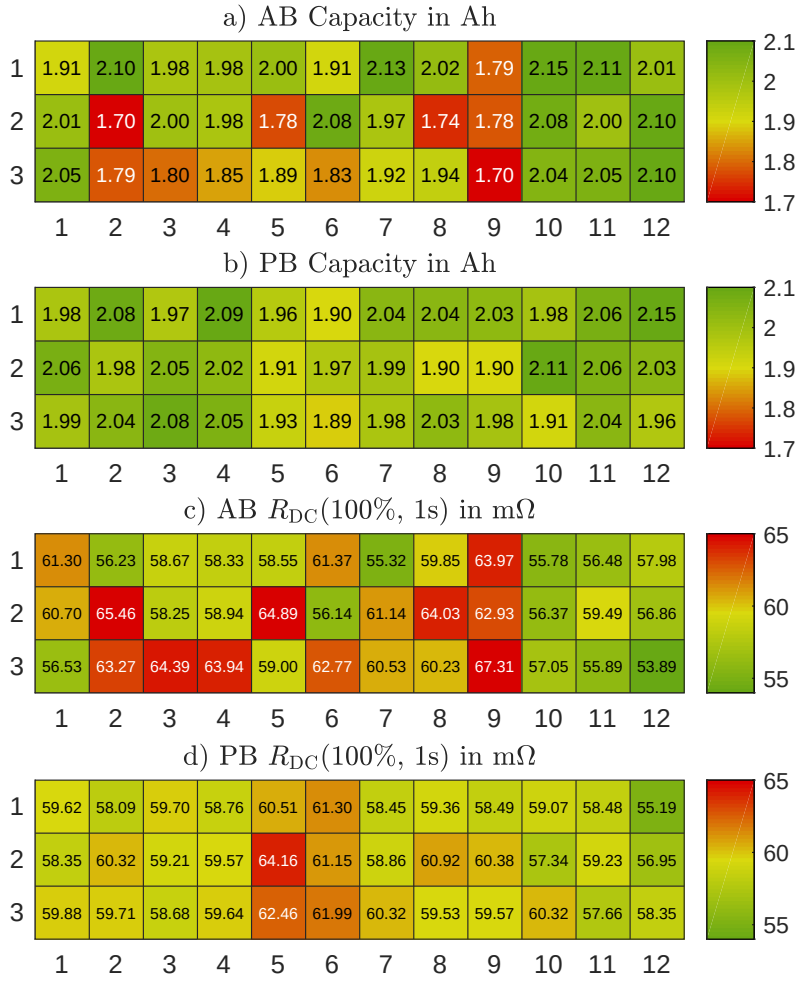

Figure 6.7: Single cell data colour-maps of 3p0.5C packs. AB pack completed 1121 EFC, PB pack 1076 EFC.

6.3.2 Data Comparison

The value overview in colour-maps provides a good physical overview of the cell data and information about battery-internal parameter distributions. However, it offers only limited possibilities of comparability between the batteries. For this purpose, a specific parameter comparison is performed by the use of box-plots. Each box-plot represents all cells within a battery of Chapter 5 and can represent their parameter variation comparably. The sub-plots in Figure 6.8 are grouped according to the battery configuration and also according to the measured values for capacitance and internal resistance.

Plot a), b) and e) show all measured capacities. They directly compare both BMS used and both battery loads. It can be seen that the data sets of the 1.0C PB batteries in plots a) and b) are the only ones with outliers downwards. In plot e), an outlier is also visible in the significantly older 1.0C AB battery, as well as one in the 0.5C PB data set. All other batteries have no outliers within the criteria of the box plot presented in Chapter 6.2.2 and are thus distributed more homogeneously. As already shown in the previous section using the colour-maps, the batteries subjected to 0.5C have lower residual capacities and higher internal resistances. This can also be seen consistently in all other plots. The only exception is again the older 1.0C AB battery in plot e). In general, it becomes visible that the parameter dispersion of the 0.5C batteries (visible in the box plot as the span of the whiskers) is generally lower than that of the 1.0C batteries. This confirms the statements made in Chapter 5, based on Figures 5.9 and 5.10. Specifically, it can be seen that the ΔQ_c values of the 1.0C batteries from Figure 5.10 also show up in the same order in the box-plots from Figure 6.8, as 4p followed by 3p and 5p has the highest variation.

Plot b), c) and f) show all measured internal resistances following the same scheme of the capacities. In contrast to the capacities, there are generally more outliers visible here. As expected the internal resistances rise out of the data set. The only exception is the data set 1.0C PB from plot a), which also shows single outliers downwards. Outliers of the internal resistance upwards, analogous to the outliers of the capacity downwards, can lead to a loss of performance of the entire pack. If the cell voltage under load gets below the switch off value due to the voltage drop at the internal resistance the BMS will switch off the battery just as early as would be the case with a lower cell voltage due to a lower cell capacity.
Basically, the variation of the internal resistances at 1.0C is smaller than that of the capacities, which favours the visible outliers due to the definition

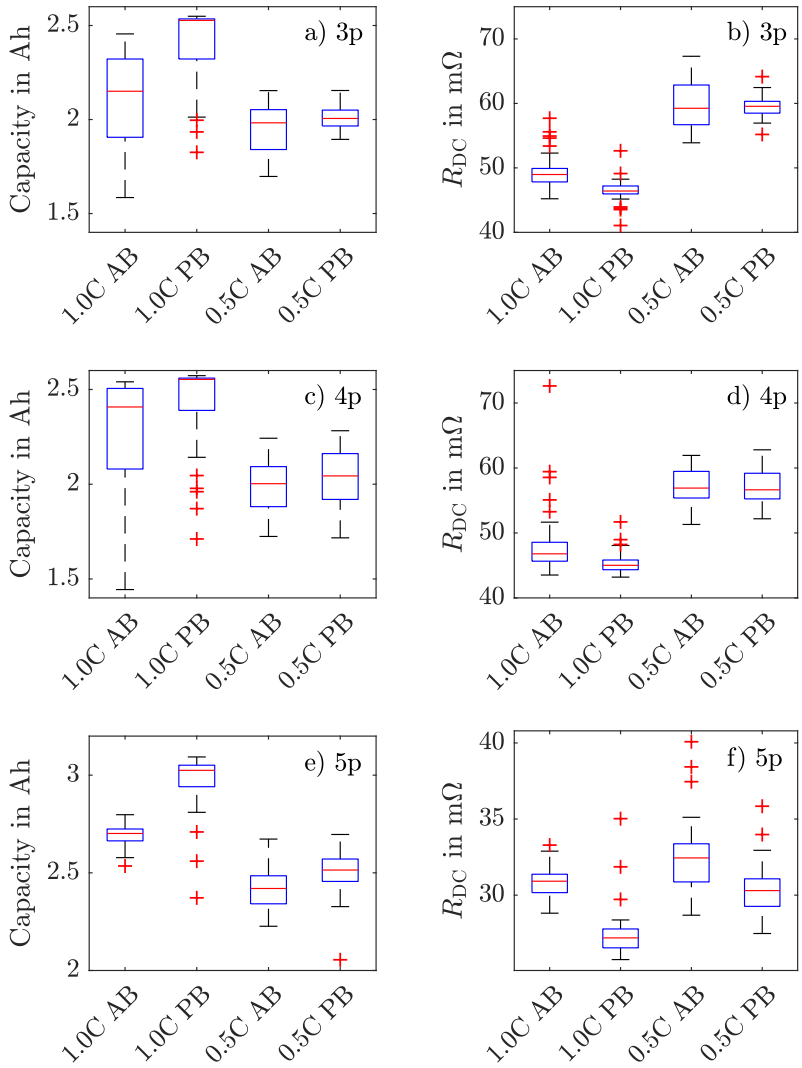

Figure 6.8: Boxplots of all single cell data-sets. Figures a) and b) show 3p batteries, c) and d) show 4p batteries and e) and f) show 5p batteries.

of the maximum box-plot whisker length. The variation of capacities and internal resistances of the 0.5C batteries are quite similar. On average, the internal resistances of the batteries subjected to 0.5C are higher than those of the 1.0C batteries, but show a slightly wider span in contrast to the capacities. This can be seen consistently in all plots and, analogous to the capacities, can be attributed to a longer service life of the 0.5C packs.

The outliers of the resistance values for the 0.5C batteries in plot f) are particularly noticeable which is most likely due to the enormously longer lifetime of the 5p batteries compared to the 3p and 4p batteries and the associated larger parameter variation.

6.4 Conclusion

In this chapter, all single cells of the aged packs from Chapter 5 were extracted and measured individually. The aim of this study was to gain further information about the chances and limits of AB and to confirm the results of the pack tests as far as possible. The following statements can be derived from the measured data:

- The values of the capacities and internal resistances differ depending on the battery load used. In principle, this is due to the different service life as a direct result of the battery load. The more cycles a battery completes, the lower the average capacity of the individual cells and the higher the measured internal resistances.

- Although the battery ageing ended approximately at identical residual capacities. Passively balanced batteries have high residual capacities of the individual cells, indicating poor utilization of the battery.

- While cell parameters show wider distribution with AB compared to PB, only few individual capacities deviate in the case of passively balanced batteries. In most cases, these celld belong to one level. The deviating values are visible in the box plot as outliers; they limit the battery capacity during operation.

- Compared to PB actively balanced batteries show a parameter distribution in a larger range, but with fewer or no outliers. The AB system thus seems to distribute the load more evenly across the cells. Again, the greater dispersion is due to the longer service life of the packs; it continues to increase with the number of cycles regardless of the BMS used.

- The measurement results indicate that AB only minimizes effects of parameter variation on the operating behaviour of the packs. It has no influence on the emergence of the parameter variation itself and cannot stop/reduce it.

- Disassembling the batteries provides valuable additional benefits, as the causes of the packs EOL and the position of the weak cells can be investigated in more detail.

With reference to the pack ageing from Chapter 5, the following results can be supplemented or confirmed by the single-cell measurement:

- **Capacity and Internal Resistance:**
  It is confirmed that cells subjected to 0.5C load achieve higher absolute values of internal resistance compared to 1.0C load.

- **Balanced Charge and Capacity Spread:**
  The parameter variation, which was already detected by the active BMS during operation, can be verified by the single cell measurement. The packs that were heavily balanced by the active BMS during operation actually have the strongest capacity deviations in the single cell measurement.

- **Service life:**
  Passively balanced batteries are limited in performance by one or few cells. They lose capacity faster and have a shorter service life. Active balancing can compensate this effect and average the capacity loss between all cells.

Chapter 7

Conclusion and Future Works

7.1 Conclusion and Contribution

This work gives an overview over lithium-ion batteries and describes their complexity, areas of application and ageing effects. In order to ensure a safe operation of the batteries, a BMS is absolutely necessary, for which a nearly unlimited variety of systems is conceivable in terms of design functionality. Basically, BMSs are divided into active and passive systems. Active BMS can be separated according to their energy transfer elements, i.e. capacitive and inductive, each with a large number of variants. So far, it has not been possible to conclusively prove the advantages and disadvantages of such an active BMS, considering the existing literature. A gap in the literature has been identified, especially regarding statistically significant measurement data. To address this fact, a self-developed, universal, inductive, active system is chosen in this work for empirical measurements. Hardware and software of the system are described, with special focus on the balancing algorithm and its calculation methods.
In an empirical experiment, a comparison between actively and passively balanced batteries is carried out in several long-term experiments using the BMS presented. Here, both the battery load and the battery configuration (number of parallel cells) is varied. The batteries are aged until a residual capacity of 60%.

Considering all the test data obtained during battery ageing and subsequent single cell measurements, the following findings emerge in summary:

- Active balancing shows positive effects with regard to battery capacity and service life when the deviation of the internal cell parameters is large or becomes large due to ageing effects during the test. In this work, this is the case at a battery load of 1.0C, but not at 0.5C. The battery configuration has no significant effect on the ageing behaviour.

- If the variation of the cell parameters is small and does not increase significantly over the ageing process, AB can only have a small or no positive effect on the battery capacity. A PB system is sufficient here.
- The energy efficiency of the battery decreases with an AB system due to losses in the power electronics, especially when high charges are transferred between the cells. However, the overall efficiency of the battery can be improved in terms of resource savings through increased exploitation of the battery capacity and a longer service life.
- An active BMS detects the variations of the cells during operation and calculates necessary charge equalisations. The data calculated by the BMS shows good correlation with the results of the single cell measurements after the EOL of the battery packs.
- Especially after ageing with high load, batteries with AB show more homogeneously distributed single cell parameters than the comparable batteries with PB. With PB, the batteries show poorer utilisation of the entire battery, since individual, heavily aged cells have a limiting effect on the complete battery pack.
- The results show in context that AB could enable a second life of passively balanced batteries, provided there are only a few aged cells within a passively balanced battery at its EOL.
- An actively balanced battery consits of several aged cells in various cell levels and can no longer be used within a second life application after its EOL. It was fully utilised in its first live application.
- The advancing of parameter variation of the cells cannot be prevented by AB. However, the associated effects (decrease in capacity, drop in battery performance) can be reduced.

Chapter 1 gave a short introduction to the subject and its background. Furthermore, the motivation, the objectives of the work and its contributions to science were explained.

Chapter 2 presented an overview of the state of the art of lithium-ion batteries. Frequently used designs, chemical compositions, important terms and definitions from battery technology, information about common ageing mechanisms and modelling possibilities were explained. Finally, the chapter contained information about the determination of important battery parameters by measurement and possible effects of parameter variation.

Chapter 3 summarized the state of the art in battery management systems, with a focus on balancing topologies. A variety of cell balancing topologies were explained and evaluated. The different possibilities for energy transport within a battery pack were explained as well as the selection of deviating cells relevant for balancing.

Chapter 4 explained a self developed, used BMS hardware and its balancing algorithms. First, the flyback converter was described as the most important component for the energy transfer. The behaviour of the balancing currents during operation of the entire system were explained in detail. Second, calculation methods and algorithms necessary for balancing were described. Three different routines and their interaction were explained.

Chapter 5 gave an insight on relevant literature which used to define the relevant literature gap and the objectives of the empirical test approach with several battery packs. A full description of the experimental study design, the test conditions, the test procedure as well as a description of all relevant measurement parameters and further evaluation methods were provided. Finally, pack test results were explained and discussed.

Chapter 6 continued the empirical test approach from Chapter 5 with single cell measurements. In analogy to the pack tests, the chapters objectives, a full description of the experimental study design, the test conditions, the test procedure as well as a description of all relevant measurement parameters and further evaluation methods were provided. To conclude the chapter, cell test results were explained, discussed and compared to battery pack tests.

Chapter 7 concluded the work and summarised the thesis. Furthermore, the contributions of this thesis were listed and possibilities and suggestions for further research were provided. A list of all publications and patent applications of the author was shown at the end of the chapter.

7.2 Future Works

In this section, thoughts and ideas for future work are presented which can be based on this thesis. These include possible changes/optimisations to the experimental set-up for further data collection as well as improvements to the configuration/hardware of the active BMS.

7.2.1 Optimized Empirical Approach

During the evaluation of the data collected in this work, several limitations of the chosen approach became visible, which should be avoided for future comparative measurements between active and passive balancing. The most important aspects are:

- Conclusions from tests with commercial batteries are restricted. As part of a further experiment, the construction of custom-made batteries should be considered. All cells used should be measured individually before the test, parameter deviations within and between the battery packs can thus be excluded before starting long term measurements.
- The chosen approach showed that the battery configuration had little to no influence on the test results in this experiment. In fact, the battery load and battery chemistry were more decisive. In a future approach, different battery chemistry and configurations should be avoided in order to exclude non-conclusive findings.

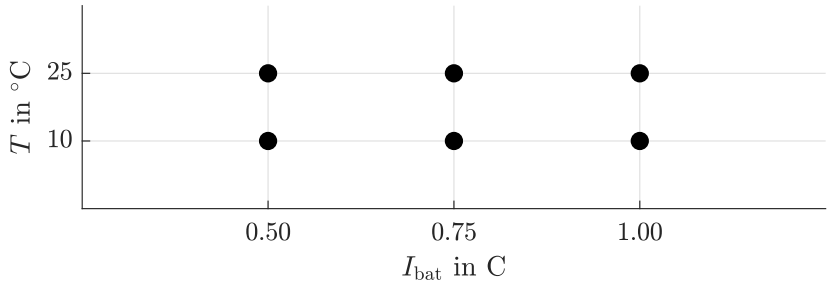

Figure 7.1: Suggested optimised test matrix with two example temperatures. Each test is a comparative long-term measurement of two identical battery packs.

- In this thesis ambient test temperature was constant and further influences of temperature were not investigated. In practice, batteries are used at different temperatures. Temperature should be varied in future tests. This requires a reliable heating/cooling system and sufficiently frequent temperature measurement in the battery housing.

The experimental design shown in Figure 7.1 can be optimised by using a constant battery design with extended variation of the battery load and at least two different temperatures.

7.2.2 Improved Active BMS

In this work he active BMS reached its performance limit during ageing with 1.0C battery load. In contrast, during measurements with 0.5C, the balancing current seemed oversized. This is due to the uniform configuration of the active BMS. The balancing current (marked in red in Figure 7.2) of the systems could be reconfigured on the hardware side for future experiments and adjusted according to requirements. Flexible adaptation during operation through control of the power electronics is conceivable.

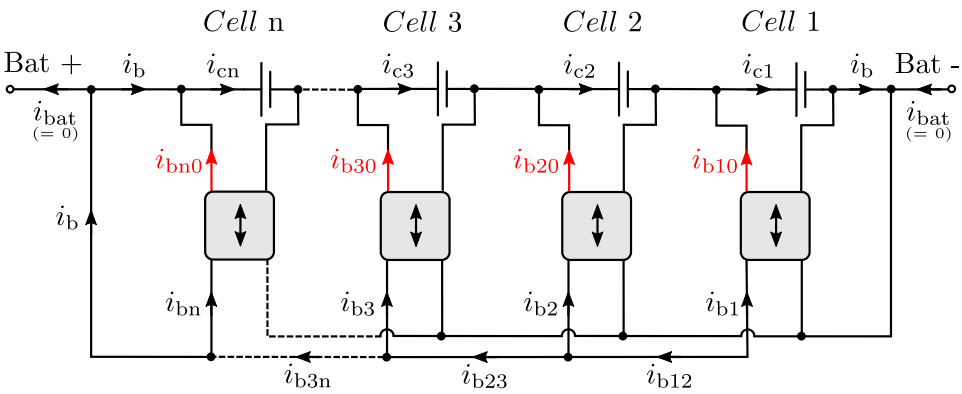

Figure 7.2: Marked adjustable balancing currents in the abstracted multiple converter topology. For detailed description see Chapter 4.1.2.

Furthermore, the operation of the two presented balancing methods can be adjusted during battery operation. For example, the predefined tolerance band voltage-based and capacity-based balancing can be adjusted. In this

work, these tolerances were designed for functionality but not optimised. When optimising the active BMS, optimisation of the predefined tolerances should take place. It is not necessarily desirable to only reduce the tolerances, but also to increase it in order to calculate fewer balancing processes and avoid unnecessary balancing processes. In any case, the tolerances are stored as variables in the software and should be adjusted during operation. Figure 7.3 shows, for example, the tolerance band of the voltage-based optimisation, which can be changed for further work within the measurement accuracy.

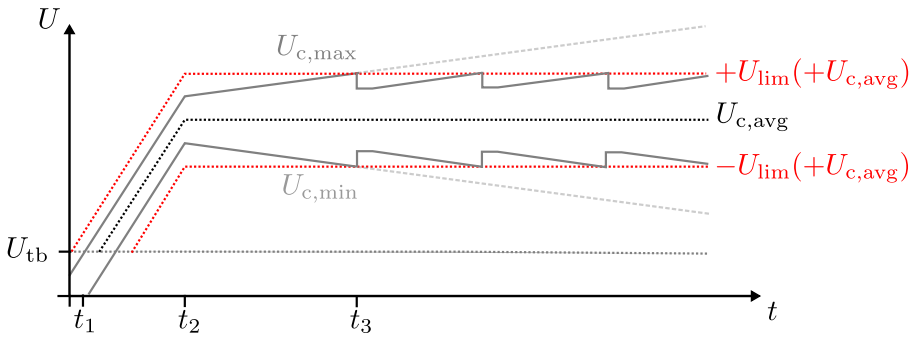

Figure 7.3: Marked adjustable tolerance band for voltage based balancing. For detailed description see Chapter 4.2.2.

7.2.3 Active Balancing for Battery Diagnosis

In this thesis it was already shown that the states of the battery cells in operation can be determined by the BMS. However, this is only achieved through an iterative approximation and not through direct measurement of the cell parameters. By choosing suitable diagnostic methods and measurement procedures, however, it is possible to calculate the cell parameters capacity and internal resistances exactly. For example, the balancing pulses of the system and the internal resistance of the cells could be measured continuously during operation using the current-pulse method from Chapter 2.5.1, illustrated in Figure 7.4. Known internal resistances would in turn be useful for accurately determining the capacity via the open circuit characteristic curve (or similar). In this work it was also shown that although the equalisation currents are set by a hardware configuration, they can often deviate during

operation. By accurately determining the actual balancing charges of each balancing pulse, it is possible to determine the cell capacity at each point in time. These further possibilities could be investigated in future.

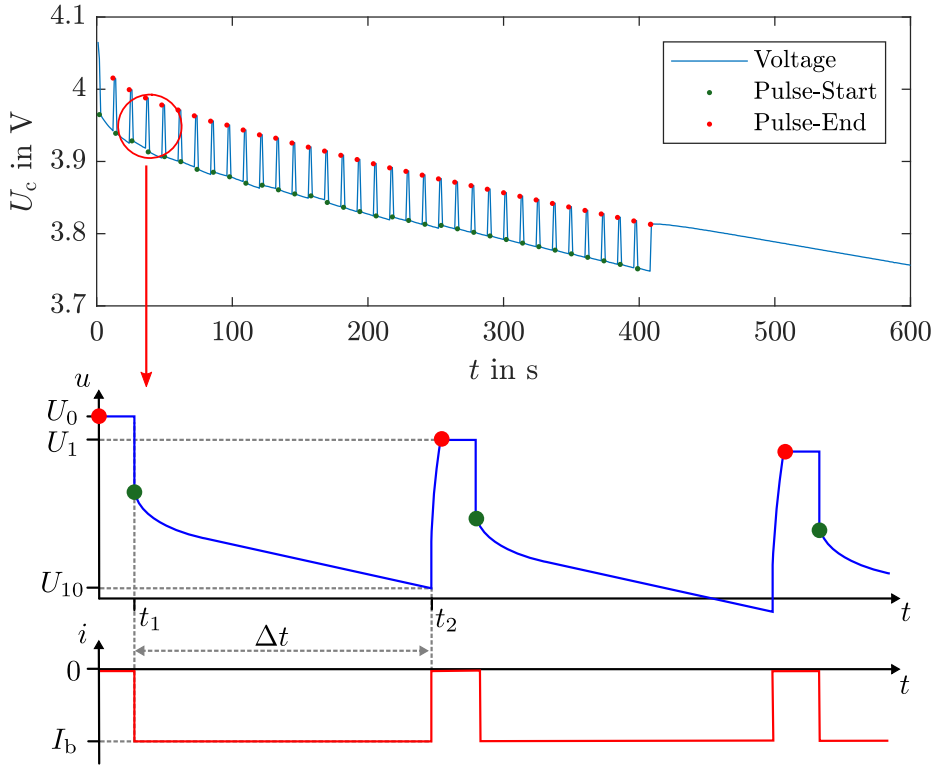

Figure 7.4: Determine internal resistances with balancing pulses. For detailed description see Chapter 2.5.1.

7.3 Publications and Patent Applications of the Author

7.3.1 Results related to battery management systems

1. A. Ziegler, D. Oeser, T. Hein, D. Montesinos-Miracle and A. Ackva, "Reducing Cell to Cell Variation of Lithium-Ion Battery Packs During Operation", *IEEE Access, vol. 9, pp. 24994-25001, 2021* [121]

   Abstract - In this work, an experimental approach to reduce the variation from cell to cell during battery operation is evaluated to reach a better battery utilization. Numerous theoretical considerations of intelligent battery management systems without long-term experimental validation of their capabilities lead to a gap in the literature, which this work aims to address. For this purpose, the ageing behaviour of two batteries is investigated over a period of almost 1.5 years. One battery is connected to an active balancing battery management system (BMS) and the other to a conventional passive balancing BMS. Important battery parameters, such as capacity and internal resistance, are recorded in each cycle. The battery behaviour is evaluated in detail by observing the voltage difference of the individual cells at the end of discharge and by calculating the amount of charge actually balanced by the BMS. Significant differences between the BMS systems used are elucidated, which illustrate the advantages of active balancing. In contrast to passive balancing, active balancing is able to reduce the ageing rate of the battery and achieve better utilization with a more than five times lower voltage spread at end of discharge, a up to 3.1% higher discharge capacity and a 7.7% longer service life.

2. T. Hein, A. Ziegler, D. Oeser, A. Ackva, "A capacity-based equalization method for aged lithium-ion batteries in electric vehicles", *Electric Power Systems Research, vol. 191, 2021* [122]

   Abstract - A capacity-based equalization method for active balancing is proposed to increase the usable capacity of aged lithium-ion batteries within a minimum of balancing effort. The main goal of the presented algorithm is to predict the equalization charge for each cell, which is needed to fully charge and discharge every cell of the battery in the next cycle. For this, State-Of-Charge (SOC) and State-Of-Health (SOH) of each cell must be determined. The predicted energy is balanced at the beginning of the cycle and further balancing is per-

formed only if the parameters of the cells change. This ensures that the minimum possible balancing effort is achieved. To validate the performance of the proposed method, a simulation is carried out. For this purpose, a battery model and Battery Management System (BMS) model are built in Matlab/Simulink. The parameters of the simulated cells differ in capacity and initial SOC to imitate an aged battery. The simulation results verify that the developed balancing method can improve the usage of aged batteries compared to conventional methods. This algorithm for active balancing can be used in second life cases of battery systems.

3. A. Ziegler, D. Oeser, T. Hein, A. Ackva, "Development and Application of an Active Balancing System for Lithium-Ion Cells", *IEEE Vehicle Power and Propulsion Conference, Hanoi, Vietnam, VPPC 2019* [123]

   Abstract - This paper describes the development of an active battery management system for lithium-ion cells and its comparison with passive battery management. For this purpose, the structure of the test hardware is described and its universal possibilities are explained. An iterative balancing algorithm is presented as a central component of the active balancing system. The algorithm is able to determine the capacitance deviations between the individual cells by measuring cell voltages and battery current. In order to compare the system built up in this work with a conventional battery management system, a realistic test is carried out on aged lithium-ion batteries. In this test, the active balancing system is able to significantly increase the removable battery capacity compared to conventional passive balancing. In addition, the disadvantage of passive balancing in second-life applications is clarified.

4. A. Ziegler, D. Oeser, B. Arndt, A. Ackva, "A Universal, Modular and Bidirectional Active Balancing System for Lithium-Ion Cells", *Proceedings of the 10th International Scientific Symposium on Electrical Power Engineering ELEKTROENERGETIKA, Stará Lesná, Slowakia, EE 2019*

   Abstract - This paper introduces a new, modular and universal active balancing system that is able to gain significantly more energy from aged and unbalanced batteries compared to other balancing concepts. One of the major issues when using battery packs is the possible unbalance within single battery cells. As this problem worsens with

increasing age state of the art passive balancing methods reach their limits in terms of energy efficiency and applicability. After identifying the issues of standard balancing systems, requirements to overcome those problems are derived. To meet those requirements a new balancing hardware and the corresponding algorithm is implemented. The applicability and energy efficiency is proofed in the laboratory on a real hardware system and demonstrated by measurement results. Furthermore, a evaluation of a realistic application with a traction battery is executed.

5. A. Ziegler, D. Oeser, B. Arndt, A. Ackva, "Comparison of Active and Passive Balancing by a Long Term Test Including a Post-Mortem Analysis of all Single Battery Cells", *IEEE International Conference and Workshop in Óbuda on Electrical and Power Engineering, Budapest, Hungary, IEEE CANDO-EPE 2018* [111]

   Abstract - Due to the fact, that there are basically no practical test comparisons between active and passive lithium-ion battery balancing systems, a long term test is carried out. Therefore two batteries with an active and a passive balancing system are cycled. After about 2600 cycles test is stopped to start with further investigations. Capacity decrease and the increase of internal resistance of the two used battery packs are presented. To investigate the influence of load cycles in combination with different battery management systems (BMS) a detailed single cell investigation is executed. Finally, active balancing increases the usable capacity by a maximum of 2balancing and reduces the cell to cell deviation of capacity and internal resistance. Furthermore it is shown that the additional stress due to frequent energy redistribution in active balancing systems has no negative ageing effects to the cells compared to passive balancing.

6. D. Oeser, A. Ziegler, B. Arndt, A. Ackva, "Effectiveness of Active Balancing on High Dispersion Batteries", *IEEE International Conference and Workshop in Óbuda on Electrical and Power Engineering, Budapest, Hungary, IEEE CANDO-EPE 2018* [110]

   Abstract - These investigations examine the benefit of an active balancing system based on an LTC-3300 IC with help of an arbitrarily configurable battery. The used structure allows creating batteries with different cell to cell variations in a 12S1P setup and to test it with the active balancing system. In total, three different combinations with varying degrees of cell to cell variation are tested. The usable capacity

of the cell combinations is compared with and without balancing. In all three tests, the capacity could be significantly increased and stabilized with help of the active system. These studies indicate that the additional benefit of an active balancing system could play a major role in the field of second-life batteries. Furthermore, the system can ensure the usability of a battery in case of cell failure.

7.3.2 Results related to battery ageing

1. A. Ziegler, D. Oeser, T. Hein, D. Montesinos-Miracle, A. Ackva, "Run to Failure: Aging of Commercial Battery Cells beyond Their End of Life" *Journal of Energies, vol. 13, no. 8: 1858, 2020* [124]

   Abstract - The aim of this work is to age commercial battery cells far beyond their expected lifetime. There is a gap in the literature regarding run to failure tests of lithium-ion batteries that this work intends to address. Therefore, twenty new Samsung ICR18650-26F cells were aged as a battery pack in a run to failure test. Aging took place with a constant load current and a constant charge current to accelerate capacity decrease. Important aging parameters such as capacity and internal resistance were measured at each cycle to monitor their development. The end of the test was initiated by the explosion of a single battery cell, after which the battery pack was disassembled and all parameters of the still intact single cells were measured. The distribution of all measured capacities and internal resistances is displayed graphically. This clearly shows the influence of the exploded cell on the cells in its immediate vicinity. Selected cells from this area of the battery were subjected to computed tomography (CT) to detect internal defects. The X-rays taken with computed tomography showed clear damage within the jelly roll, as well as the triggered safety mechanisms.

2. G. Bohn, J. Taub, A. Linke, S. Bayer, D. Oeser, A. Ziegler, P. Ettl, A. Ackva, "High-resolution interferometric measurement of thickness change on a lithium-ion pouch battery", *3rd International Conference on Environmental and Energy Engineering, IOP Confernece Series Vol. 281, Nr. 012030, Shanghai, China, IC3E 2019* [125]

   Abstract - Volume change of graphite leads to change in thickness of battery storage layers during discharging and charging. Pouch cell lithium ion batteries are used in the field of electric vehicles and solar home storage. This paper shows a measurement setup for the three-dimensional measurement of thickness change on a flat 6.7 mm thick pouch cell using a white light interferometer. With a measuring field of 7.05 mm diameter the resulting 3D thickness change record contains 226000 3D readings. The measuring points have a lateral distance of 13.1 μm. The repeatability of the measurement is 312.8 nm for the individual values and 64.1 nm for the average value. In addition, this paper shows how the storage capacity of this pouch cell drops over 30

charge cycles.

3. D. Oeser, A. Ziegler, A. Ackva, "Single Cell Analysis of Lithium-Ion E-Bike Batteries Aged under Various Conditions", *Journal of Power Sources, vol. 397, pp. 25-31, 2018* [126]

   Abstract - In most cases, batteries consist of multiple cells with different interconnections in which the weakest cells determine the usable capacity, performance and lifetime. Since data on initial production-related cell to cell parameter variance is well known, only little data on variance change over lifetime is available. This work investigates how variance spreads with age. Twenty differently aged electric bike (pedelec) batteries are disassembled and the state of health, as well as the internal resistance, are measured cell by cell for each of these batteries. The results show the development of cell to cell variation of aged batteries. Gathered data is also used to calculate capacity limitations through progressed variation. The methodology of the investigation can be used to analyse potential use cases for active balancing systems.

4. S. Bayer, D. Oeser, A. Ziegler, A. Ackva, "Laboratory ageing of commercial e-bike battery packs", *15th Design&Elektronik Batterieforum, 2018, Munich, Germany*

   Abstract - Due to the growing market for e-bikes in Europe and a gap in the knowledge about Li-ion technology a set of aging tests has been carried out using Li-ion batteries. The integrated NMC (Nickel Manganese Cobaltoxide) cells are manufactured by Samsung, labelled as ICR18650-26F. These cells are a commercial off-the-shelf product. The tests comprise of cycling in the field and laboratory. The laboratory aging concentrates on testing at different ambient temperatures. Discharging is done with an average from collected field-test data. The study shows impact of the ambient temperature on the remaining capacity and the internal resistance. In addition a post-mortem analysis of one battery has been done.

7.3.3 Patent Applications

1. Patent Application: A. Ziegler, A. Molchanov, D. Oeser, P. Ponomarov, "Verfahren und Vorrichtung zum Zellspanungsausgleich von Batteriezellen mehrzelliger Energiespeicher",
   Application Number: DE 10 2019 108 579.9
2. Patent Application: A. Ziegler, D. Oeser, "Verfahren zur Bestimmung eines bevorstehenden Fehlerfalls einer Batteriezelle sowie Batterie-Management-System",
   Application Number: DE 10 2019 134 510.3
3. Patent Application: A. Ziegler, D. Oeser, T. Hein, P. Ponomarov, "Verfahren und Vorrichtung zum aktiven Balancieren von Batteriezellen mehrzelliger Energiespeicher" (Part I),
   Application Number: DE 10 2020 123 864.9
4. Patent Application: A. Ziegler, D. Oeser, T. Hein, P. Ponomarov, "Verfahren und Vorrichtung zum aktiven Balancieren von Batteriezellen mehrzelliger Energiespeicher" (Part II),
   Application Number: DE 10 2021 119 237.4

Bibliography

[1] Martin Lange, Ralf Menzel, Lars Mönch, and Ling He. Elektromobilität - schneller als gedacht. *Umweltbundesamt Germany*, pages 1–13, 2017.

[2] John Warner. *The handbook of lithium-ion battery pack design: Chemistry, components, types and terminology.* 2015.

[3] Davide Andrea. *Battery Management Systems.* Artech House, 2010.

[4] Languang Lu, Xuebing Han, Jianqiu Li, Jianfeng Hua, and Minggao Ouyang. A review on the key issues for lithium-ion battery management in electric vehicles. *Journal of Power Sources*, 226:272–288, 2013.

[5] Jian Cao, Nigel Schofield, and Ali Emadi. Battery balancing methods: A comprehensive review. *2008 IEEE Vehicle Power and Propulsion Conference, VPPC 2008*, pages 3–8, 2008.

[6] Mohamed Daowd, Noshin Omar, Peter van den Bossche, and Joeri van Mierlo. A review of passive and active battery balancing based on MATLAB/Simulink. *International Review of Electrical Engineering*, 6(7):2974–2989, 2011.

[7] Xiaosong Hu; Changfu Zou; Caiping Zhang; Yang Li Yang. Technological Developments in Batteries. *IEEE Power and Energy Magazine*, (July):42–44, 2017.

[8] Peter Kurzweil and Otto K. Dietlmeier. *Elektrochemische Speicher.* Springer Verlag, 2015.

[9] Reiner Korthauer. *Handbuch Lithium-Ionen- Batterien.* Springer Verlag, 2013.

[10] Jeffrey W. Fergus. Recent developments in cathode materials for lithium ion batteries, 2010.

[11] Buchman Isidor. Types of Lithium-ion Batteries - Battery University, 2017.

[12] Naoki Nitta, Feixiang Wu, Jung Tae Lee, and Gleb Yushin. Li-ion battery materials: Present and future, 2015.

[13] Christian M. Julien, Alain Mauger, Karim Zaghib, and Henri Groult. Comparative issues of cathode materials for Li-ion batteries. *Inorganics*, 2014.

[14] Christian Glaize and Sylvie Geniès. *Lithium-Ion Batteries and other Electrochemical Storage Systems*. ISTE Ltd and John Wiley & Sons, Inc., 2013.

[15] Manuel Brühl. *Aktive Balacing-Systeme für Lithium-Ionen Batterien und deren Auswirkungen auf die Zellalterung*. PhD thesis, 2017.

[16] M. Broussely, Ph Biensan, F. Bonhomme, Ph Blanchard, S. Herreyre, K. Nechev, and R. J. Staniewicz. Main aging mechanisms in Li ion batteries. *Journal of Power Sources*, 146(1-2):90–96, 2005.

[17] A. Jossen and W. Weydanz. Moderne Akkumulatoren richtig einsetzen. *Moderne Akkumulatoren richtig einsetzen*, (January 2006):204–213, 2006.

[18] Matthieu Dubarry, Bor Yann Liaw, Mao Sung Chen, Sain Syan Chyan, Kuo Chang Han, Wun Tong Sie, and She Huang Wu. Identifying battery aging mechanisms in large format Li ion cells. *Journal of Power Sources*, 196(7):3420–3425, 2011.

[19] Yuejiu Zheng, Minggao Ouyang, Languang Lu, and Jianqiu Li. Understanding aging mechanisms in lithium-ion battery packs: From cell capacity loss to pack capacity evolution. *Journal of Power Sources*, 278:287–295, 2015.

[20] Matthew B. Pinson and Martin Z. Bazant. Theory of SEI Formation in Rechargeable Batteries: Capacity Fade, Accelerated Aging and Lifetime Prediction. *Journal of The Electrochemical Society*, 160(2):A243–A250, 2013.

[21] Madeleine Ecker. *Lithium plating in lithium-ion batteries : an experimental and simulation approach*. Dissertation, Rheinisch-Westfälische Technische Hochschule Aachen, 2016.

[22] Simon F. Schuster, Tobias Bach, Elena Fleder, Jana Müller, Martin Brand, Gerhard Sextl, and Andreas Jossen. Nonlinear aging characteristics of lithium-ion cells under different operational conditions. *Journal of Energy Storage*, 2015.

[23] Matthieu Dubarry, Nan Qin, and Paul Brooker. Calendar aging of commercial Li-ion cells of different chemistries - A review, 2018.

[24] Madeleine Ecker, Nerea Nieto, Stefan Käbitz, Johannes Schmalstieg, Holger Blanke, Alexander Warnecke, and Dirk Uwe Sauer. Calendar and cycle life study of Li(NiMnCo)O2-based 18650 lithium-ion batteries. *Journal of Power Sources*, 248:839–851, 2014.

[25] Jan Philipp Schmidt. *Verfahren zur Charakterisierung und Modellierung von Lithium-Ionen Zellen.* PhD thesis, Karlsruher Institut für Technologie Fakultät für Elektrotechnik und Informationstechnik, 2013.

[26] Peter Keil and Andreas Jossen. Aufbau und Parametrierung von Batteriemodellen. *19. DESIGN&ELEKTRONIK-Entwicklerforum Batterien & Ladekonzepte*, 2012.

[27] Bernhard Schweighofer, Klaus M. Raab, and Georg Brasseur. Modeling of high power automotive batteries by the use of an automated test system. *IEEE Transactions on Instrumentation and Measurement*, 52(4):1087–1091, 2003.

[28] Min Chen and Gabriel A. Rincon-Mora. Accurate Electrical Battery Model Capable of Predicting Runtime and I-V Performance. *IEEE TRANSACTIONS ON ENERGY CONVERSION*, 21(2):504–511, 2006.

[29] Hongwen He, Rui Xiong, and Jinxin Fan. Evaluation of lithium-ion battery equivalent circuit models for state of charge estimation by an experimental approach. *Energies*, 4(4):582–598, 2011.

[30] Ryan C. Kroeze and Philip T. Krein. Electrical battery model for use in dynamic electric vehicle simulations. *PESC Record - IEEE Annual Power Electronics Specialists Conference*, pages 1336–1342, 2008.

[31] Wladislaw Waag, Stefan Käbitz, and Dirk Uwe Sauer. Experimental investigation of the lithium-ion battery impedance characteristic at various conditions and aging states and its influence on the application. *Applied Energy*, 2013.

[32] Jan Philipp Schmidt, André Weber, and Ellen Ivers-Tiffée. A novel and fast method of characterizing the self-discharge behavior of lithium-ion cells using a pulse-measurement technique. *Journal of Power Sources*, 2015.

[33] M. Strauch, N. Klumpp, and A. Binder. Parameteridentifikation und Modellierung von Lithium-Eisen-Phosphat-Akkumulatoren für die Verwendung in Modellen elektrischer Fahrzeuge. In *Elektromobilitätsausstellung (EMA)*, 2012.

[34] Sophia Gantenbein. *Impedanzbasierte Modellierung von Lithium-Ionen Zellen und deren Degradationsverhalten*. PhD thesis, Karlsruher Institut für Technologie Fakultät für Elektrotechnik und Informationstechnik, 2019.

[35] D. Andre, M. Meiler, K. Steiner, Ch Wimmer, T. Soczka-Guth, and D. U. Sauer. Characterization of high-power lithium-ion batteries by electrochemical impedance spectroscopy. I. Experimental investigation. *Journal of Power Sources*, 2011.

[36] Dirk Uwe Sauer. Grundlagen der Impedanzspektroskopie fur die Charakterisierung von Batterien. (January 2006):0–14, 2016.

[37] D. Andre, M. Meiler, K. Steiner, H. Walz, T. Soczka-Guth, and D. U. Sauer. Characterization of high-power lithium-ion batteries by electrochemical impedance spectroscopy. II: Modelling. *Journal of Power Sources*, 2011.

[38] J. T.B.A. Kessels, B. Rosca, H. J. Bergveld, and P. P.J. Van Den Bosch. On-line battery identification for electric driving range prediction. *2011 IEEE Vehicle Power and Propulsion Conference, VPPC 2011*, pages 0–5, 2011.

[39] Taesic Kim and Wei Qiao. A hybrid battery model capable of capturing dynamic circuit characteristics and nonlinear capacity effects. *IEEE Transactions on Energy Conversion*, 26(4):1172–1180, 2011.

[40] Simone Barcellona and Luigi Piegari. Lithium ion battery models and parameter identification techniques, 2017.

[41] DIN ISO 12405-4:2018-07 Electrically propelled road vehicles –Test specification for lithium-ion traction battery packs and systems - Part 4: Performance testing, 2018.

[42] Thorsten Baumhöfer, Manuel Brühl, Susanne Rothgang, and Dirk Uwe Sauer. Production caused variation in capacity aging trend and correlation to initial cell performance. *Journal of Power Sources*, 247:332–338, 2014.

[43] Sabine Piller, Marion Perrin, and Andreas Jossen. Methods for state-of-charge determination and their applications. *Journal of Power Sources*, 96(1):113–120, 2001.

[44] Habiballah Rahimi-Eichi and Mo Yuen Chow. Adaptive parameter identification and State-of-Charge estimation of lithium-ion batteries. In *IECON Proceedings (Industrial Electronics Conference)*, 2012.

[45] Mathias Petzl and Michael A. Danzer. Advancements in OCV measurement and analysis for lithium-ion batteries. *IEEE Transactions on Energy Conversion*, 28(3):675–681, 2013.

[46] Lei Pei, Rengui Lu, and Chunbo Zhu. Relaxation model of the open-circuit voltage for state-of-charge estimation in lithium-ion batteries. *IET Electrical Systems in Transportation*, 3(4):112–117, 2013.

[47] Valer Pop, Henk Jan Bergveld, Dmitry Danilov, Paul P.L. Regtien, and Reter H.L. Notten. *Battery Management Sytems - State-of-Charge indication for battery-powered applications*. Springer Verlag, 2008.

[48] Robert A. Huggins. *Advanced batteries*. Springer Verlag, 2009.

[49] Allen J. Bard and Larry R. Faulkner. *ELECTROCHEMICAL METHODS Fundamentals and Applications*. JOHN WILEY & SONS, INC., 2001.

[50] Ira Bloom, Andrew N. Jansen, Daniel P. Abraham, Jamie Knuth, Scott A. Jones, Vincent S. Battaglia, and Gary L. Henriksen. Differential voltage analyses of high-power, lithium-ion cells 1. Technique and application. *Journal of Power Sources*, 139(1-2):295–303, 2005.

[51] Jürgen Remmlinger, Michael Buchholz, Markus Meiler, Peter Bernreuter, and Klaus Dietmayer. State-of-health monitoring of lithium-ion batteries in electric vehicles by on-board internal resistance estimation. *Journal of Power Sources*, 196(12):5357–5363, 2011.

[52] Zhen Guo, Xinping Qiu, Guangdong Hou, Bor Yann Liaw, and Changshui Zhang. State of health estimation for lithium ion batteries based on charging curves. *Journal of Power Sources*, 249:457–462, 2014.

[53] Nadana Ayzah Azis, Endra Joelianto, and Augie Widyotriatmo. State of Charge (SoC) and State of Health (SoH) Estimation of Lithium-Ion Battery Using Dual Extended Kalman Filter Based on Polynomial Battery Model. *Proceedings of the 2019 6th International Conference on Instrumentation, Control, and Automation, ICA 2019*, (August):88–93, 2019.

[54] M. Berecibar, I. Gandiaga, I. Villarreal, N. Omar, J. Van Mierlo, and P. Van Den Bossche. Critical review of state of health estimation methods of Li-ion batteries for real applications, 2016.

[55] Kong Soon Ng, Chin Sien Moo, Yi Ping Chen, and Yao Ching Hsieh. Enhanced coulomb counting method for estimating state-of-charge and state-of-health of lithium-ion batteries. *Applied Energy*, 86(9):1506–1511, 2009.

[56] Markus Lelie, Thomas Braun, Marcus Knips, Hannes Nordmann, Florian Ringbeck, Hendrik Zappen, and Dirk Uwe Sauer. Battery management system hardware concepts: An overview. *Applied Sciences (Switzerland)*, 8(4), 2018.

[57] Kuan Cheng Chiu, Chi Hao Lin, Sheng Fa Yeh, Yu Han Lin, Chih Sheng Huang, and Kuo Ching Chen. Cycle life analysis of series connected lithium-ion batteries with temperature difference. *Journal of Power Sources*, 263:75–84, 2014.

[58] Simon F. Schuster, Martin J. Brand, Philipp Berg, Markus Gleissenberger, and Andreas Jossen. Lithium-ion cell-to-cell variation during battery electric vehicle operation. *Journal of Power Sources*, 2015.

[59] I. Aizpuru, U. Iraola, J. M. Canales, E. Unamuno, and I. Gil. Battery pack tests to detect unbalancing effects in series connected Li-ion cells. *4th International Conference on Clean Electrical Power: Renewable Energy Resources Impact, ICCEP 2013*, pages 99–106, 2013.

[60] Barrie Lawson. Elektropaedia - Battery and Energy Technologies. *Woodbank Communications Ltd*, 2005.

[61] Ashraf Bani Ahmad, Dahaman Ishak, and Jiashen Teh. Cell Balancing Topologies in Battery Energy Storage Systems: A Review. 10th International Conference on Robotics, Vision, Signal Processing and Power Applications, pp.159-165, 2019.

[62] Javier Gallardo-Lozano, Enrique Romero-Cadaval, M. Isabel Milanes-Montero, and Miguel A. Guerrero-Martinez. Battery equalization active methods. *Journal of Power Sources*, 246:934–949, 2014.

[63] B. Lindemark. Individual Cell voltage Equalizers (ICE) For Reliable Battery Performance. In *IEEE 13th International Telecommunications Energy Conference, INTELEC '91*, pages 196–201, 1991.

[64] Gerald Landrum, Thomas A. Stuart, and Wei Zhu. Fast equalization for large lithium ion batteries. *Oceans 2008*, (July):27–31, 2008.

[65] Maurice Caspar, Torsten Eiler, and Sören Hohmann. Comparison of active battery balancing systems. *2014 IEEE Vehicle Power and Propulsion Conference, VPPC 2014*, 2014.

[66] Moon Young Kim, Chol Ho Kim, Jun Ho Kim, and Gun Woo Moon. A chain structure of switched capacitor for improved cell balancing speed of lithium-ion batteries. *IEEE Transactions on Industrial Electronics*, 61(8):3989–3999, 2014.

[67] Andrew Baughman and Mehdi Ferdowsi. Double-tiered capacitive shuttling method for balancing series-connected batteries. *2005 IEEE Vehicle Power and Propulsion Conference, VPPC*, 2005:50–54, 2005.

[68] Andrew C. Baughman and Mehdi Ferdowsi. Double-tiered switched-capacitor battery charge equalization technique. *IEEE Transactions on Industrial Electronics*, 55(6):2277–2285, 2008.

[69] Carmelo Speltino, Anna Stefanopoulou, and Giovanni Fiengo. Cell equalization in battery stacks through State Of Charge estimation polling. *Proceedings of the 2010 American Control Conference, ACC 2010*, pages 5050–5055, 2010.

[70] Sang Hyun Park, Tae Sung Kim, Jin Sik Park, Gun Woo Moon, and Myung Joong Yoon. A new battery equalizer based on buck-boost topology. *7th Internatonal Conference on Power Electronics, ICPE'07*, pages 962–965, 2007.

[71] Thanh Hai Phung, Jean Christophe Crebier, Alexandre Chureau, Alexandre Collet, and Van Nguyen. Optimized structure for next-to-next balancing of series-connected lithium-ion cells. *Conference Proceedings - IEEE Applied Power Electronics Conference and Exposition - APEC*, pages 1374–1381, 2011.

[72] Abusaleh M. Imtiaz, Faisal H. Khan, and Haresh Kamath. A low-cost time shared cell balancing technique for future lithium-ion battery storage system featuring regenerative energy distribution. *Conference Proceedings - IEEE Applied Power Electronics Conference and Exposition - APEC*, pages 792–799, 2011.

[73] Seonwoo Jeon, Myungchin Kim, and Sungwoo Bae. Analysis of a symmetric active cell balancer with a multi-winding transformer. *Journal of Electrical Engineering and Technology*, 12(5):1812–1820, sep 2017.

[74] Markus Einhorn, Werner Roessler, and Juergen Fleig. Improved performance of serially connected Li-ion batteries with active cell balancing in electric vehicles. *IEEE Transactions on Vehicular Technology*, 60(6):2448–2457, 2011.

[75] Siqi Li, Chris Mi, and Mengyang Zhang. A high efficiency low cost direct battery balancing circuit using a multi-winding transformer with reduced switch count. *Conference Proceedings - IEEE Applied Power Electronics Conference and Exposition - APEC*, pages 2128–2133, 2012.

[76] Dorin V. Cadar, Dorin M. Petreus, and Toma M. Patarau. An energy converter method for battery cell balancing. *ISSE 2010 - 33rd International Spring Seminar on Electronics Technology: Polymer Electronics and Nanotechnologies: Towards System Integration - Conference Proceedings*, pages 290–293, 2010.

[77] Kong Zhi-Guo, Zhu Chun-Bo, Lu Ren-Gui, and Cheng Shu-Kang. Comparison and Evaluation of Charge Equalization Technique for Series Connected Batteries. In *37th IEEE Power Electronics Specialists Conference*, pages 1–6. IEEE, 2006.

[78] Chol Ho Kim, Hong Sun Park, Chong Eun Kim, Gun Woo Moon, and Joong Hui Lee. Individual charge equalization converter with parallel primary winding of transformer for series connected Lithium-Ion battery strings In an hev. *Journal of Power Electronics*, 9(3):472–480, 2009.

[79] Wei Hong, Kong Soon Ng, Jin Hsin Hu, and Chin Sien Moo. Charge equalization of battery power modules in series. *2010 International Power Electronics Conference - ECCE Asia -, IPEC 2010*, pages 1568–1572, 2010.

[80] T. Gottwald, Z. Ye, and Stuart T. Equalization of EV and HEV Batterie With a Ramp Converter. In *Ieee Transactions On Aerospace And Electronic Systems*, 1997.

[81] Yuang Shung Lee, Chun Yi Duh, Guo Tian Chen, and Shen Ching Yang. Battery equalization using bi-directional Cûk converters in DCVM operation. *PESC Record - IEEE Annual Power Electronics Specialists Conference*, 2005:765–771, 2005.

[82] Yunlong Shang, Chenghui Zhang, Naxin Cui, and Josep M. Guerrero. A cell-to-cell battery equalizer with zero-current switching and zero-voltage gap based on quasi-resonant lc converter and boost converter. *IEEE Transactions on Power Electronics*, 30(7):3731–3747, 2015.

[83] Laxman Maharjan, Shigenori Inouc, Hirofumi Akagi, and Jun Asakura. State-of-Charge (SOC)-Balancing Control of a Battery Energy Storage System Based on a Cascade PWM Converter. *IEEE Transactions on Power Electronics*, 24(6):1628–1636, 2009.

[84] Jong Hoon Kim, Jong Won Shin, Chang Yoon Jeon, and Bo Hyung Cho. Screening process of Li-Ion series battery pack for improved voltage/SOC balancing. *2010 International Power Electronics Conference - ECCE Asia -, IPEC 2010*, pages 1174–1179, 2010.

[85] Maurice Caspar, Viktor Polinski, and Soren Hohmann. Structural Comparison of Battery Balancing Architectures with Optimal Control. *2015 IEEE Vehicle Power and Propulsion Conference, VPPC 2015 - Proceedings*, 2015.

[86] Federico Baronti, Roberto Roncella, Roberto Saletti, and Walter Zamboni. Experimental validation of an efficient charge equalization system for Lithium-ion batteries. *IEEE International Symposium on Industrial Electronics*, pages 1811–1816, 2014.

[87] Michael Evzelman, M. Muneeb Ur Rehman, Kelly Hathaway, Regan Zane, Daniel Costinett, and Dragan Maksimovic. Active Balancing System for Electric Vehicles With Incorporated Low-Voltage Bus. *IEEE Transactions on Power Electronics*, 31(11):7887–7895, 2016.

[88] Yuejiu Zheng, Minggao Ouyang, Languang Lu, Jianqiu Li, Xuebing Han, and Liangfei Xu. On-line equalization for lithium-ion battery packs based on charging cell voltages: Part 1. Equalization based on remaining charging capacity estimation. *Journal of Power Sources*, 2014.

[89] Linfeng Zheng, Jianguo Zhu, and Guoxiu Wang. A comparative study of battery balancing strategies for different battery operation processes. *2016 IEEE Transportation Electrification Conference and Expo, ITEC 2016*, pages 1–5, 2016.

[90] Yujie Wang, Chenbin Zhang, Zonghai Chen, Jing Xie, and Xu Zhang. A novel active equalization method for lithium-ion batteries in electric vehicles. *Applied Energy*, 145:36–42, 2015.

[91] Chol-ho Kim, Student Member, Moon-young Kim, Student Member, Hong-sun Park, Associate Member, and Gun-woo Moon. A Modularized Two-Stage Charge Equalizer With Cell Selection Switches for Series-Connected Lithium-Ion Battery String in an HEV. 27(8):3764–3774, 2012.

[92] A. Hande and T. A. Stuart. A selective equalizer for NiMH batteries. *Journal of Power Sources*, 138(1-2):327–339, 2004.

[93] Markus Einhorn, Werner Rößler, Fiorentino Valerio Conte, Hartmut Popp, and Jürgen Fleig. Charge balancing of serially connected lithium-ion battery cells in electric vehicles. *Elektrotechnik und Informationstechnik*, 129(3):167–173, 2012.

[94] Linfeng Zheng, Jianguo Zhu, Guoxiu Wang, Dylan Dah Chuan Lu, Peter McLean, and Tingting He. Model predictive control based balancing strategy for series-connected lithium-ion battery packs. *2017 19th European Conference on Power Electronics and Applications, EPE 2017 ECCE Europe*, 2017-Janua:9–11, 2017.

[95] Markus Einhorn, Fiorentino Valerio Conte, and Juergen Fleig. Improving of active cell balancing by equalizing the cell energy instead of the cell voltage. *World Electric Vehicle Journal*, 4(1):400–404, 2011.

[96] Chang Yoon Chun, B. H. Cho, and Joonhoon Kim. State-of-charge and remaining charge estimation of series-connected lithium-ion batteries for cell balancing scheme. In *INTELEC, International Telecommunications Energy Conference (Proceedings)*, 2016.

[97] Lina Huang, Prasanth Thummala, Zhe Zhang, and Michael A.E. Andersen. Battery powered high output voltage bidirectional flyback converter for cylindrical DEAP actuator. *Proceedings of the 2012 IEEE International Power Modulator and High Voltage Conference, IPMHVC 2012*, pages 454–457, 2012.

[98] Mohd Kashif. Bidirectional flyback DC-DC converter for hybrid electric vehicle: Utility, working and PSPICE computer model. *Asia Pacific Conference on Postgraduate Research in Microelectronics and Electronics*, (December):61–66, 2012.

[99] Daiming Yang, Shengyong Li, and Guoguang Qi. A bidirectional flyback cell equalizer for series-connected lithium iron phosphate batteries. *2015 6th International Conference on Power Electronics Systems and Applications: Electric Transportation - Automotive, Vessel and Aircraft, PESA 2015*, pages 1–5, 2016.

[100] Sebastian Paul, Christian Diegelmann, Herbert Kabza, and Werner Tillmetz. Analysis of ageing inhomogeneities in lithium-ion battery systems. *Journal of Power Sources*, 239:642–650, 2013.

[101] David Oeser. *From the Production of the Single Cell to the End of Life of the Battery Module: The Development of Parameter Variation of Lithium-Ion Cells.* PhD thesis, UPC Barcelona, 2022.

[102] Wai Chung Lee, David Drury, and Phil Mellor. Comparison of passive cell balancing and active cell balancing for automotive batteries. *2011 IEEE Vehicle Power and Propulsion Conference, VPPC 2011*, 2011.

[103] Christian Fleischer, Bastian Ostendorp, Dirk Uwe Sauer, Simulative Comparison, Lithium-ion Batteries, Advanced Automotive, and Battery Aabc. Reprinted from Simulative Comparison of Balancing Algorithms for Active and Passive Cell Balancing Systems for Lithium-Ion Batteries. (February), 2013.

[104] Federico Baronti, Roberto Roncella, and Roberto Saletti. Performance comparison of active balancing techniques for lithium-ion batteries. *Journal of Power Sources*, 267:603–609, 2014.

[105] Lukas Valda and Kamil Kosturik. Comparison of Li-ion active cell balancing methods replacing passive cell balancer. *International Conference on Applied Electronics*, 2015-Octob:267–270, 2015.

[106] Martin Lukasiewycz, Matthias Kauer, and Sebastian Steinhorst. Synthesis of Active Cell Balancing Architectures for Battery Packs. *IEEE Transactions on Computer-Aided Design of Integrated Circuits and Systems*, 35(11):1876–1889, 2016.

[107] Youngchul Lee, Seonwoo Jeon, Hongyeob Lee, and Sungwoo Bae. Comparison on cell balancing methods for energy storage applications. *Indian Journal of Science and Technology*, 2016.

[108] Thuc Minh Bui, Myungchin Kim, and Sungwoo Bae. Comparative survey on modular cell-equalizing circuits for battery management systems. *Medico-Legal Update*, 18(1):372–379, jan 2018.

[109] Yang Hua, Sida Zhou, Haigang Cui, Xinhua Liu, Cheng Zhang, Xingwu Xu, Heping Ling, and Shichun Yang. A comprehensive review on inconsistency and equalization technology of lithium-ion battery for electric vehicles. *International Journal of Energy Research*, 44(14):11059–11087, 2020.

[110] D. Oeser, A. Ziegler, B. Arndt, and A. Ackva. Effectiveness of active balancing on high dispersion batteries. In *CANDO-EPE 2018 - Proceedings IEEE International Conference and Workshop in Obuda on Electrical and Power Engineering*, 2018.

[111] A. Ziegler, D. Oeser, B. Arndt, and A. Ackva. Comparison of active and passive balancing by a long term test including a post-mortem analysis of all single battery cells. In *CANDO-EPE 2018 - Proceedings IEEE International Conference and Workshop in Obuda on Electrical and Power Engineering*, 2018.

[112] Peter Keil and Andreas Jossen. Aging of lithium-ion batteries in electric vehicles:. *Dissertation*, 7(1):41–51, 2017.

[113] Kristen A. Severson, Peter M. Attia, Norman Jin, Nicholas Perkins, Benben Jiang, Zi Yang, Michael H. Chen, Muratahan Aykol, Patrick K. Herring, Dimitrios Fraggedakis, Martin Z. Bazant, Stephen J. Harris, William C. Chueh, and Richard D. Braatz. Data-driven prediction of battery cycle life before capacity degradation. *Nature Energy*, 4(5):383–391, 2019.

[114] David Oeser, Andreas Ziegler, and Ansgar Ackva. Single cell analysis of lithium-ion e-bike batteries aged under various conditions. *Journal of Power Sources*, 397(May):25–31, 2018.

[115] Michael Baumann, Leo Wildfeuer, Stephan Rohr, and Markus Lienkamp. Parameter variations within Li-Ion battery packs - Theoretical investigations and experimental quantification. *Journal of Energy Storage*, 18(February):295–307, 2018.

[116] Christian Campestrini, Peter Keil, Simon F. Schuster, and Andreas Jossen. Ageing of lithium-ion battery modules with dissipative balancing compared with single-cell ageing. *Journal of Energy Storage*, 6:142–152, 2016.

[117] Simon F. Schuster, Martin J. Brand, Philipp Berg, Markus Gleissenberger, and Andreas Jossen. Lithium-ion cell-to-cell variation during battery electric vehicle operation. *Journal of Power Sources*, 297:242–251, 2015.

[118] Susanne Rothgang, Thorsten Baumhöfer, and Dirk Uwe Sauer. Necessity and methods to improve battery lifetime on system level. *28th International Electric Vehicle Symposium and Exhibition 2015, EVS 2015*, (May):0–9, 2015.

[119] Johannes Schmalstieg, Stefan Käbitz, Madeleine Ecker, and Dirk Uwe Sauer. A holistic aging model for Li(NiMnCo)O2 based 18650 lithium-ion batteries. *Journal of Power Sources*, 257:325–334, 2014.

[120] Thomas Waldmann, Marcel Wilka, Michael Kasper, Meike Fleischhammer, and Margret Wohlfahrt-Mehrens. Temperature dependent ageing mechanisms in Lithium-ion batteries - A Post-Mortem study. *Journal of Power Sources*, 262:129–135, 2014.

[121] Andreas Ziegler, David Oeser, Thiemo Hein, Daniel Montesinos-Miracle, and Ansgar Ackva. Reducing Cell to Cell Variation of Lithium-Ion Battery Packs during Operation. *IEEE Access*, 2021.

[122] Thiemo Hein, Andreas Ziegler, David Oeser, and Ansgar Ackva. A capacity-based equalization method for aged lithium-ion batteries in electric vehicles. *Electric Power Systems Research*, 191:106898, feb 2020.

[123] Andreas Ziegler, David Oeser, Thiemo Hein, and Ansgar Ackva. Development and Application of an Active Balancing System for Lithium-Ion Cells. In *2019 IEEE Vehicle Power and Propulsion Conference (VPPC)*, pages 1–6. IEEE, oct 2019.

[124] Andreas Ziegler, David Oeser, Thiemo Hein, Daniel Montesinos-Miracle, and Ansgar Ackva. Run to Failure: Aging of Commercial Battery Cells beyond Their End of Life. *Energies*, 13(8):1858, apr 2020.

[125] G Bohn, J Taub, A Linke, S Bayer, D Oeser, A Ziegler, P Ettl, and A Ackva. High-resolution Interferometric Measurement of Thickness Change on a Lithium-Ion Pouch Battery. *IOP Conference Series: Earth and Environmental Science*, 281:012030, jun 2019.

[126] D. Oeser, A. Ziegler, and A. Ackva. Single cell analysis of lithium-ion e-bike batteries aged under various conditions. *Journal of Power Sources*, 397, 2018.

Appendix A

Hardware and Testbench

A.1 Active Balancing BMS

This section gives an overview and technical information of the used active balancing battery management system.

Multiple Flyback-Converter Board

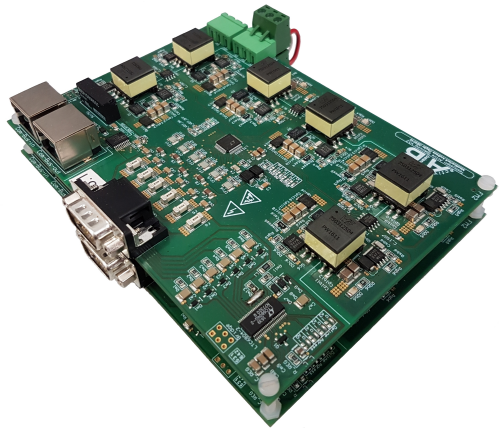

Figure A.1: Multiple Flyback-Converter board.

Description	Value/Type
Flyback controller	Linear Technology LTC3300-2
Measurement IC	Linear Technology LTC6804
Nominal voltage	48V (12s configuration)
Max. cell current	12x ± 4 A
Max. cell count	stackable up to 96s
Flyback switching frequency	150 kHz
Current Measurement IC	MicroChip MCP3426

Table A.1: Multiple Flyback-Converter board specification.

Balancing Controller

Figure A.2: STM32 microcontroller with stacked adapter board.

Description	Value/Type
Name	STM32F407VGT6
CPU	32-bit Arm Cortex M4, FPU core
Memory	1-Mbyte Flash, 192-Kbyte RAM
Supported protocols	USB/UART, SPI, I2C, CAN
USB IC	FTDI FT232
DC supply	muRata NCS12S4805C

Table A.2: Balancing controller specification.

A.2 Battery Pack Test-Bench

This section gives an overview and technical information of the used battery test system and temperature chamber for pack tests.

Battery Test System

Figure A.3: BaSyTec battery pack test system.

Description	Value/Type
Name	BaSyTec HPS
Voltage range	3 V - 60 V
Voltage accuracy	± 1 mV
Current range	-40 A / +20 A
Current accuracy	± 20 mA
Current rise time	< 1 ms

Table A.3: Battery pack test system specification.

Temperature Chamber

Figure A.4: ThermoTEC temperature chamber.

Description	Value/Type
Name	ThermoTEC PU-1 J
Temperature range	-40 °C / +100 °C
Temperature fluctuation	± 0.3 °C
Temperature variation in space	1.5 °C
Temperature change rate	+3.0 °C/min, -2.0 °C/min
Chamber volume	120 l

Table A.4: ThermoTEC temperature chamber specification.

A.3 Single Cell Test-Bench

This section gives an overview and technical information of the used cell test system and temperature chamber for cell tests.

Figure A.5: Rack setup with BaSyTec cell test system and Memmert temperature chamber.

Description	Value/Type
Name	BaSyTec CTS
Voltage range	0 V - 6 V
Voltage accuracy	± 1 mV
Current range	-5 A / +5 A
Current accuracy	± 1 mA
Time delay	± 1 μs

Table A.5: Single cell test system specification.

Description	Value/Type
Name	Memmert IPP55
Temperature range	0 °C to +70 °C
Temperature accuracy	± 0.1 °C
Chamber volume	53 l

Table A.6: Memmert temperature chamber specification.

Appendix B

Calculated Balanced Charges

In this section the calculated data for Q_{b} of all batteries is presented. The data is determined according to the explanation in Chapter 5.3.2. This is to supplement the plots for ΔQ_{c} in Figure 5.10, Chapter 5.4.4.

Note: Q_{b}-values of the passive batteries can also be positive, even if the passive BMS can only discharge cells according to its topology. The reason for this can be found in the battery test system, which regulates the current during the constant voltage phase based on the actual pack voltage. If passive balancers are active, the voltage of the balanced cells drops slightly, which is noticed by the battery tester and the current of the entire battery is readjusted (increased). Cells that are not balanced in that moment receive a higher current and therefore a positive voltage change. This corresponds to an additional charge of the cell and thus a positive Q_{b}-value.

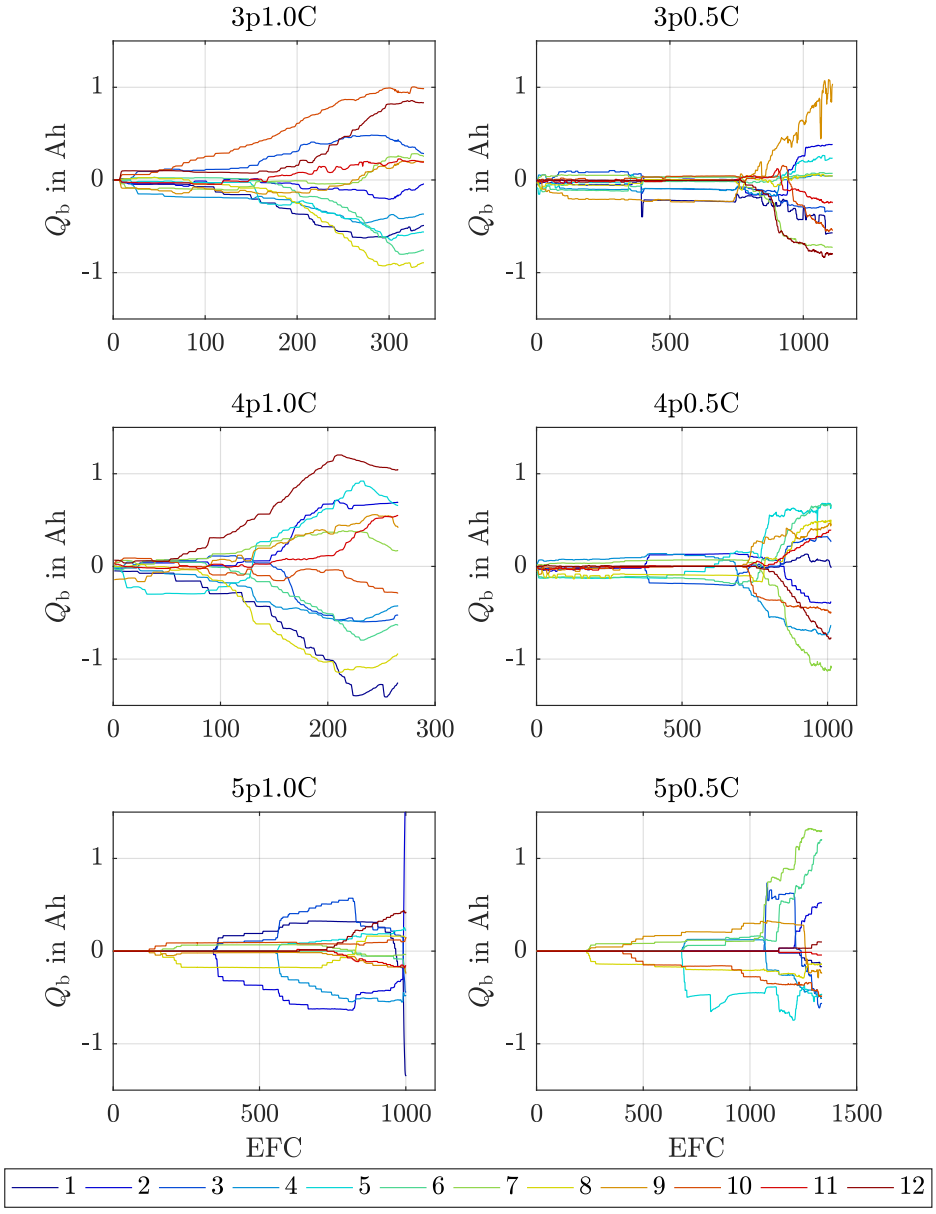

Figure B.1: Calculated Q_b-Data for all active BMS batteries. Legend shows the cell levels in ascending order.

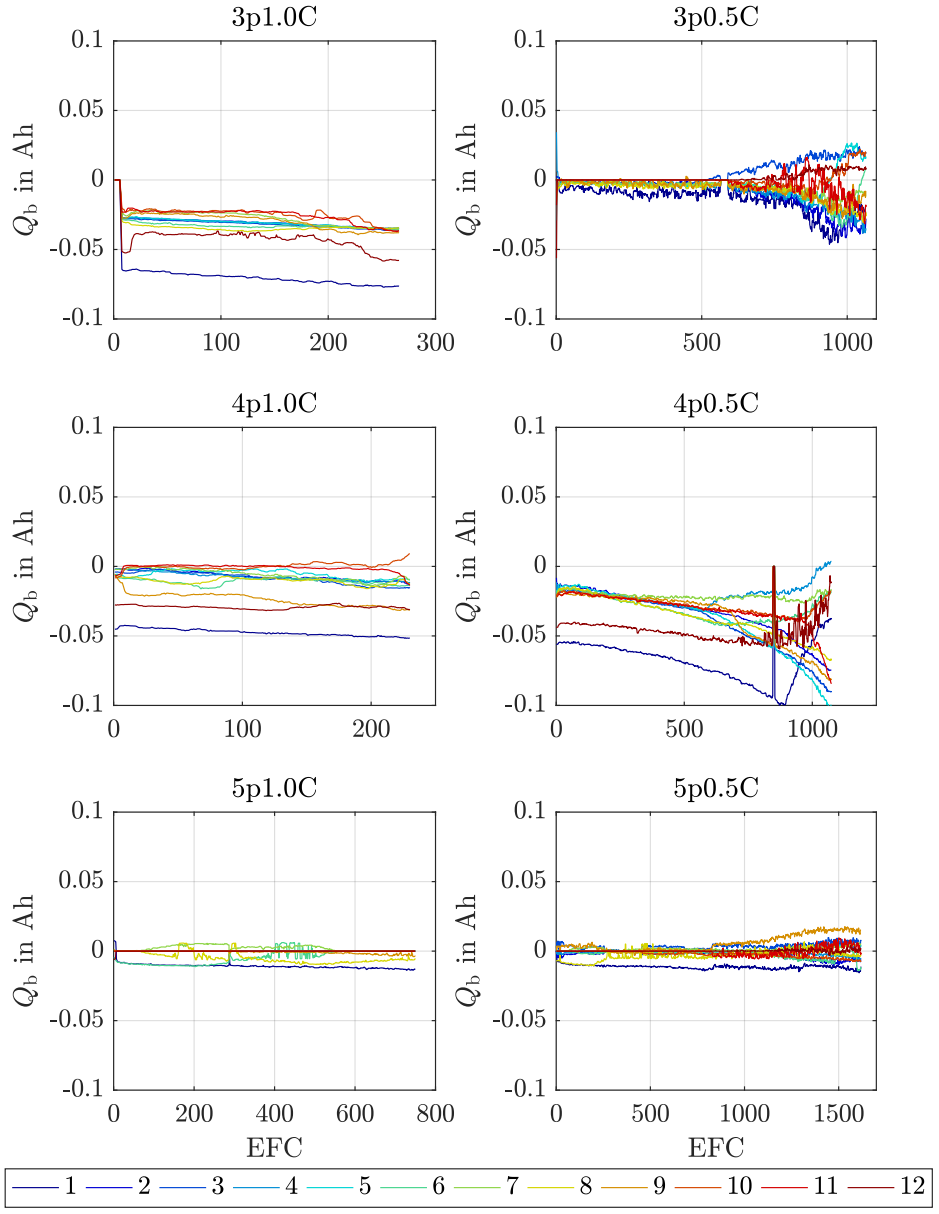

Figure B.2: Calculated Q_b-Data for all passive BMS batteries. Legend shows the cell levels in ascending order.

Appendix C

Single Cell Data

This section provides additional data of single cell parameters. For further explanations see Chapter 6.2.2.

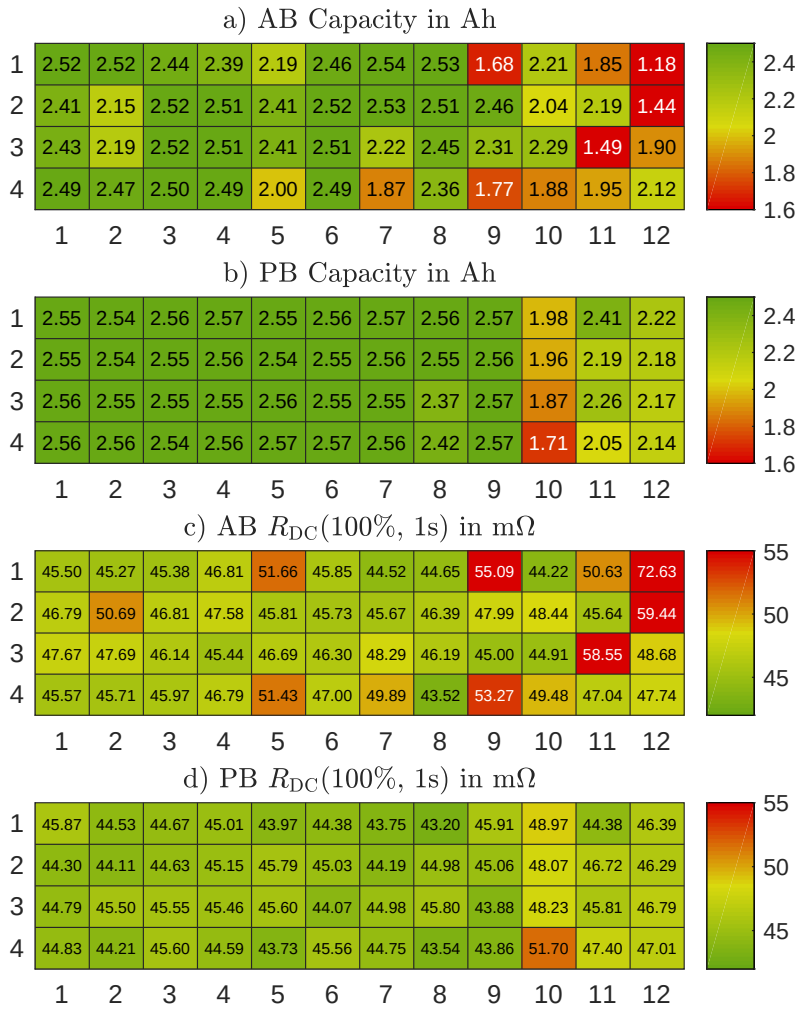

Figure C.1: Single cell data colour-maps of 4p1.0C packs. AB pack completed 266 EFC, PB pack 230 EFC.

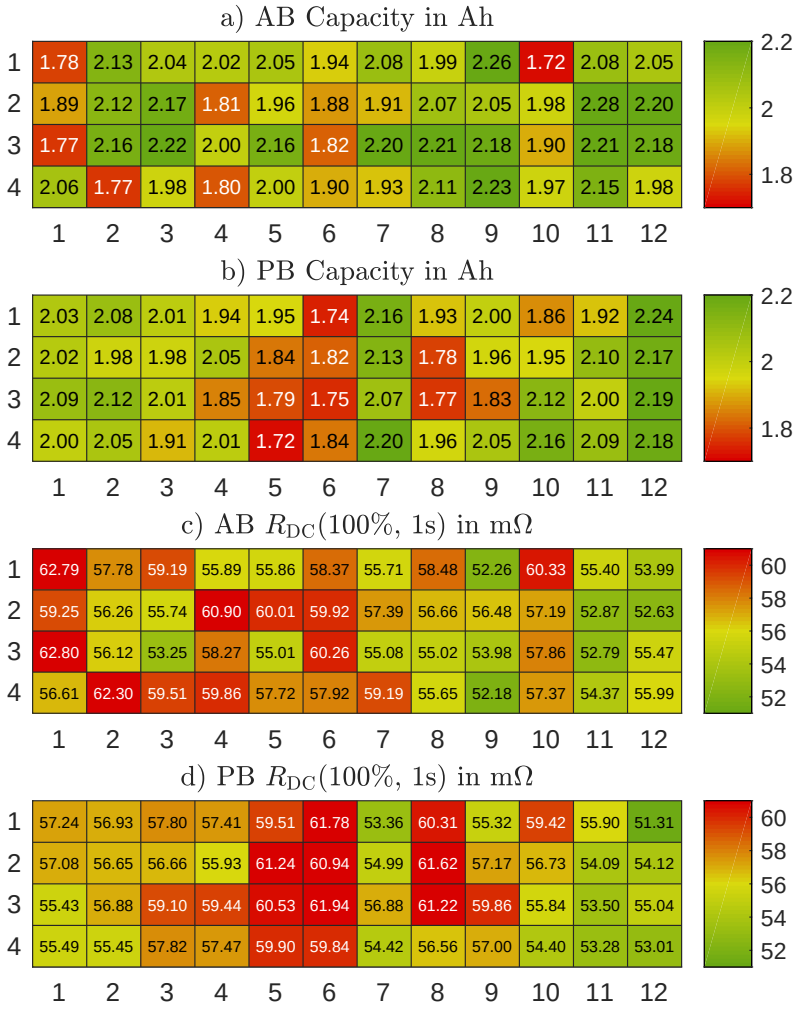

Figure C.2: Single cell data colour-maps of 4p0.5C packs. AB pack completed 1013 EFC, PB pack 1074 EFC.

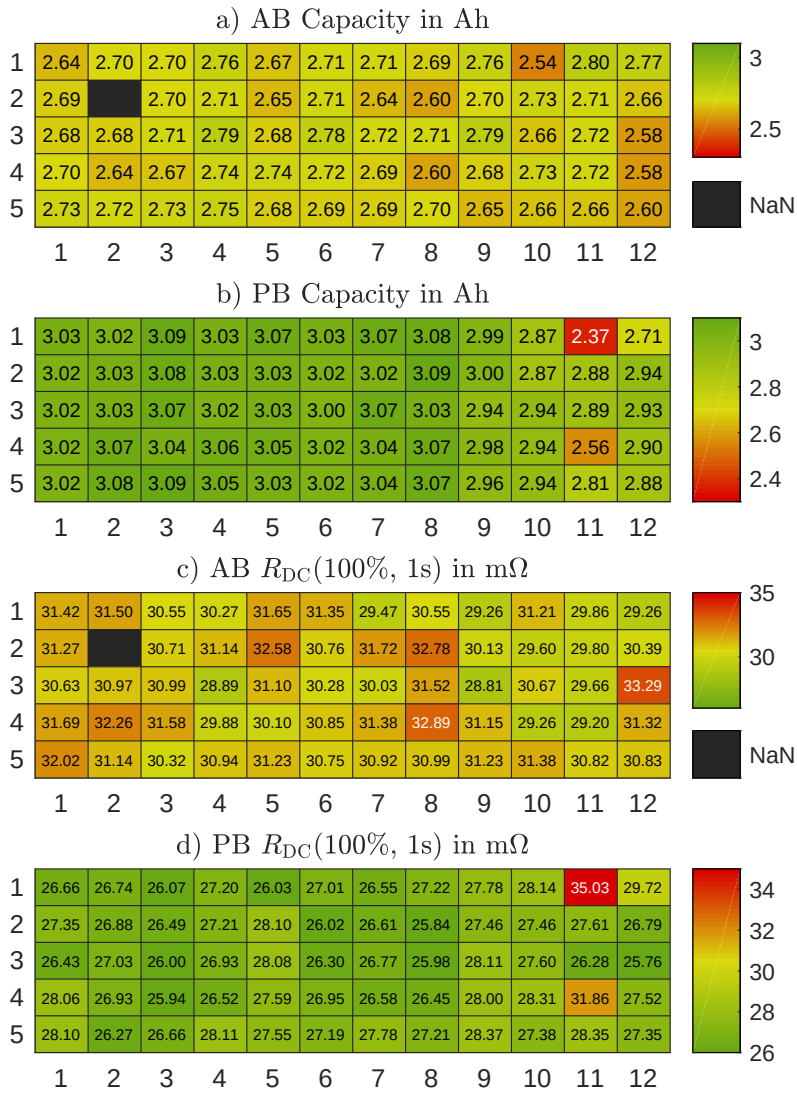

Figure C.3: Single cell data colour-maps of 5p1.0C packs. AB pack completed 994 EFC, PB pack 750 EFC.

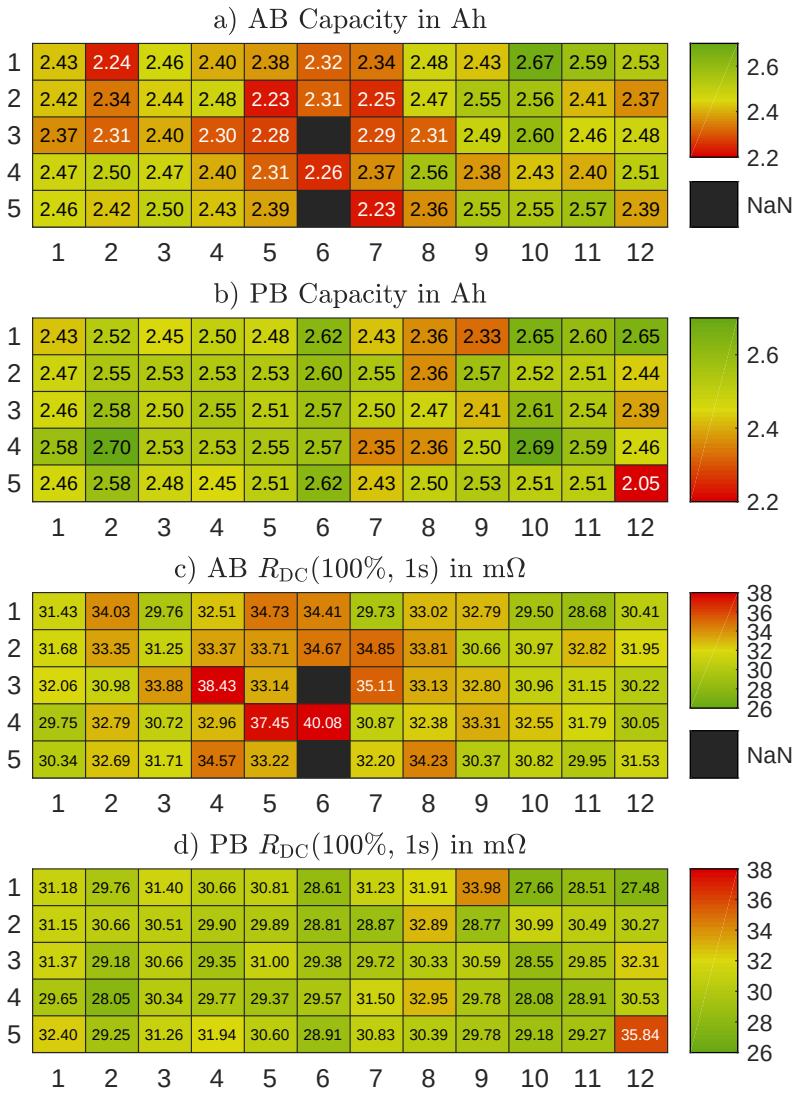

Figure C.4: Single cell data colour-maps of 5p0.5C packs. AB pack completed 1337 EFC, PB pack 1618 EFC.